DIRECTED-POLYMER SYSTEMS EXPLORED VIA THEIR QUANTUM ANALOGS

BY

DAVID Z. ROCKLIN

DISSERTATION

Submitted in partial fulfillment of the requirements
for the degree of Doctor of Philosophy in Physics
in the Graduate College of the
University of Illinois at Urbana-Champaign, 2013

Urbana, Illinois

Doctoral Committee:

Professor Michael Stone, Chair
Professor Paul M. Goldbart, Director of Research
Professor Peter Abbamonte
Professor Richard L. Weaver

ABSTRACT

The equilibrium statistical mechanics of classical directed polymers in $D+1$ dimensions is well known to be equivalent to the imaginary-time quantum dynamics of a quantum many-particle system in D spatial dimensions, with polymer configurations corresponding to particle world-lines. This equivalence motivates the application of techniques originally designed for one-dimensional many-particle quantum systems to the exploration of many-polymer systems, as first recognized and exploited by P.-G. de Gennes [J. Chem. Phys. **48**, 2257 (1968)]. In two dimensions, interactions give rise to an emergent polymer fluid, and I shall examine how topological constraints on this polymer fluid (e.g., due to uncrossable pins or barriers) and their geometry give rise to strong, entropy-driven forces. I shall also apply quantum techniques such as Bethe's Ansatz and bosonization to shed light on the structure of the polymer system. These techniques allow us to examine how polymer system correlations, thermodynamic properties, and response to impurities are influenced by strong polymer-polymer interactions.

In three dimensions, polymers wind around one another and polymer topology may be incorporated via coupling to a Chern-Simons field. As I discuss, this approach reveals the somewhat reduced role played by interactions in this higher-dimensional setting, leading to qualitatively different polymer correlations, thermodynamic properties, and response to impurities.

To my father and the memory of my mother.

ACKNOWLEDGMENTS

It was my great fortune and pleasure to have Paul Goldbart as my advisor. I am indebted to him for his guidance, encouragement, support and advice. Paul's unflagging enthusiasm for and fascination with physics has deepened my own. The breadth of his expertise has allowed us to explore and combine various ideas from many areas of condensed matter and statistical physics. He has taught me to think through all of the stages of research, from problem identification to publication and communication, not merely going through each step but thinking about how and why we do it. He has gone to extraordinary lengths to ensure that our work together has gotten the support it needs.

I thank the many friends and group members in and outside of the department who have offered me help and moral support. There are too many to name, but I mention specifically Bing Sui Lu, Fangfu Ye, Florin Bora, Anton Souslov, David Ferguson, Sarang Gopalakrishnan, Harrison Mebane, Yun Liu, Ben Hsu, Wade DeGottardi, Jeremy McMinis, Carrie Meldgin, Tomoki Ozawa, Norm Tubman, Janet Sheung, Erik Huemiller, Ethan Brown, and Siddhartha Lal. Sarang in particular was always there to show me the ropes.

I thank Professors Nigel Goldenfeld, Paul M. Goldbart, Michael Stone, Philip W. Phillips, Eduardo Fradkin, Gordon Baym, Brian DeMarco and Smitha Vishveshwara for informative and engaging classes. I also thank Professor David Goodstein of the California Institute of Technology for teaching an introductory physics class with enough creativity and flair to capture the attention of an impressionable freshman.

I am grateful to Professor Shina Tan of the Georgia Institute of Technology for collaborating with Paul and me. His quick insights into difficult problems and his clear communication thereof were invaluable for our work. His cheerful help with my professional development was also invaluable.

I am grateful to Professor Nadya Mason for the opportunities to collaborate

with her and her group, especially Scott Scharfenberg, Cesar Chialvo and Malcolm Durkin. I am also grateful to Professor Richard L. Weaver for sharing his expertise in elastic media in collaboration on this project. I also thank Nadya for her valuable advice and help with my professional development.

I thank Professor Jennifer Curtis of the Georgia Institute of Technology, whose research probing pericellular coats first motivated us to consider how polymers reconfigure around obstacles.

I thank Professors Michael Stone, Peter Abbamonte and Richard L. Weaver for graciously serving on my committee.

I thank my parents for their love, support and guidance. While my mother passed away during the completion of this work, the example that she set continues to inspire me. I thank the rest of my family, especially my grandfathers, whose careers in engineering served as examples to me.

During my graduate career, I have received fellowship support from the Department of Defense through a National Defense Science and Engineering Graduate Fellowship (NDSEG) Program and from the Department of Physics at the University of Illinois at Urbana-Champaign. Additionally, I was supported through the National Science Foundation via grant nos. DMR09-06780 and DMR12-07026.

TABLE OF CONTENTS

CHAPTER 1

INTRODUCTION

The ensemble of configurations of a set of directed, one-dimensional objects embedded in $(D+1)$-dimensional space can be envisioned as the ensemble of worldlines of a corresponding set of nonrelativistic quantum-mechanical point particles evolving in time in D spatial dimensions. In particular, a standard mapping which we discuss in detail below relates the classical canonical-ensemble equilibrium statistical mechanics of the set of directed one-dimensional objects to the imaginary-time evolution of the state of the corresponding set of point particles. This mapping was introduced and exploited by de Gennes [1] in order to shed light on the equilibrium structure of a system of many directed fibrous polymers that are confined to two dimensions, thus providing a scheme for accounting, nonperturbatively, for strong local polymer-polymer interactions that serve to prohibit configurations in which pairs of polymers cross one another.

In a parallel development, a suite of powerful techniques—specifically, Bethe's Ansatz, bosonization, and quantum hydrodynamics—have been developed to address the quantum mechanics of one-dimensional systems of many interacting particles or spins. The aim of the research presented in this thesis is to employ these advances in quantum many-body (QMB) physics, together with the de Gennes analogy between the quantum-fluctuating, many-particle system and the classical, thermally fluctuating directed-polymer system, to uncover new information about the equilibrium structure of systems comprising polymers that are either rigorously prohibited from passing through one another (i.e., noncrossing) or subject to other interactions, such as energetic penalizations of crossings, or systems with long-range interactions between polymers. In addition, we apply these advances in technique to determine the equilibrium forces acting on particles included in interacting polymer systems that serve to exclude the polymers from certain spatial regions, as well as the effective forces that act between such particles as a result of their exclusion of polymers. Such constraints force the polymer system to assume configurations that would otherwise correspond to large fluctuations. A global theme of the present work is that, due to the reduced dimensionality of the polymer system, interactions dramatically influence the structure and correlations that characterize the polymer system, and do so both, as we shall see, in topologically—and also geometrically—rich settings. This is a lesson already well known in the quantum-particle domain. We use the quantum analogy to describe the structure, thermodynamic properties,

and response to impurities of two-dimensional interacting directed polymer systems.

We also address systems of directed polymers in three dimensions. We show that, much like de Gennes' use of Fermi statistics to account for the noncrossing condition in $1+1$ dimensions, a nonintersecting condition can be implemented for polymers in $2+1$ via a transmutation of polymer statistics. Despite a somewhat reduced role of interactions in this higher-dimensional setting, polymer interactions and topology serve to strongly modify polymer behavior and response to strong constraints.

This work is organized as follows. In the remainder of this introduction (Chapter 1) the polymer system is described and the application of the techniques used here and related techniques to various physical systems is discussed to motivate the analysis. In Chapter 2, a quantum system is considered and the mapping between the classical polymer system and the quantum many-body system is described. In Chapter 3, the response of the system to a generic strong constraint, or alternately the probability of a large fluctuation, is analyzed. In Chapter 4 the response of a system of noncrossing polymers to a topological pin which forces some polymers to one side of the system is given. In Chapter 5 the noncrossing condition is relaxed and the effect of polymer crossings is considered. In Chapter 6 the consequences of long-range interactions between polymers are investigated. In Chapter 7 a polymer system possessing generic interactions is studied through the technique of bosonization. In Chapter 8 directed polymers in three dimensions are investigated. Concluding remarks are given in Chapter 9.

1.1 Directed two-dimensional classical polymers in thermal equilibrium

We consider a system of N two-dimensional (2D) directed lines, indexed by $n = 1, \ldots, N$, that are noncrossing or otherwise subject to interactions. Although these lines may generally represent a wide variety of statistical objects— vortex lines [3, 4, 5, 6], crystalline step edges [7], levels of growing interfaces [8] or generic "vicious walkers" [9]— we shall typically refer to them specifically as polymer lines. The configuration of the n^{th} polymer is described by $x_n(\tau)$, where τ is the coordinate along the directed axis of the

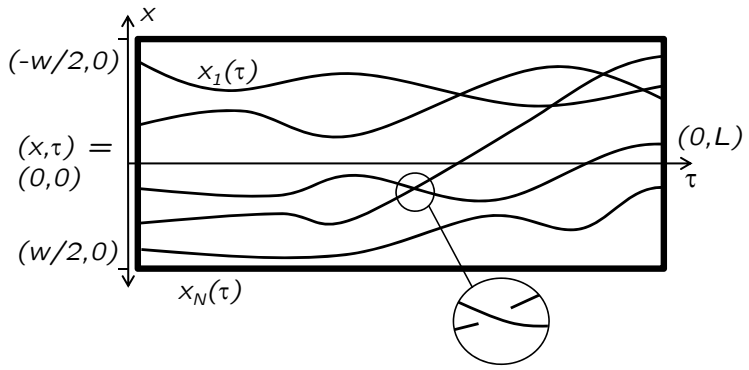

Figure 1.1: The paths $\{x_n(\tau)\}$ describe a possible configuration of the directed polymer system. Thermal fluctuations permit the system to adopt energetically disfavored configurations. When polymers appear to intersect in the (x, τ) plane, in reality one crosses over the other by exploiting the presence of a third dimension. From Rocklin et al. [2].

system (which we call the longitudinal direction), and x_n gives the location of the n^{th} polymer in the perpendicular direction (which we call the lateral direction); see Fig. 1.1. We take the energy cost of the deflections of the polymers from the longitudinal direction to be

$$\frac{A}{2}\sum_{n=1}^{N}\int_0^L d\tau\,(\partial_\tau x_n)^2, \tag{1.1}$$

where L is the extent of system in the longitudinal direction, and A is the deflection energy per unit length, which penalizes configurations for straying from the preferred (i.e., longitudinal) direction.

There are a number of possible origins of such an energetic cost. For polymer lines, the most conceptually simple is tension in the line. Then, for a line subject to tension of magnitude A, the cost of deflections would be as given in Eq. (1.1), provided that the polymers remain sufficiently straight, in a way that we shall define later, to permit us to neglect higher-order gradients in this expression. Alternatively, one could imagine that the polymers are of some fixed length L_p slightly greater than L, and one then adjusts the effective parameter A to enforce the average condition

$$L_p = \left\langle \int_0^L d\tau\,\sqrt{1+(\partial_\tau x_n)^2} \right\rangle \approx L + (L/2)\big\langle(\partial_\tau x_n)^2\big\rangle, \tag{1.2}$$

where $\langle \cdots \rangle$ denotes a thermal expectation value.

Another possibility is for the polymers to couple to a directional field that causes them to orient in the τ-direction, leading to a deflection energy for small deflections of the same form as already considered. One possible source of such a field, at least for polymers in $2+1$ dimensions, is for polymers to spontaneously acquire a preferred direction, at which point the average effect of a polymer's neighbors could lead to a deflection energy of the given form [10].

In addition to the deflection energy, we include an interaction $V(\cdot)$ between the polymers, which we take to be translationally and parity invariant, and sufficiently short-ranged that it may be taken to operate only between monomers (i.e., polymer segments) having common τ coordinates. In fact, we often take the interaction to be purely local, in which case it would take the form $V\big(x_n(\tau) - x_{n'}(\tau)\big) = c\,\delta\big(x_n(\tau) - x_{n'}(\tau)\big)$, where $\delta(x)$ is the one-dimensional Dirac delta function. Much of the present work is devoted to considering polymers that are strictly noncrossing, so that $c \to \infty$, although, as we shall see, many of the results derived therefrom apply more broadly. Incorporating a generic one-body potential $\Phi(\cdot)$, we arrive at the following energy functional $U[\cdot]$ of a configuration $\{x_n(\cdot)\}_{n=1}^N$ of the polymer system:

$$U\left[\{x_n(\cdot)\}\right] = \frac{A}{2}\sum_{n=1}^{N}\int_0^L d\tau\,\big(\partial_\tau x_n(\tau)\big)^2 + \frac{1}{L}\sum_{n=1}^{N}\int_0^L d\tau\,\Phi\big(x_n(\tau)\big) + \frac{1}{L}\sum_{1\le n<n'\le N}\int_0^L d\tau\,V\big(x_n(\tau) - x_{n'}(\tau)\big). \qquad (1.3)$$

According to this model, in the absence of polymer-polymer interactions or external potentials the polymer configurations have a thermal distribution that is Gaussian, in the sense that increments in their deflections [i.e., $x_n(\tau+\delta\tau) - x_n(\tau)$] are independent Gaussian random variables having mean zero and variance $\delta\tau k_B T/A$, where T is the system temperature and k_B is Boltzmann's constant, which we generally set to unity via a suitable choice of units. We note that we shall not be considering the *dynamics* of the polymer system, so we shall not need to take note of the kinetic energy of the polymer system. Additionally, we characterize the system via conditions on the configurations of the polymers at their ends, via the distributions $P^i(\{x_n\})$ and $P^f(\{x_n\})$, which respectively give the probability densities for

the configurations $\{x_n\}$ of the polymer ends at $\tau = 0$ and $\tau = L$.

We take the polymer system to be at thermal equilibrium at inverse temperature $\beta = 1/k_B T$. Thus, we have for the canonical ensemble partition function

$$Z[P^f, P^i] = \int d\{X_n^f\}\, P^f(\{X_n^f\})\, d\{X_n^i\}\, P^i(\{X_n^i\}) \times \int_{\{x_n(0)=X_n^i\}}^{\{x_n(L)=X_n^f\}} \mathcal{D}\left[\{x_n(\cdot)\}\right]\, \mathrm{e}^{-\beta U[\{x_n(\cdot)\}]}, \tag{1.4}$$

which depends functionally on $P^i(\cdot)$ and $P^f(\cdot)$. Here, the measures are defined via

$$d\{X_n^f\}\, d\{X_n^i\} \equiv \prod_{n=1}^{N} dX_n^f\, dX_n^i, \tag{1.5a}$$

$$\mathcal{D}\left[\{x_n(\cdot)\}\right] \equiv \prod_{n=1}^{N} \mathcal{D}\left[x_n(\cdot)\right]. \tag{1.5b}$$

If the polymers are indistinguishable, an additional Gibbs factor of $1/N!$ is owed in the partition function. To complete the definition of this multiple path integral we also need to impose some form of lateral boundary conditions on the polymer configurations; we return to this point in Chapter 2.

As for the thermal expectation value $\langle O\left[\{x_n(\cdot)\}\right]\rangle$ of a generic observable (i.e., a functional of the polymer configuration) $O\left[\{x_n(\cdot)\}\right]$, this is given by

$$\langle O\left[\{x_n(\cdot)\}\right]\rangle = Z[P^f, P^i]^{-1} \int d\{X_n^f\}\, P^f(\{X_n^f\})\, d\{X_n^i\}\, P^i(\{X_n^i\}) \times \int_{\{x_n(0)=X_n^i\}}^{\{x_n(L)=X_n^f\}} \mathcal{D}\left[\{x_n(\cdot)\}\right]\, \mathrm{e}^{-\beta U[\{x_i(\cdot)\}]}\, O\left[\{x_n(\tau)\}\right]. \tag{1.6}$$

For an observable that depends not on the behavior of the polymers across their entire length, but only at some position $\tau = \tau_p$, the observable may be written more simply as

$$\langle O(\{x_n\}, \tau_p)\rangle = \int d\{x_n\}\, O(\{x_n\})\, \Pr(\{x_n\}, \tau_p), \tag{1.7}$$

where, as we shall see, the probability $\Pr(\{x_n\}, \tau_p)$ that the polymers pass through positions $\{x_n\}$ at time τ_p will be independent of τ_p and the longitudinal boundary conditions, provided that τ_p is sufficiently far from the edges of the system.

As we have noted above and shall see below, owing to the low dimensionality of this thermally fluctuating polymer system, even short-range interactions produce qualitative alterations of the structure and correlations that it exhibits, relative to those exhibited by its noninteracting counterpart. Moreover, even interactions that are weak, microscopically, are fundamentally nonperturbative, in that they induce correlations that are long-ranged.

1.2 Physical systems described by directed lines in two dimensions

Because the model discussed in this introduction describes polymers confined to two dimensions, it applies most readily to polymers adsorbed on a surface or confined at an interface between two fluids. However, such two-dimensional models have also at times been applied to three-dimensional polymer systems. In particular, de Gennes' original free fermion model of fibrous polymers has been applied to the hydrocarbon chains of lipid bilayers [11]. Such chains, tens of angstroms in length, interact via an excluded volume effect.

Although our focus is on polymer systems, our treatment extends to other physical realizations of two-dimensional systems characterized by fluctuating linelike degrees of freedom, and it may find the most ready experimental realizations therein. We now briefly survey such systems.

1.2.1 Crystal surfaces

Consider wandering step edges on a miscut crystal surface such as Silicon(111). Such step edges have a preferred direction, an energetic cost to

wandering, and do not cross one another. They may thus be mapped onto a system of noncrossing polymer lines governed by an energy functional such as Eq. (1.3) and thence to free one-dimensional fermions via the techniques we shall describe. Indeed, such a mapping has been performed to elucidate the distribution of step widths [7]. The width of a crystalline terrace is then mapped onto the distance between two nearest-neighbor fermions. The effect of the thermal wandering, coupled with the noncrossing condition, is to increase the likelihood that any given step width is nearer to the average step width than would be the case for statistically independent (i.e., freely crossing) lines.

1.2.2 Vortex lines

The quantum analogy has also been applied to systems of flux-carrying vortex lines in superconductors. The lines are treated as purely classical objects having a preferred direction and a contact repulsion. The quantum technique of bosonization (see e.g., Giamarchi [12]) allows the system to be described via a continuous field, resembling an isotropic elastic medium, while still preserving the short-distance behavior of the vortex lines. Also present in such systems are columnar and point-like impurities, and pinning centers compete with the thermal fluctuations of the lines to produce a rich variety of phases [3, 4, 5, 6]. We shall discuss the application of bosonization to polymer systems in Chapter 7.

1.2.3 Kardar-Parisi-Zhang universality class

Consider now the classical problem of particles being deposited on an interface in one dimension. This dynamical process is described by the height $h(x,t)$ of the interface expressed as a function of position x and time t. The process is governed by the Kardar-Parisi-Zhang (KPZ) equation [13]

$$\frac{\partial h}{\partial t} = \nu\,\partial_x^2 h + \frac{\lambda}{2}\left(\partial_x h\right)^2 + \eta(x,t). \tag{1.8}$$

The first term on the right-hand side describes relaxation of the interface to a flat profile, e.g. from particles rearranging themselves to minimize surface

tension. The second term comes from the tendency of new particles to be deposited normal to the local orientation $(1, \partial_x h)$ of the interface, so that the steepest portions of the interface receive the most depositions per unit of lateral distance x. To be specific, the second term is the lowest-order nonconstant term in the expansion of the area element. The third term is a Gaussian random variable.

The KPZ equation was originally applied to, among other things, a directed polymer in two dimensions in a random medium [14, 15], a system closely related to interacting polymers in a uniform medium. More recently [8], the KPZ model has been related to one-dimensional bosonic systems, which we will relate to our directed polymer system.

CHAPTER 2

FROM CLASSICAL LINES TO QUANTUM PARTICLES

2.1 A quantum system

Let us turn now to the consideration of a one-dimensional quantum system of N nonrelativistic particles each of mass m and having coordinates $\{q_n\}_{n=1}^N$, subject to a one-body interaction $\Phi(q_n(t))$ and to a (translationally and parity invariant) two-body interaction $V(q_n - q_{n'})$. For this system, and introducing the (unsymmetrized) simultaneous particle-position eigenkets $|\{q_n^i\})$, a matrix element of the imaginary-time propagator $(\{X_n^f\}|\mathrm{e}^{-H\mathcal{T}/\hbar}|\{X_n^i\})$ can be expressed as the following Feynman integral over paths $\{q_n(t)\}$; (see, e.g.,Feynman [16]):

$$(\{X_n^f\}|\mathrm{e}^{-H\mathcal{T}/\hbar}|\{X_n^i\}) = \int_{\{q_n(0)=X_n^i\}}^{\{q_n(\mathcal{T})=X_n^f\}} \mathcal{D}\left[\{q_n(\cdot)\}\right]\, \mathrm{e}^{-S_E[\{q_n(\cdot)\}]/\hbar}, \tag{2.1}$$

where the Euclidean action S_E is given by

$$S_E = \int_0^{\mathcal{T}} dt \Big\{ \sum_{n=1}^N \frac{m}{2} \left(\partial_t q_n\right)^2 + \sum_{n=1}^N \Phi(q_n) + \sum_{1\le n<n'\le N} V\big(q_n(t) - q_{n'}(t)\big)\Big\}. \tag{2.2}$$

The "non-Lagrangian" sign of the interaction term in Eq. (2.2) and the terminology of the Euclidean action reflect the fact that we are considering imaginary-time propagation, in which the paths of the Feynman integral are referred to as imaginary-time world-lines. As usual, the propagator can be used to construct the transition amplitude between generic initial and final quantum states $|\Psi^i\rangle$ and $|\Psi^f\rangle$:

$$\langle\Psi^f|\mathrm{e}^{-H\mathcal{T}/\hbar}|\Psi^i\rangle = \int d\{X_n^f\}\, d\{X_n^i\}\, \langle\Psi^f|\{X_n^f\}) \times(\{X_n^f\}|\mathrm{e}^{-H\mathcal{T}/\hbar}|\{X_n^i\})(\{X_n^i\}|\Psi^i\rangle. \tag{2.3}$$

In order to relate this quantum-mechanical system to the classical polymer systems, we make the following identifications. We match the wave functions

with the probability distributions, i.e., we choose

$$(\{X_n\}|\Psi^i\rangle = P^i(\{X_n\}), \tag{2.4a}$$

$$(\{X_n\}|\Psi^f\rangle^* = P^f(\{X_n\}). \tag{2.4b}$$

Note that the identification is not between classical and quantal probability distributions but, rather, between classical probability distributions and quantal wave functions. Thus, to be appropriate, the wave functions should be restricted to being real, non-negative, and integrating to unity. The equivalence between the quantal and classical problems is completed by adding the following identifications:

$$\mathcal{T} = \hbar\beta, \tag{2.5a}$$

$$t = \mathcal{T}\tau/L, \tag{2.5b}$$

$$q_n(t) = x_n(\tau), \tag{2.5c}$$

$$m = \hbar^2\beta^2 A/L. \tag{2.5d}$$

In order to maintain the analogy to the polymer system, we refer to the 1D quantum system as having a *width* rather than a length, and denote the widths of both systems by w. Then we have a result that is central to this work, viz., that the quantal matrix element of the imaginary-time evolution operator is equal to the classical partition function of the polymer system:

$$\langle\Psi^f|\mathrm{e}^{-H\mathcal{T}/\hbar}|\Psi^i\rangle = Z[P^f, P^i]. \tag{2.6}$$

In particular, the imaginary-time worldlines of the quantum particles correspond to the configurations of the directed polymers, and the quantum fluctuations of the particle system (the strength of which is governed by $\hbar$) correspond to the thermal fluctuations of the polymer system (the strength of which is governed by $1/\beta$). Strictly speaking, the path integral is defined only up to a constant factor that depends on a short-distance cutoff. This factor does not affect the physics of the system at length scales above the scale of the cutoff. We will discuss this point and its physical consequences later in this Chapter.

In order to apply many of the techniques of QMB physics it is useful to impose a choice of quantum statistics upon the initial and final quantum

states $|\Psi^i\rangle$ and $|\Psi^f\rangle$. The condition that the initial and final wave functions $(\{X_n\}|\Psi^i\rangle$ and $(\{X_n\}|\Psi^f\rangle$ be non-negative, so that they may match the polymer end distributions, Eqs. (2.4), precludes the direct choice of fermionic statistics (although, as we shall see, such statistics can be applied indirectly, following a Jordan-Wigner–type transformation). Thus, we choose to consider situations in which the polymer endpoint distributions P^i and P^f are each symmetric functions—respectively under the exchange of initial endpoints amongst themselves and final endpoints amongst themselves—from which it follows that the initial and final quantum end states be symmetric under particle exchange, and hence that they describe identical *bosons*.

One valuable notion made accessible and sharpened via the tools of one-dimensional quantum many-body systems (such as bosonization, quantum hydrodynamics, and Bethe-Ansatz-rooted methods) is that of the *emergent directed-polymer liquid* (cf. Kafri et al. [17]). This state is a classical analog of the Luttinger-Tomonaga liquid, which can be exhibited by interacting QMB systems in one dimension, and is qualitatively distinct from, e.g., the Landau liquid state of many-fermion systems, i.e., a state that can be exhibited by such systems in higher dimensions. Thus, we shall see, e.g., that the manner in which density correlations decay spatially in the emergent directed-polymer liquid resembles the space-time decay of superfluid fluctuation correlations in one-dimensional interacting QMB systems.

2.2 Eigenfunction expansion of the imaginary-time propagator

Due to the association of polymer configurations with particle paths, discussed in the previous subsection, it is the path-integral (i.e., covariant) formulation of the quantization of the system that is the one most clearly associated with the physical degrees of freedom of the fluctuating polymer system. However, the quantum mechanics of the same particle system can also be formulated in terms of the time-dependent Schrödinger equation (i.e., via canonical quantization).

Consider the partition function of a thin longitudinal slice (in the quantum picture, a time slice) of the total polymer system, stretching from some $\tau = 0$ to $\tau = \ell$, subject to polymer coordinates $\{x_n^i\}$ and $\{x_n^f\}$ at the boundaries.

Over a sufficiently short slice, the tension energy in Eq. (1.3) will dominate the other terms, and the polymer configurations will be straight lines:

$$x_n(\tau) = x_n^i + \frac{\tau}{\ell}\left(x_n^f - x_n^i\right). \tag{2.7}$$

The tension energy of the configuration is then

$$\frac{A}{2}\sum_n \int_0^\ell d\tau \left(\partial_\tau x_n(\tau)\right)^2 = \frac{A}{2\ell}\sum_n \left(x_n^f - x_n^i\right)^2, \tag{2.8}$$

and the one-body term in the energy of the configuration is

$$\begin{aligned}\frac{1}{L}\int_0^\ell d\tau\, \Phi\left(x_n^i + \frac{\tau}{\ell}\left(x_n^f - x_n^i\right)\right) \\ \approx \frac{\ell}{L}\Phi(x_n^i) + \frac{\ell}{2L}\Phi'(x_n^i)\left(x_n^f - x_n^i\right) + \frac{\ell}{6L}\Phi''(x_n^i)\left(x_n^f - x_n^i\right)^2 + \ldots\end{aligned} \tag{2.9}$$

with a similar expression for the expansion of the two-body interaction $V(x_n(\tau) - x_{n'}(\tau))$. Provided that the length ℓ of our slice is sufficiently small, we may concern ourselves only with those configurations where $x_n^f - x_n^i$ is small, and so retain only the first term in the expansion. We retain the $O\left(x_n^f - x_n^i\right)^2$ term in the tension energy only because it includes the large prefactor ℓ^{-1}. Combining these terms, the partition function for this small longitudinal slice of the polymer system is

$$\exp\left[-\frac{\beta A}{2\ell}\sum_n \left(x_n^f - x_n^i\right)^2 - \beta\frac{\ell}{L}\sum_n \Phi(x_n^i) - \beta\frac{\ell}{L}\sum_{n<n'} V(x_n^i - x_{n'}^i)\right]. \tag{2.10}$$

We now wish to consider how such a partition function changes as one minutely varies either the length of the slice, ℓ, or the boundary conditions $\{x_n^f\}$. One may readily show that it obeys the differential equation

$$-\frac{\partial}{\partial \ell}\mathcal{Z}\left(\{x_n^i\},\{x_n^f\},\ell\right)\approx \tag{2.11}$$
$$\left[-\frac{1}{2A\beta}\sum_n \frac{\partial^2}{\partial (x_n^f)^2}+\sum_n \frac{\beta}{L}\Phi(x_n^i)+\sum_{n<n'}\frac{\beta}{L}V(x_n^i-x_{n'}^i)\right]\mathcal{Z}\left(\{x_n^i\},\{x_n^f\},\ell\right).$$

This is the equivalent of an imaginary-time Schrödinger equation, with the partition function serving the role of a Green's function describing the imaginary-time evolution between two quantum states. Thus, it is straightforward to ascertain that the propagator can be expressed in terms of the expansion

$$(\{x_n^f\}|\mathrm{e}^{-Ht/\hbar}|\{x_n^i\})\propto \sum\nolimits_k e^{-E_k t/\hbar}\,\psi_k(\{x_n^f\})\,\psi_k^*(\{x_n^i\}) \tag{2.12}$$

over the exact normalized eigenfunctions $\{\psi_k\}$ and corresponding energy eigenvalues $\{E_k\}$, with many-body quantum numbers k, of the associated many-body quantum Hamiltonian

$$H=\sum_{n=1}^{N}\frac{p_n^2}{2m}\quad+\sum_{n=1}^{N}\Phi\big(x_n(\tau)\big)+\sum_{1\le n<n'\le N}V(x_n-x_{n'}). \tag{2.13}$$

For a system of finite size, the eigenspectrum will consist of discrete energy levels $\{E_k\}$ with a finite ground-state energy. An important special case is made evident via this expansion. Suppose one is concerned with a statistical-mechanical expectation value involving polymer observables all taken at a single value of the longitudinal coordinate τ and, moreover, obeying $(t,\mathcal{T}-t)\gg\hbar/\Delta E$, where ΔE is the spacing between the ground many-body state $|\psi_{gs}\rangle$ of the QMB system and its first excited state. The wave functions ψ_k decay over longitudinal length scales $L/\beta E_k$, so that for a sufficiently long system it can be adequate to retain only the ground state in the eigenfunction expansion, i.e., to take

$$\mathrm{e}^{-Ht/\hbar}=\sum\nolimits_k |\psi_k\rangle\,\mathrm{e}^{-E_k t/\hbar}\,\langle\psi_k|\approx|\psi_{gs}\rangle\,\mathrm{e}^{-E_{gs}t/\hbar}\,\langle\psi_{gs}|, \tag{2.14}$$

a situation referred to as ground-state dominance. In particular, within the ground-state dominance approximation and far from the system ends, the

equilibrium expectation value of the polymer density

$$\Big\langle \sum_n \delta\big(x - x_n(\tau)\big)\Big\rangle \tag{2.15}$$

is given, as a function of lateral position x, by the quantum-mechanical ground-state expectation value of the density operator $\sum_n \delta(x-\hat{q}_n)$, a result that holds regardless of the longitudinal boundary conditions on the polymer configurations. Thus, properties deep in the longitudinal interior of a long system (i.e., one for which $\mathcal{T} \gg \hbar/\Delta E$) are associated with the ground-state properties of the quantum system.

Much can be said about the ground state of the general Hamiltonian in Eq. (2.14) (see argument by Feynman [16], Chapter 11). Our choice of boundary conditions ensures that we need consider only bosonic wave functions. Clearly, such a wave function can be chosen to be real: if ψ is an eigenstate of the Hamiltonian, then so are its real and imaginary parts, at least one of which must be nonzero. Furthermore, the ground state must not generally have any nodes. Consider a point $x = x^*$ at which the wave function did pass from positive to negative (keeping the other coordinates $\{x_i\}$ at some fixed values). In such a case the absolute value of the wave function would have the same energy, with a kink at $x = x^*$. But smoothing out said kink could lower the kinetic energy while only negligibly increasing the potential and interaction energies. Thus could the energy expectation be lowered, indicating that ψ was not a true ground state. The exception to this is when smoothing out the kink would necessarily have a high energy cost— that is, when the potential or interaction energies diverged at some set of coordinates. For example, an infinite contact repulsion can and will cause the wave function to vanish whenever two particle coordinates coincide. Nevertheless, the wave function must be taken to be positive on either side of this crossing, to ensure Bose symmetry. Thus, we find that the groundstate wave function is strictly real and nonnegative, an important requirement that permits its association with a probability distribution in Eq. (2.4). We also find that for polymers in the interior of a system (where the groundstate approximation is appropriate) any set of polymer coordinates $\{x_i\}$ has finite probability of occurring so long as such a configuration has finite energy.

2.3 Noncrossing polymers

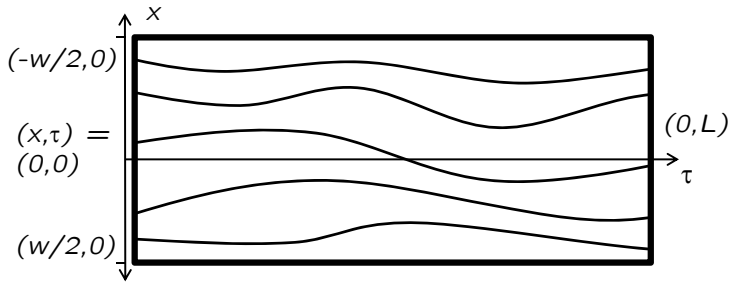

Figure 2.1: Snapshot of a configuration for the case of noncrossing polymers. Such polymers are not permitted to cross one another, but are otherwise noninteracting. From Rocklin et al. [2].

Our focus is on systems comprising strictly *noncrossing* polymers. Such systems do not adopt configurations in which any polymer crosses any other but, beyond this important element, they are not subject to any polymer-polymer interactions; see Fig. 2.1. As we shall see in later chapters, QMB physics techniques enable the study of polymer systems having a wide range of interactions; we shall show there that in the presence of such interactions many of the results obtained in this chapter and the next will continue to hold, at least qualitatively. To enforce noncrossing, the polymers are taken to feature an infinitely strong excluded-volume effect, so that the partition function contains only those paths for which $x_n(\tau) \neq x_{n'}(\tau)$ for all $n \neq n'$. This restriction can be enforced for the polymer system via the inclusion of the interaction term

$$V\big(x_n(\tau) - x_{n'}(\tau)\big) = c\,\delta\big(x_n(\tau) - x_{n'}(\tau)\big), \tag{2.16}$$

with $c/LA \to \infty$. The corresponding quantum system can therefore be taken to comprise many identical particles, bosonic in their quantum statistics and subject to an interparticle interaction having the same form. This system is known as the hard-core (or impenetrable) point-like boson model. (A finitely strong interpolymer repulsion corresponds to a quantum Lieb-Liniger system [18], as will be discussed in Chapter 5.) We mention that, despite its short range, this interaction is strong, and we may therefore expect the qualitative behavior of noncrossing polymer systems to be replicated in systems having more general interactions.

2.3.1 From bosons to fermions

It was demonstrated by Girardeau [19] that any system of interacting, one-dimensional, bosonic particles for which the wave functions vanish when pairs of particles coincide in space can be mapped to an equivalent system of fermionic particles, subject to the same interaction $V(x_i - x_j)$ whenever $x_i \neq x_j$. Girardeau's mapping is particularly useful in the case of hard-core boson systems, as these can be mapped to systems of *free* fermions. Thus, as first noted and exploited by de Gennes [1], the noncrossing condition on polymers can be accounted for entirely by the quantum statistics of fermions, without the need to include any interaction term. We mention that Girardeau's mapping preserves the modulus of the quantum wave function in the *position* basis; however, the forms of the bosonic and fermionic momentum-space wave functions are not preserved. This means that the local density of polymers is correctly described under the mapping but, e.g., quantities involving the slopes of polymer configurations—the analogs of the momenta of the quantum particles—are not. De Gennes applied this free fermion picture of two-dimensional noncrossing fibrous polymers to describe the structure of such systems. In particular, he showed that there is a logarithmic divergence in the "x-ray form factor" (i.e., the longitudinally-averaged correlator between lateral Fourier components of the density fluctuations of the polymer system), at a length scale associated with the Fermi momentum of the quantum system (or, equivalently, the mean lateral inter-polymer spacing).

2.3.2 Fermi statistics from the method of images

When de Gennes first mapped noncrossing lines onto fermion worldlines [1], he did not first map them onto interacting bosons. Rather, he relied upon physical insights similar to those developed by Michael Fisher [9] to describe the paths of "vicious drunks"— i.e., paths of antisocial individuals who wander randomly, with the requirement that their paths never cross. Consider first of all a single random walker, traveling from the point $(x_i, 0)$ to the point (x_f, L), with both x-coordinates positive. In the absence of any interactions or potentials, we have an unnormalized (normalization will be discussed later in this chapter) partition function

$$\mathcal{Z}_0(x_i \to x_f) \sim \exp\left[-\frac{A\beta}{2L}\left(x_f - x_i\right)^2\right]. \tag{2.17}$$

Now suppose we have a wall located at $x = 0$, so that only paths where $x(\tau) > 0$ may be included in the partition function. We wish then to subtract from our partition function any paths which cross the line $x = 0$ at least once. We do this by including an "image" destination at $(-x_f, L)$.

Consider any path between x_i and x_f that crosses $x = 0$ at least once and let $(0, \tau^*)$ be the position at which it first does so. Then, the mapping

$$x(\tau) \to x(\tau)\theta(\tau^* - \tau) - x(\tau)\theta(\tau - \tau^*) \tag{2.18}$$

takes it uniquely to a path between $(x_i, 0)$ and $(-x_f, L)$ with *the same* Boltzmann weight (a kink introduced at τ^* does not contribute significant additional cost). Here, $\theta(\cdot)$ is the usual Heaviside step function, which takes the values 0 and 1, respectively, for negative and positive arguments. Alternatively, one can map in the same way *any* path between $(x_i, 0)$ and $(-x_f, L)$ (which will by necessity cross $x = 0$ at least once) onto one of the paths between $(x_i, 0)$ and (x_f, L) which is forbidden by the condition $x(\tau) > 0$. Thus, there is a one-to-one correspondence between the paths disallowed by the wall at $x = 0$ and paths of an unconstrained polymer between $(x_i, 0)$ and $(-x_f, L)$. Thus, the partition function of the polymer constrained by the wall may be obtained by subtracting off paths to this image destination:

$$\mathcal{Z}_c(x_i \to x_f) \sim \mathcal{Z}_0(x_i \to x_f) - \mathcal{Z}_0(x_i \to -x_f), \tag{2.19}$$

where $\mathcal{Z}_c$ and $\mathcal{Z}_0$ denote partition functions of polymer systems with and without the condition $x(\tau) > 0$. Here it is understood that the partition function is zero if $x_f < 0$, as there are then no valid paths.

Now, rather than a single polymer line and a static wall, we may consider two fluctuating polymer lines that may not cross one another. Again, we wish to eliminate from the ensemble any paths where the two polymer lines touch. Again, this can be done via the method of images:

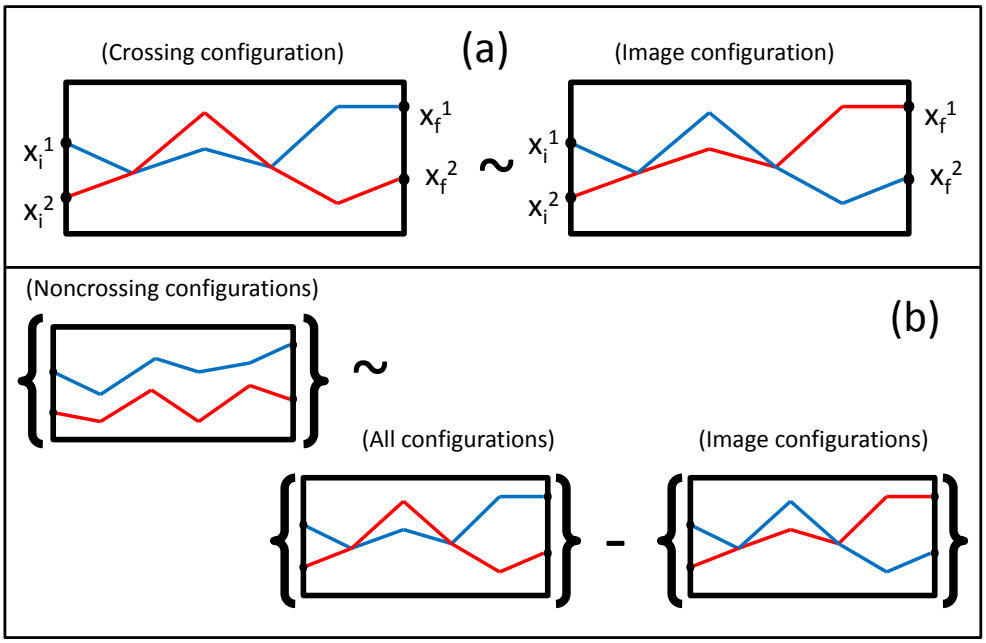

Figure 2.2: Part (a) shows on the left a generic polymer configuration where two polymers cross. On the right, the paths of the polymers have been exchanged everywhere after the first crossing. This new configuration has the polymer endpoints exchanged, but has the same Boltzmann weight as the original path. Polymer configurations which have at least one crossing have a one-to-one correspondence in this way with equal-weight configurations with exchanged boundary conditions. Thus, as indicated in Part (b), the total weight of all noncrossing polymer configurations is equal to the weight of all polymer configurations (crossing and noncrossing) minus the weight of all polymer configurations subject to exchanged boundary conditions. For N polymers, one generates the weight of the noncrossing configurations by summing over the $N!$ permutations of the boundary conditions, adding or subtracting depending on the sign of the permutation.

$$\mathcal{Z}_c\left((x_i^1, x_i^2) \to (x_f^1, x_f^2)\right) \sim \mathcal{Z}_0\left((x_i^1, x_i^2) \to (x_f^1, x_f^2)\right) - \mathcal{Z}_0\left((x_i^1, x_i^2) \to (x_f^2, x_f^1)\right). \tag{2.20}$$

Here, the paths in the second partition function are

$$(x_1(\tau), x_2(\tau)) \to (x_1(\tau), x_2(\tau))\theta(\tau^* - \tau) - (x_2(\tau), x_1(\tau))\theta(\tau - \tau^*). \tag{2.21}$$

Note that such paths have the same Boltzmann weight even in the presence of interactions and potentials, provided that these are symmetric under the exchange of polymers.

One can continue this procedure for N polymers, so that the partition function for N polymer lines which are not allowed to cross is

$$\mathcal{Z}_c\left(\{x_i\} \to \{x_f\}\right) \sim \sum_P (-1)^P \mathcal{Z}_0\left(x_i \to P(\{x_f\})\right), \tag{2.22}$$

where $P(\{x_f\})$ is any permutation on the N endpoints $\{x_f\}$. Thus, we can enforce the noncrossing condition automatically by considering polymer configurations *without* the noncrossing condition but *with* antisymmetrized boundary conditions in Eq. (1.4). As noted in Eq. (2.4), the boundary conditions correspond to a quantum wave function (not its squared modulus), so in the quantum picture we enforce noncrossing precisely by antisymmetrizing the wave function (i.e., choosing a fermionic wave function). As we will see in Chapter 8, for polymers in $(2+1)$ dimensions the nonintersecting condition may be enforced by a different set of quantum statistics in higher dimensions.

2.4 Ground state and ground-state dominance

As noted earlier in this chapter, the ground state of the quantum Hamiltonian plays a key role in the behavior of the polymer system over long distances. In order to make use of this idea, we now obtain the ground-state wave function for the many-hard-core boson system, subject to hard-wall boundary conditions, in a form that is convenient for the subsequent analysis. To do this, we begin with the ground-state wave function $\psi^p_{gs}(\{x_n\})$ of a system of N hard-core bosons on a ring of circumference w, subject to *periodic* (rather than hard-wall) boundary conditions (see e.g. [19]); this is given by

$$\psi^p_{gs}(\{x_n\}) = \frac{2^{N(N-1)/2}}{w^{N/2}\sqrt{N!}} \prod_{1 \le n < n' \le N} \left| \sin \frac{\pi}{w}\big(x_n - x_{n'}\big) \right|. \tag{2.23}$$

Such boundary conditions are appropriate for a system of polymers that lie on a cylindrical surface and are directed along the cylinder axis. Our aim, however, is to consider a system of polymers that are confined to a strip with

hard-wall boundary conditions, and this system corresponds to a quantum system also subject to hard-wall boundary conditions. To that end, we give the groundstate wave function of a system of N bosons subject to vanishing boundary conditions at $x_n = \pm w/2$ (see Appendix A):

$$\psi_{gs}(\{x_n\}) = \frac{2^{N^2/2}}{w^{N/2}\sqrt{N!}} \left(\prod_{n=1}^{N} \cos \frac{\pi x_n}{w} \right) \prod_{1 \le n < n' \le N} \left| \sin \frac{\pi x_n}{w} - \sin \frac{\pi x_{n'}}{w} \right|. \quad (2.24)$$

The wave function ψ_{gs} reflects the inter-polymer repulsion. Although the corresponding polymers are forbidden energetically only from actually intersecting one another, continuity and thermal fluctuations have the combined effect of "carving out" a spatial region around the polymers so that the probability of finding one polymer very near another (compared with the mean inter-polymer spacing w/N) vanishes as the square of the separation. A similar effect occurs near the hard boundaries, i.e., at $x = \pm w/2$. The preceding results pertain to infinitely strong contact interactions. However, as is known from the work of Lieb and Liniger [18], the physical properties of a system of bosons subject even to *weak* contact interactions differ nonperturbatively from those of a system of free bosons.

Whereas the lateral *correlations* amongst the polymer segments depend additionally on the quantum-mechanical energy eigenfunctions, the thermodynamic properties of the polymer system are determined solely by the spectrum of energy eigenvalues. The ground-state energy and energy spacing to the first excited state of the quantum system are, respectively, given by

$$E_{gs} = \frac{\pi^2}{6} \frac{\hbar^2}{m w^2} N^3 = \frac{\pi^2}{6} \frac{L}{w^2 \beta^2 A} N^3, \quad (2.25a)$$

$$\Delta E = \pi^2 \frac{\hbar^2}{m w^2} N = \pi^2 \frac{L}{w^2 \beta^2 A} N \quad (2.25b)$$

for $N \gg 1$. The partition function of a long system is dominated by the term $\exp(-E_{gs}\mathcal{T}/\hbar)$.

Thus, the free energy density of a long system of noncrossing polymers is given, to leading order, by

$$\frac{\mathcal{F}}{wL} = \frac{\pi^2}{6} \left(\frac{N}{w} \right)^3 \frac{1}{\beta^2 A}. \quad (2.26)$$

This is the free energy cost density of imposing the noncrossing condition. This condition essentially restricts each polymer to a region of width of order w/N, leading to a strong reduction in entropy and therefore an increase in free energy. Even a weak inter-polymer repulsion would suffice to generate a free energy proportional to N^3 rather than N.
We conclude this section on ground state dominance by remarking that the length scale over which the ground-state dominance approximation holds is $\tau \gg L/\beta\Delta E$, or

$$\tau \gg \frac{w^2 \beta A}{N}. \tag{2.27}$$

2.5 Short-distance behavior of the polymer system

The polymer partition functions that we consider in this work contain certain pathologies that must be controlled via a short-distance regularization. Consider the partition function for a single polymer not subject to interactions or external potential, which formally reads

$$\mathcal{Z} = \int \mathcal{D}x(\cdot) \exp\left(-\frac{A\beta}{2}\int d\tau\, \dot{x}^2(\tau)\right). \tag{2.28}$$

To make sense of this object, let us divide the longitudinal coordinate into $M+1$ discrete sections, so that

$$\mathcal{Z}_{(M)} = \int d\{x_m\} \exp\left(-\frac{A\beta}{2}\sum_{m=0}^{M}\frac{M}{L}\left(x_m - x_{m-1}\right)^2\right) \tag{2.29}$$

Note that, here, the $\{x_m\}$ are the coordinates of longitudinally separated segments of a single polymer, rather than the $\{x_n\}$ considered elsewhere in this work which are laterally separated segments of N different polymers along the line $\tau = \tau_p$. Proceeding in the manner of time-slicing for a quantum path integral (see, e.g., Kleinert [20], Feynman and Hibbs [21]), one may make use of the following mathematical relationship to eliminate the interior degrees of freedom:

$$\int_{-\infty}^{\infty} dy \, \exp\left(-C\left[(x-y)^2+(y-z)^2\right]\right) = \sqrt{\frac{\pi}{2C}} \exp\left(-\frac{C}{2}\left[x-z\right]^2\right) \quad (2.30)$$

By using this relationship, we see that the partition function for a single polymer line that travels from x_0 to x_f and has $M-1$ interior segments is

$$\mathcal{Z}_{(M)} = \frac{1}{\sqrt{M!}} \left(\frac{2\pi L}{A\beta M}\right)^{(M-1)/2} \exp\left(-\frac{A\beta}{2L}\left[x_f - x_0\right]^2\right). \quad (2.31)$$

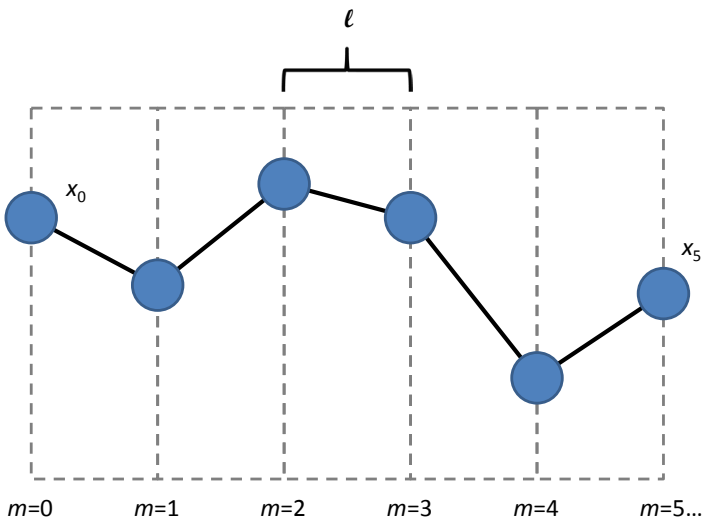

Figure 2.3: A configuration of the first five primitive segments of a single polymer. Although the polymer configurations over longer distances do not depend on the primitive segment length ℓ, the root mean squared polymer slope is proportional to ℓ^{-1}.

We see thus that the free polymer fluctuates with a Gaussian distribution that does not depend on the number of internal segments. The polymer structure over long distances will not depend on this short-distance behavior.

However, this does not mean that the short-distance behavior can be ignored entirely in the determination of thermodynamic properties of the polymer fluid. Let us define the short-distance portion of the partition function for N polymers with a short-distance cutoff $\ell \equiv L/M$. Then, the portion of the partition function dealing with the short-distance behavior is

$$\mathcal{Z}_\ell \equiv \left(\frac{2\pi\ell}{A\beta}\right)^{NL/2\ell}. \tag{2.32}$$

This factor is not connected to the structure of the polymer lines $\{x_n(\tau)\}$ over distances long compared to ℓ, but it does influence thermodynamic observables that depend on temperature or the tension parameter. For example, the mean squared deflection $\langle \dot{x}(\tau)^2 \rangle$ of a free long polymer line is given by

$$\langle \dot{x}(\tau)^2 \rangle = -\frac{2}{\beta LN} \partial_A \ln \mathcal{Z} = \frac{1}{A\beta\ell}. \tag{2.33}$$

Thus, if we try to take $\ell \to 0$ we find that short-distance polymer deflections diverge. That is, the closer we examine an ideal polymer line within our model, the steeper its slope seems to be. More generally, the short-distance behavior of polymers encoded in the short-distance portion of the partition function $\mathcal{Z}_\ell$ will depend on polymer interactions $V(x_n - x'_n)$ and on one-body potentials $\Phi(x_n)$, and it is this prefactor that must be inserted to make the eigenfunction expansion of Eq. (2.12) an equality:

$$\begin{aligned} \mathcal{Z} &= \mathcal{Z}_\ell \left(\{x_n^f\}|\mathrm{e}^{-Ht/\hbar}|\{x_n^i\}\right) \\ &= \mathcal{Z}_\ell \sum\nolimits_k e^{-E_k t/\hbar}\, \psi_k(\{x_n^f\})\, \psi_k^*(\{x_n^i\}). \end{aligned} \tag{2.34}$$

Now incorporating the noncrossing condition through the use of the fermionic wave functions as discussed earlier in this chapter, we have a mean squared polymer deflection

$$\langle \dot{x}(\tau)^2 \rangle = -\frac{2}{\beta LN} \partial_A \ln \left[\mathcal{Z}_\ell \exp\left(-E_{gs}\mathcal{T}\right)\right] = \frac{1}{A\beta\ell} - \frac{\pi^2}{3}\left(\frac{N}{w}\right)^2 \left(\frac{1}{\beta A}\right)^2. \tag{2.35}$$

It is this expression that must be small in order to justify the form of the tension energy in Eq. (1.3).

Without taking the short-distance behavior into account, we would have

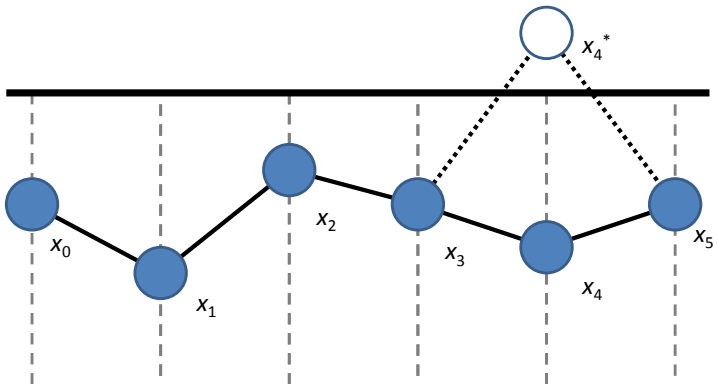

Figure 2.4: A configuration of the first five primitive segments of a single polymer near to the hard wall of its container. Because polymer segments cannot cross this wall, a configuration that includes x_4^* is not permitted, whereas x_4 is. Note that the configurations eliminated by the wall have on average greater polymer deflections than those permitted, so the wall decreases, e.g., $\langle (x_3 - x_4)^2 \rangle$ and therefore decreases the average slope of polymer lines in its vicinity. Similarly, noncrossing polymers decrease the average slopes of their neighbors (and see their own average slopes reduced in turn). Even polymers with a finite contact interaction see this effect, with configurations with steep slopes crossing more neighbors and thus suffering a finite energetic penalty.

only the second term on the right-hand side of Eq. (2.35) and thus suppose that the noncrossing condition led to *negative* polymer tension energy, an impossibility. In fact, the noncrossing condition merely decreases the average polymer slope (as do hard walls). This is because the polymer configurations eliminated (or energetically discouraged, for finite contact interactions) tend to be the ones having the greatest slopes; see Fig. 2.3.

Let us return to the partition function originally obtained for the system of noncrossing polymers (i.e., the one not including the short-distance behavior, which led to the free energy density obtained in Eq. (2.26)):

$$\mathcal{Z} \approx \exp(-E_{gs}\mathcal{T}) = \exp\left(-\frac{\pi^2}{6} N^3 L \frac{1}{\beta A} \frac{1}{w^2}\right). \tag{2.36}$$

We can now interpret this expression for the partition function either as the fraction of total polymer configurations (weighted by their Boltzmann factors) that are noncrossing or as the probability that a system of non-interacting polymers would spontaneously assume a configuration in which

no polymer line crossed another. As one would expect, this probability becomes exponentially small as either the length of the system, the density of polymers, the temperature, or the number of polymers is increased.

CHAPTER 3

LARGE FLUCTUATIONS AND STRONG CONSTRAINTS IN THE POLYMER SYSTEM

3.1 Introduction to large fluctuations

We turn our attention now to a series of related questions central to this work. Consider a line $\tau = \tau_p$ deep in the interior of the system. Denote the positions at which the N polymers cross this line as $\{x_n\}$. Let $\mathcal{C}$ denote some constrained class of these positions $\{x_n\}$. For example, $\mathcal{C}$ might denote configurations where all polymers crossed the line $\tau = \tau_p$ on the left side of the system ($x_n < 0$) or the configurations where, on this line, no polymer came within some distance a of another ($|x_n - x_{n'}| > a$). We will focus on constraints that are *strong* in the sense that any polymer configuration consistent with them is exponentially less likely than the dominant polymer configuration (i.e., an almost uniform polymer density) of the unconstrained system.

For any constraint $\mathcal{C}$, we may ask: what is the free energy cost of imposing the constraint $\mathcal{C}$ on the polymer system? Equivalently, we may ask: what is the probability that an unconstrained system will assume spontaneously a configuration consistent with $\mathcal{C}$? In either case, we may ask: when the polymer system obeys the constraints embodied in $\mathcal{C}$ what is the polymer structure on and around the line $\tau = \tau_p$?

Let us begin by constructing the partition function of a polymer system confined to pass exactly through some set of coordinates $\{x_n\}$ on the line $\tau = \tau_p$:

$$\mathcal{Z}(\{x_n\}) = \langle \Psi_f | \mathrm{e}^{-H(\mathcal{T}-t_p)/\hbar} | \{x_n\} \rangle \langle \{x_n\} | \mathrm{e}^{-Ht_p/\hbar} | \Psi_i \rangle. \tag{3.1}$$

Making the ground-state approximation in describing the evolution from $t = 0$ to $t = t_p$ and from $t = t_p$ to $t = \mathcal{T}$, one obtains

$$\mathcal{Z}(\{x_n\}) \approx \langle \Psi_f | \Psi_{gs} \rangle \langle \Psi_{gs} | \Psi_i \rangle \mathrm{e}^{-\mathcal{T}E_{gs}/\hbar} \left| \langle \Psi_{gs} | \{x_n\} \rangle \right|^2. \tag{3.2}$$

We recognize the first portion of this partition function as the partition function pertaining to the unconstrained polymer system. We may then write a partition function for the polymer segments on the line $\tau = \tau_p$ as separate from the bulk of the polymers:

$$\mathcal{Z}(\{x_n\}) = \int d\{x_n\} \left|\langle\{x_n\}|\Psi_{gs}\rangle\right|^2. \tag{3.3}$$

We may use this partition function to determine the probability that the coordinates $\{x_n\}$ satisfy the constraint. Equivalently, we may construct the partition function of the constrained system:

$$\mathcal{Z}_{\mathcal{C}} = \int_{\mathcal{C}} d\{x_n\} \left|\langle\{x_n\}|\Psi_{gs}\rangle\right|^2. \tag{3.4}$$

Here, the integration is only over those coordinates $\{x_n\}$ consistent with the constraint $\mathcal{C}$. The normalization of the groundstate wave function ensures that the unconstrained partition function is unity and that the constrained partition function gives the probability that the constraint is obeyed spontaneously.

We may interpret our system now as describing a one-dimensional classical system of particles subject to some interaction and external potential. Then, we may write our partition function as

$$\mathcal{Z}_{\mathcal{C}} = \int d\{x_n\} \, \exp\left(-\beta U(\{x_n\})\right); \tag{3.5}$$

$$\beta U(\{x_n\}) = -\ln\left|\langle\Psi_{gs}|\{x_n\}\rangle\right|^2. \tag{3.6}$$

Let us consider systems whose quantum wave functions are of a modified product form, so that the effective energy of a configuration takes the form

$$\beta U(\{x_n\}) = \sum_n f(x_n) + \sum_{n<n'} g(x_n, x_{n'}). \tag{3.7}$$

This form is sufficiently general that it includes polymers which are non-interacting, noncrossing, or subject to long-range interactions [22]. It also encompasses a wide variety of lateral boundary conditions: periodic (for which $f(\cdot)$ is constant and $g(\cdot,\cdot)$ depends only on the relative coordinate), hard-wall, and a confining harmonic potential.

Note that the effective potential and interaction *are not* the bare potential

or interaction of the actual polymer lines as given in Eq. (1.3). Consider for example the wave function of noncrossing polymers subject to hard walls at $x = \pm w/2$ from Eq. (2.24). The effective potential is

$$f(x) = -2 \ln \left(\cos \frac{\pi x}{w} \right), \tag{3.8}$$

and the effective interaction is

$$g(x, x') = -2 \ln \left| \sin \frac{\pi x}{w} - \sin \frac{\pi x'}{w} \right|. \tag{3.9}$$

Rather than polymers which experience a uniform potential on $-w/2 < x(\tau) < w/2$, we see a particle system which has a unique potential minimum at $x = 0$ and actually diverges as x approaches the walls. This is from the bulk of the polymers, which we have integrated out. Ignoring for the moment interactions, the partition function is proportionate to the number of polymer configurations (with their Boltzmann weights) which pass from $\tau = 0$ to $\tau = L$ without violating the constraint $-w/2 < x(\tau) < w/2$. And indeed, this number is greatest for those paths which obey $x(\tau_p) = 0$ (this follows simply from the fact that $x = 0$ is the most likely place to find the polymer). The number of allowed configurations becomes vanishingly small as $x(\tau_p)$ is brought to either wall due to the large number of nearby polymer segments at $x(\tau_p \pm \ell), x(\tau_p \pm 2\ell), \ldots$ that would be confined by the wall. Taking into account the finite short-distance cutoff ℓ would lead to an ℓ-dependent finite value for $f(\pm w/2)$.

Similarly, the contact repulsion embodied in the noncrossing condition becomes a long-range repulsion. The closer two particles at x and x' are brought to each other, the more likely it is that the corresponding polymers would encounter one another at some "earlier" or "later" τ. For polymer systems whose quantum wave functions vanish as a power law as two coordinates are brought close to one another, the effective interaction $g(\cdot, \cdot)$ is logarithmic repulsion at short ranges. This is the same as a two-dimensional Coulomb interaction between particles of like charge (though recall that our particles are confined to a one-dimensional line, not the two-dimensional plane). For this reason, we refer generally to the classical system subject to potentials and

interactions of the form given in Eq. (3.7) as having *charge*. This does not indicate, of course, that the polymers themselves necessarily have an electrical charge, any more than the quantum picture indicates that the polymers behave nonclassically.

This form permits us to determine any number of statistical observables provided that they are confined to some line $\tau = \tau_p$. For example, the free fermion wave function may be used to determine the terrace width distribution [7], that is the probability that two nearest neighbor lines x_n and x_{n+1} are separated by a given width. However, we shall focus on large fluctuations and strong constraints.

3.2 Large numbers of polymers

For systems of only a few polymers, one may evaluate the integrals in Eq. (3.4) directly. We are interested in the opposite limit, in which the number of polymers is sufficiently large that their distribution resembles a continuous density. To this end, we may write the partition function of our effective 1D classical system as

$$\mathcal{Z}_{\mathcal{C}} = \int \mathcal{D}\rho(\cdot) d\{x_n\}\, \hat{\delta}\left[N\rho(x) - \sum_n \delta(x - x_n)\right] \exp\left(-\beta U_0\left[\rho(\cdot)\right]\right);$$
$$\beta U_0\left[\rho(\cdot)\right] = \int dx N\rho(x) f(x) + (N^2/2)\int dx dx' \rho(x) g(x,x') \rho(x'), \quad (3.10)$$

where $\hat{\delta}\left[\cdot\right]$ is the functional version of the Dirac delta function. Performing the functional integration in $\rho(\cdot)$ would exactly recover our original partition function in terms of the individual particle coordinates. Instead, we make use of the Fourier representation of a Dirac delta function and introduce an auxiliary field $K(\cdot)$ so that

$$\hat{\delta}\left(N\rho(x) - \sum_n \delta(x - x_n)\right) \quad (3.11)$$
$$\sim \int \mathcal{D}K(\cdot) \exp(i \int dx K(x) \left(N\rho(x) - \sum_n \delta(x - x_n)\right).$$

With this transformation, the partition function becomes

$$\mathcal{Z}_{\mathcal{C}} = \int \mathcal{D}\rho(\cdot)\mathcal{D}K(\cdot) \left(\int dx e^{-iK(x)} \right)^N \times \exp\left(iN \int dx K(x)\rho(x) - \beta U_0 \left[\rho(\cdot)\right] \right). \quad (3.12)$$

Until now, our introduction of the auxiliary field has been exact. Now, we make a saddlepoint approximation in $K(\cdot)$ and retain only the configuration which satisfies the first-order conditions. This approximation is best when the number of particles is large, so that the set of particle coordinates most closely resembles a continuous density distribution. The saddlepoint approximation yields

$$\rho(x) = \frac{e^{-iK(x)}}{\int dx e^{-iK(x)}}. \quad (3.13)$$

Using this relationship to eliminate $K(x)$, one obtains the effective potential energy of the continuous density distribution:

$$\beta U\left[\rho(\cdot)\right] = \int dx \left[N\rho(x)\ln\rho(x) + N\rho(x)f(x)\right] + (N^2/2)\int dx dx' \rho(x)g(x,x')\rho(x'). \quad (3.14)$$

The first term arises in the method of collective coordinate [23]. It is essentially a statistical degeneracy factor [24], appropriate when we consider length scales such that the number of polymers in any region is large. Additionally, our definition of the density profile (enforced by the Dirac delta function) introduces the additional requirements

$$\rho(x) \geq 0, \quad (3.15)$$

$$\int dx\, \rho(x) = 1. \quad (3.16)$$

As before, the interaction $g(\cdot,\cdot)$ suggests a Coulomb-type repulsion, but now one that acts on a continuous fluid. For this reason, we refer to the energy

functional in Eq. (3.14) subject to the requirements in Eq. (3.15) as *the charged fluid model*. This model also describes the statistics of the eigenvalues of certain ensembles of random matrices, as discussed in Appendix B.

3.3 Introduction of a constraint

We now wish to impose some additional constraint $\mathcal{C}$ on the density profile $\rho(\cdot)$ inherited from the constraint on the original particle coordinates. To this end, we include an additional source term $-Ns(x)\rho(x)$. The factors of N in the exponent suggest that we may treat this functional integral via the functional version of Laplace's method, and therefore via finding the maximum of the leading term of the exponent. Retaining only the dominant contribution (that from interpolymer interactions), the first-order conditions thus obtained are

$$N \int dx' g(x, x')\rho(x') = s(x). \tag{3.17}$$

For a clean polymer system without any constraint or varying potential, $s(x)$ is merely a constant, an effective chemical potential used to fix the number of polymers. Alternatively, $s(x)$ can represent a continuous potential that acts on the polymers only on the line $\tau = \tau_p$. However, as we will discuss more fully in the next chapter, $s(x)$ can be chosen to represent a topological constraint on the polymers. If certain polymers are required to pass through certain portions of the line $\tau = \tau_p$, then even in the absence of a true potential $s(x)$ can assume different values on the different portions of the $\tau = \tau_p$ into which the topological constraint partitions the system. The different values $s(x)$ serve as Lagrange multipliers that fix the number of polymers passing through each region.

3.4 Enforcing positive polymer density

There is no guarantee that the solution of this integral equation in Eq. (3.17) will obey the positivity required of the density profile. How do we reconcile the positivity condition with the first-order conditions?

Let us briefly consider some separate well-behaved function $B(\{z_i\})$ by means of example. We wish to maximize this function over the variables $\{z_i\}$ subject to the constraint that all z_i are nonnegative. Thus, basic calculus tells us that at the point $\{z_i^*\}$ that maximizes $B(\cdot)$ (if such a point exists) *either* $\partial B/\partial z_i = 0$ *or* $z_i = 0$ for all z_i. The functional equivalent applicable to our system is simply this: for any x *either* the first-order conditions of Eq. (3.17) are obeyed *or* the constraint $\rho(x) \geq 0$ is satisfied with equality (i.e., $\rho(x) = 0$).

So, we may proceed thusly: First, we shall simply attempt to satisfy the first-order conditions on $\rho(\cdot)$, while ignoring the positivity requirement. As we will see, though, this can result in density profiles that violate positivity. If this occurs, we will assume that the true profile that minimizes energy subject to positivity includes at least one *gap*, a region of finite width in which polymer density is zero. We then go back to our first-order conditions and *assume* the existence of a gap, and exclude this region from the integration in Eq. (3.17). If this results in a profile which satisfies positivity we may adjust the size and width of the gap so as to minimize the energy of the configuration. If this second set of profiles also violates positivity, then we must include assume the existence of at least two separate gaps, and continue in this fashion until positivity is eventually achieved. We will discuss this procedure in more detail for the particular case of the *pin*, discussed in the next chapter.

CHAPTER 4

TOPOLOGICAL PINS CONSTRAINING THE POLYMER SYSTEM

4.1 Constraints on the partition function due to a single pin

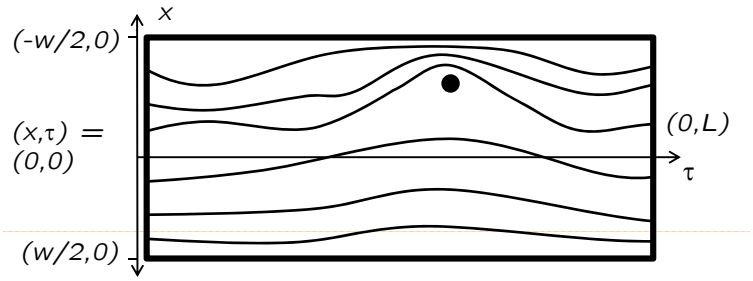

Figure 4.1: A topological obstruction (a *pin*), located at $(x, \tau) = (x_p, \tau_p)$. Thermal fluctuations cannot carry a polymer across this pin, so a fixed number of polymers N_L pass to one side of the pin, and the remainder $N_R \equiv N - N_L$ pass to the other side. From Rocklin et al. [2].

In the previous chapter, we considered a generic polymer system subject to a generic constraint. We now specialize to the concrete example of a system of noncrossing polymers subject to a *pin*. As we shall see, the pin renders the system nontrivial, topologically. By a pin we mean a region of the polymer system, sharply localized near the point $(x, \tau) = (x_p, \tau_p)$, at which the one-body potential experienced by any polymer segment is taken to be so large and repulsive that the polymers never cross it during the course of an experiment:

$$\Phi_p(x, \tau) = c_p \delta(x - x_p)\delta(\tau - \tau_p); \qquad (4.1)$$
$$c_p \to \infty.$$

Because polymers cannot cross over the pin, it serves as a *topological constraint* and, because the polymers are directed and have no free ends, *it partitions the configuration space* of the polymer system into sectors labeled by the number N_L of polymers that have the property that as they pass through the line $\tau = \tau_p$ they obey $-w/2 < x(\tau_p) < x_p$; see Fig. 4.1. Then, the corresponding number of polymers that pass the pin on its other side [i.e., obey $x_p < x(\tau_p) < w/2$] is given by $N_R \equiv N - N_L$. We note that on the line $\tau = \tau_p$ the mean polymer densities to the left and right of the pin are, respectively, $\rho_L = N_L/\big((w/2) + x_p\big)$ and $\rho_R = N_R/\big((w/2) - x_p\big)$. Evidently,

the constraint created by the pin eliminates polymer configurations from the thermal ensemble, and thereby reduces the entropy of the system. For a generically located pin, the only configurations remaining in the ensemble correspond to large fluctuations of the original system. The pin therefore raises the free energy of the system and, as a result, there is generically an equilibrium force on the pin.

To determine the increase in the free energy due to the presence of the pin, it is convenient to analyze the partition function of the polymer system, restricted to having N_L polymers constrained to pass on one side of the pin (as described more precisely in the previous paragraph), normalized by the unrestricted partition function. This amounts to computing Eq. (1.7) with the observable $O(\{x_n\})$ given by

$$\delta\Big(N_L, \sum_{n=1}^{N} \theta\big(x_p - x_n\big)\Big), \tag{4.2}$$

where $\delta(N, N')$ is the Kronecker delta function (i.e., 1 for $N = N'$ and 0 for $N \neq N'$) and $\theta(\cdot)$ is the usual Heaviside step function, which takes the value 0 and 1, respectively, for negative and positive arguments. We now set about computing this free energy increase, as well as the impact of the pin on the spatial variation of the polymer density.

4.2 The charged fluid model with a pin

As discussed in the previous chapter, the polymer segments $\{x_n\}$ on the line $\tau = \tau_p$ behave as charged particles, with thermal fluctuations of the polymer lines at "earlier" and "later" τ generating long-range repulsion driving the segments away from one another and from the walls of the system. For a large number of polymers we may treat these segments as a continuous polymer density $N\rho(x)$ on the line $\tau = \tau_p$. The effective energy of a polymer system may be expressed as in Eq. (3.14). For the particular case of noncrossing polymers contained within hard walls, whose correlations are are encoded in the wave function in Eq. (2.24), the charged fluid energy functional is

$$\beta U\left[\rho(\cdot)\right] = \int_{-\pi/2}^{\pi/2} dx \left[N\rho(x)\ln\rho(x) - 2N\rho(x)\ln|\cos x|\right] \tag{4.3}$$
$$-N^2\int_{-\pi/2}^{\pi/2}\int_{-\pi/2}^{\pi/2} dx dx' \rho(x)\ln|\sin x - \sin x'|\,\rho(x'),$$

where, to shorten the equations, we have set the width of the system equal to π.

We now impose on this system the constraint associated with the pin. In terms of the original polymer coordinates, this is

$$-\pi/2 < x_1, \ldots, x_{N_L} < x_p < x_{N_L+1}, \ldots, x_N < \pi/2. \tag{4.4}$$

In terms of the polymer density, this constraint is

$$\int_{-\pi/2}^{x_p} dx\,\rho(x) = N_L/N; \tag{4.5}$$
$$\int_{x_p}^{\pi/2} dx\,\rho(x) = N_R/N. \tag{4.6}$$

In addition, we have the standard requirement that the polymer density be nonnegative:

$$\rho(x) \geq 0, \quad \text{for} \quad -\pi/2 < x < \pi/2. \tag{4.7}$$

4.3 Obtaining the density profile

We now apply the functional version of Laplace's method in order to obtain the density profile which minimizes the energy functional subject to the constraint. Because of the factors of N in the energy functional, for large numbers of polymers the fluctuations around this dominant density profile should be small. Including now a source term that will allow us to enforce the pin constraint, as discussed in Chapter 3, the first-order condition which the dominant density profile $\bar{\rho}(\cdot)$ obeys are

$$\int_{-\pi/2}^{\pi/2} dx\, \bar{\rho}(x) \ln|\sin x - \sin x'| = s_L + (s_R - s_L)\, \theta(x_p - x'). \tag{4.8}$$

Here, s_L and s_R are the effective chemical potentials to add particles (i.e., polymer segments) on the left and right sides of the pin, respectively. These parameters may be adjusted in order to enforce the pin conditions of Eq. (4.5). It is important to note that this condition is only obeyed at values of x' for which $\bar{\rho}(x)$ is strictly greater than zero.

In the absence of the pin constraint, s_L would be equal to s_R and the condition would be trivially satisfied via a uniform polymer density profile (short-distance behavior such as Friedel oscillations near the walls are averaged out over the length scales embodied in $\rho(x)$). This uniform density profile is also the correct mean density profile in the presence of a pin for the exceptional case in which the pin demands that the average polymer densities on the two sides of it be equal to one another (i.e., for the case in which $\rho_L = \rho_R = 1/\pi$). We refer to such a constraint as an *equilibrium pin*. Generically, however, the pin has a profound effect on the mean polymer density.

To analyze the stationarity condition, Eq. (4.8), it is convenient to make the following transformations of the dependent and independent variables:

$$\bar{\rho}(x) \;\rightarrow\; Q(s) \equiv \bar{\rho}(x)/\cos x, \tag{4.9a}$$

$$x \;\rightarrow\; s \equiv \sin x, \tag{4.9b}$$

so that $dx = ds/\sqrt{1-s^2}$, and similarly for x'. In terms of these new variables the stationarity condition becomes

$$\int_{-1}^{1} ds\, Q(s)\, \ln|s - s'| = s_L + (s_R - s_L)\theta(s - s_p) \tag{4.10}$$

where $s_p \equiv \sin x_p$. This form of the stationarity condition must be met at values of s for which $Q(s) > 0$.

If we were to ignore the positivity condition that a physically acceptable density profile $Q(\cdot)$ must satisfy then it would be straightforward to solve the integral equation (4.10) for all s (by following a technique that we shall, in fact, eventually adopt; see, e.g., Ref. [25]). However, the result we would

obtain for $Q(\cdot)$ would be invalid, as it would diverge to negative infinity near the pin. Thus, we search for a solution that violates the first-order conditions over one or more segments of $-1 < s < 1$; within these segments $Q(s) = 0$ and we refer to any such a segment as a *gap*.

Nonequilibrium pins necessarily cause compression of the the polymers either on one side of the pin or on the other. Without loss of generality, we may take the compressed region to correspond to $-1 < s < s_p$; then the rarefied region corresponds to $s_p < s < 1$. For the profile that minimizes the energy functional (4.3), it is physically reasonable to assert that any gap would form on the rarefied side and, furthermore, that it would lie directly adjacent to the pin and extend over a region that more strongly disfavors the presence of polymers, as a result of its proximity to the dense region of polymers that is created by the pin on the other side of the pin. Indeed, it is this region that would, in the absence of the positivity condition, acquire a negative density of polymers. (This assertion will be verified as we proceed.) Thus, we look for non-negative profiles for which we require $Q(s) = 0$ for s lying within the range $s_p < s < s_g$. If a gap were to be present anywhere else, the system free energy could be lowered by moving polymer density into that gap. Thus, any solution found that (i) has this gap and (ii) elsewhere satisfies the constraints on $\bar{\rho}(x)$ is the unique minimizer of our effective free energy.

As we shall see, the formation of a *single* gap yields a suitable profile (i.e., one that satisfies the positivity constraint automatically). What remains, then, for the case of a single pin, is to determine the value of the density profile and, in particular, the width of the gap $(s_g - s_p)$ that together ensure that the necessary conditions on the profile are obeyed by it. Following the approach reviewed in Ref. [25], we have that the family of solutions to this integral equation is given in terms of parameters A_0 and A_1 by

$$Q(s) = \begin{cases} \dfrac{(A_0 + A_1 s)\,\mathrm{sgn}(s - s_g)}{\sqrt{(1 - s^2)(s - s_p)(s - s_g)}}, & \text{for } -1 < s < s_p \\ & \text{or } s_g < s < 1; \\ 0, & \text{for } s_p < s < s_g. \end{cases} \tag{4.11}$$

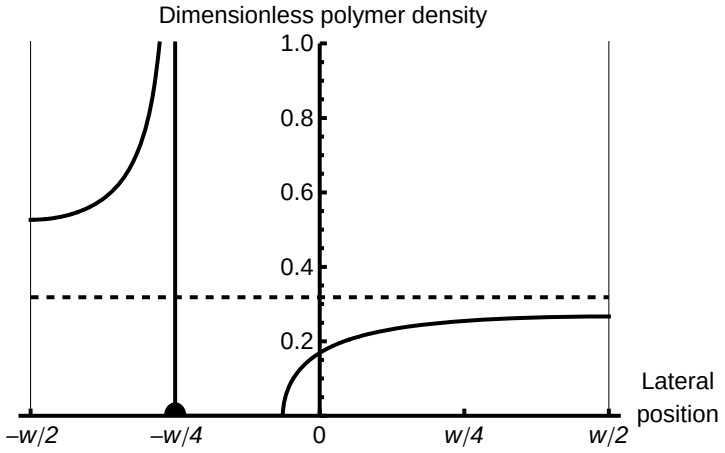

Figure 4.2: Transverse variation of the equilibrium directed polymer density along the line $\tau = \tau_p$ for a system subject to a pinning constraint located at $(x, \tau) = (-w/4, \tau_p)$, the location of which is marked by a black dot. The physical polymer density is the plotted quantity scaled by $N\pi/w$. Within the present approximation scheme, a finite gap (i.e., an area of zero polymer density) extends from the pin. The dashed line represents the equilibrium polymer density in the absence of a pin. From Rocklin et al. [2].

Transforming back to polymer coordinates, using Eq. (4.9), we thus have

$$\bar{\rho}(x) = \begin{cases} \dfrac{(A_0 + A_1 \sin x)\,\mathrm{sgn}(\sin x - \sin x_g)}{\sqrt{(\sin x - \sin x_p)(\sin x - \sin x_g)}}, & \text{for } -\pi/2 < x < x_p \\ & \text{or } x_g < x < \pi/2; \\ 0, & \text{for } x_p < x < x_g. \end{cases} \tag{4.12}$$

The next step in determining $\bar{\rho}(x)$ is to adjust A_0 and A_1 to ensure that there is no divergence at $x = x_g$; this requires that $A_0 + A_1 \sin x_g = 0$. Physically, this choice is motivated by the expectation that the equilibrium density does not diverge on the rarefied side of the pin. Next, we invoke the normalization condition and thus determine that $A_1 = 1/\pi$; and, finally, we adjust x_g to ensure that the pin constraint (4.5) is met. Thus, we arrive at the profile that dominates the constrained partition function:

$$\bar{\rho}(x) = \begin{cases} \dfrac{1}{\pi}\sqrt{\dfrac{\sin x - \sin x_g}{\sin x - \sin x_p}}, & \text{for } -\pi/2 < x < x_p \\ & \text{or } x_g < x < \pi/2; \\ 0, & \text{for } x_p < x < x_g. \end{cases} \tag{4.13}$$

Restoring the physical lengths, this becomes

$$\bar{\rho}(x) = \begin{cases} \dfrac{1}{w}\sqrt{\dfrac{\sin(\pi x/w) - \sin(\pi x_g/w)}{\sin(\pi x/w) - \sin(\pi x_p/w)}}, & \text{for } -w/2 < x < x_p \\ & \text{or } x_g < x < w/2; \\ 0, & \text{for } x_p < x < x_g. \end{cases} \tag{4.14}$$

Note the essential features of this solution for the polymer density along the line $\tau = \tau_p$, as shown in Fig. 4.2: throughout the width of the system (i.e., for $-w/2 < x < w/2$) the density is non-negative; at the system edges (i.e., $x = \pm w/2$) the density is finite; at the pin (i.e., for $x = x_p$) the density has a square-root divergence approaching x_p from the compressed side and a square-root vanishing approaching x_g from the rarefied side; and within the segment $x_p < x < x_g$ the density is zero. It is striking that merely as a result of inter-polymer interactions that are local in the two-dimensional plane the topological restriction presented by the pin causes the opening up of a finite gap in the polymer density and, in particular, that the reach of its impact extends over many times the intrinsic inter-polymer separation, at least at the level of the present mean-field type of approximation. The mechanism responsible for this is that—over a longitudinal distance that is nonzero—the polymers are energetically disfavored from entirely filling in the gap by the cost in deflection energy they would have to incur to depart from their long-distance equilibrium positions. Note that while the mean density $\bar{\rho}(x)$, as calculated within our approach, is zero within the gap, fluctuations can only increase it, leading to there being a small positive polymer density within this region.

A closed-form expression for the gap edge x_g associated with a partitioning may be found in terms of elliptic integrals, as in Appendix C. For a pin near its equilibrium position x_e, the pin displacement $x_p - x_e \equiv \delta$ and the gap $x_p - x_g \equiv \gamma$ are both small. Then the gap size is related to pin displacement to leading order by

$$\delta \approx \frac{\gamma}{2} \ln\left(\frac{2w}{\pi|\gamma|}\cos^2\frac{\pi x_p}{w}\right) + O(\gamma). \tag{4.15}$$

Thus for a pin near its equilibrium position the gap size is sublinear in the

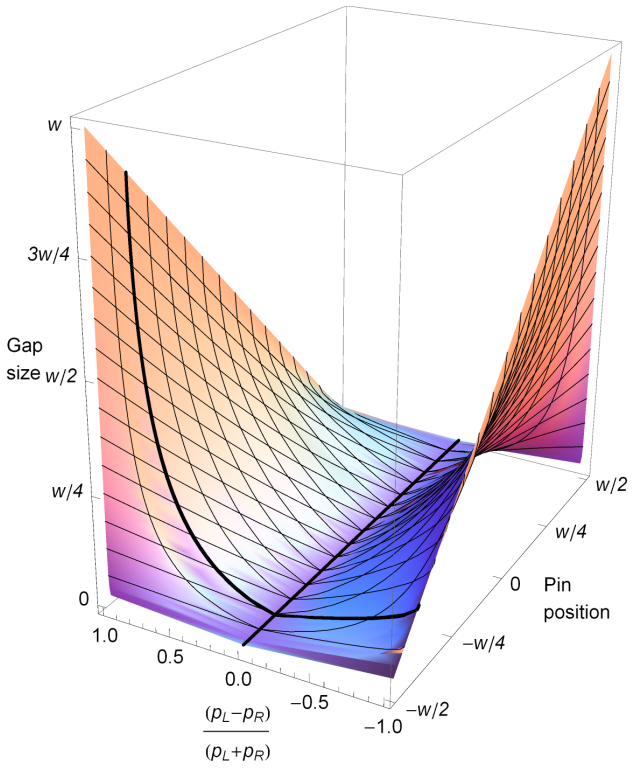

Figure 4.3: Dependence of the width of the gap that opens in the polymer density adjacent to a pin on the pin location and polymer density imbalance. Note that the gap width increases from zero as the pin position is varied, parametrically, from its equilibrium position. At the equilibrium position ($\rho_L = \rho_R$), the gap vanishes and the polymer density is spatially uniform, as it is for a system in the absence of a pin. From Rocklin et al. [2].

pin displacement.

In Fig. 4.3 we show the gap size more generally as a function of the pin position and the parameter $\nu \equiv (\rho_L - \rho_R)/(\rho_L + \rho_R)$, which we introduce to characterize the imbalance between the densities on either side of the pin. When all the polymers are on one side of the pin (in which case $\nu = \pm 1$) then the gap size is simply the pin displacement. More generally, the polymers on the rarefied side expand towards the pin so that the gap is smaller than the pin displacement.

4.4 Force on a pin

Having determined the mean density profile on the lateral line through the pin, viz. $\rho(x,\tau)|_{\tau=\tau_p}$, we now return to our formulation of the dominant contribution to the partition function, and hence the free energy, to determine the increase in the free energy due to the pin, viz. $\Delta\mathcal{F}$. To do this, we begin with the energy functional Eq. (4.3) and seek to compute its value at the mean density profile. To simplify this computation, we employ the first-order stationarity condition (4.8) to eliminate the combination $-\int_{-w/2}^{w/2} dx'\,\rho(x')\,\ln\left|\sin(\pi x/w)-\sin(\pi x'/w)\right|$ in favor of $s_L+(s_R-s_L)\,\theta(x_p-x)$. We also use the stationarity condition evaluated at $x=\pm w/2$ to obtain the Lagrange multipliers s_L and $(s_R-s_L$ in terms of the (known) mean profile. Then, in the resulting expression for $\Delta\mathcal{F}$, we use the normalization of $\rho(\cdot)$ and the constraint on it that the pin introduces, Eq. (4.5), and thus arrive at the result

$$\Delta\mathcal{F}(x_p,N_L,N,T,w) = -N^2T\int_{-w/2}^{w/2} dx\,\bar{\rho}(x,x_p,x_g)$$
$$\times\Big((N_L/N)\ln 2\big(1+\sin(\pi x/w)\big)+(N_R/N)\ln 2\big(1-\sin(\pi x/w)\big)\Big), \quad (4.16)$$

We remind the reader that the gap edge location x_g is not an independent variable but is determined in terms of the independent variables, via the pin constraint, Eq. (4.5).

As a special case, we first consider the situation in which all polymers lie to one side of the pin, i.e. $N_L=N$, so that the pin can in effect be taken to be a septum emerging normally from one wall of the system. In this case, the formula for the free energy increase, Eq. (4.16), simplifies to the explicit form

$$\Delta\mathcal{F} = -\frac{N^2T}{w}\int_{-w/2}^{x_p} dx\,\sqrt{\frac{\sin(\pi x/w)-1}{\sin(\pi x/w)-\sin(\pi x_p/w)}}\,\ln 2\big(1+\sin(\pi x/w)\big)$$
$$= -N^2T\ln\big(\,[1+\sin(\pi x_p/w)]\,/2\big). \quad (4.17)$$

Remaining with the case $N_L=N$, we note that for mild compressions (i.e, those obeying $(w/2)-x_p \ll w$) the force exerted on the pin is Hookean in

nature:

$$\Delta\mathcal{F} = \frac{\pi^2}{4} N^2 T \left(\frac{(w/2) - x_p}{w} \right)^2 , \tag{4.18}$$

as established by making a Taylor expansion of Eq. (4.17) about $x = w/2$. On the other hand, for strong compressions [for which $(w/2) + x_p \ll w$], so that the polymers are forced through an opening the width of which is only a small fraction of the full width of the system, we have the form

$$\Delta\mathcal{F} = 2N^2 T \ln \left(\frac{2}{\pi} \left(\frac{w}{(w/2) + x_p} \right) \right) . \tag{4.19}$$

Residing, as it does, beyond the linear-response regime, it is not surprising that this form is non-Hookean. Indeed, a similar term, with N_L^2 replacing N^2, dominates the free energy for highly compressed systems with polymers on both sides of the pin.

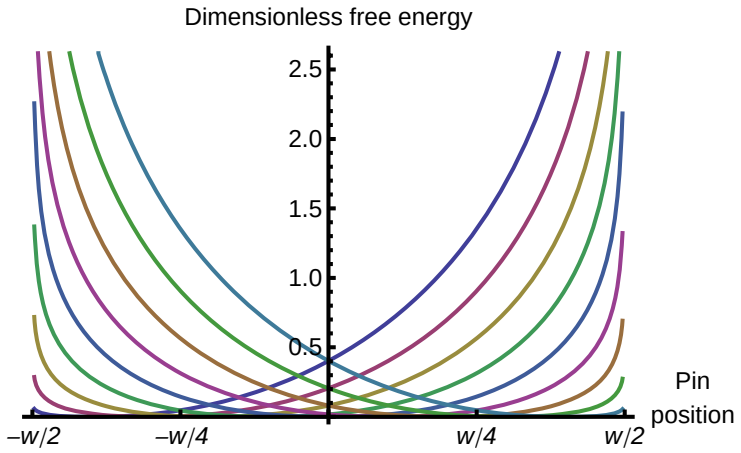

Figure 4.4: Increase in free energy as a function of pin position, for various values of the number of directed polymers N_L passing to one side of the pin. The physical free energy is the plotted quantity scaled by N^2T. The free energy cost due to the pin is less than harmonic for a generic pin that is near its equilibrium position, and it diverges logarithmically as the pin nears an edge of the system. The curves plotted here are for pins having equilibrium (and free energy-minimizing) positions $-.4w,\ -.3w,\ -.2w\ \ldots\ .4w$. From Rocklin et al. [2].

In the more general case, in which $N_R > 0$ polymers pass to the right of the pin, the force on the pin obeys (see Appendix C)

$$-\frac{d\mathcal{F}}{dx_p} = -\frac{\pi N^2 T}{w}\left(\frac{\sin(\pi x_p/w) - \sin(\pi x_g/w)}{\cos(\pi x_p/w)}\right). \tag{4.20}$$

For a pin near its equilibrium position this force is simply proportionate to the gap size $x_p - x_g$, and the above expression may be integrated to obtain the leading term in the free energy

$$\mathcal{F} \approx \frac{N^2 T}{4}\left(\frac{\pi\gamma}{w}\right)^2 \ln\left[\frac{2w}{\pi|\gamma|}\cos^2\frac{\pi x_p}{w}\right]. \tag{4.21}$$

Note that although the free energy of the pin near its equilibrium position grows faster than quadratically in the gap size γ it is sub-Hookean in (i.e., grows slower than quadratically with) the pin displacement $x_p - x_e$. In contrast, in the limit in which the pin position approaches the boundary of the system and highly compresses the polymers, the free energy diverges logarithmically. Fig. 4.4 shows the free energy as a function of pin position for polymer partitionings corresponding to various equilibrium positions of the pin.

4.5 Effects of a barrier on noncrossing polymers

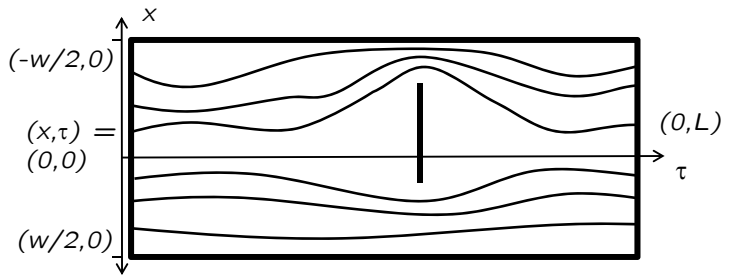

Figure 4.5: A barrier (i.e., a laterally oriented topological obstruction of nonzero width) that constrains the number of directed polymers that pass on either side. By using the techniques developed in the present work one can readily analyze the effects of such barriers. From Rocklin et al. [2].

The approach we have developed so far addresses the case of a topological constraint created by an infinitesimally wide pin. We now generalize the

approach to allow consideration of the case in which the constraint is a barrier of finite width, so that polymers are prohibited from passing through an extended line segment $(x,\tau)|_{\tau=\tau_p}$ (with $-w/2 \le x_p^L < x < x_p^R \le w/2$), as shown in Fig. 4.5. We note that the effect of single barrier is, from the standpoint of directed-polymer statistical mechanics, entirely equivalent to the effect of a pair of pins, provided that polymers are forbidden from passing between the pins.

To analyze the situation of a barrier and, in particular, to compute the change in free energy arising from the presence of this barrier, we return to the task of minimizing the energy functional (4.3), but we replace the pin constraints (4.5), by the following ones, appropriate for a barrier in which precisely N_L polymers pass to the left of the barrier and N_R pass to its right:

$$\int_{-\pi/2}^{x_p^L} dx\, \rho(x) = N_L/N, \tag{4.22a}$$

$$\int_{x_p^R}^{\pi/2} dx\, \rho(x) = N_R/N. \tag{4.22b}$$

These constraints along with normalization and positivity imply the barrier condition: $\int_{x_p^R}^{x_p^L} dx\, \rho(x) = 0$.

Physically, it is evident that there are two distinct situations. Consider a barrier of given width, and with a partitioning specified by N_L and N_R. Relative to the situation without the barrier, the polymers are compressed on at least one side of the barrier, and possibly both. Let us focus on a compressed side, at which the polymer density diverges, and imagine shrinking the barrier into a pin located at x_P^L. On the other side of the pin, there would now be a gap in the polymer density, the width of which is determined, as before, by the pin constraints. Now, imagine widening the pin into a barrier. As long as the barrier width does not exceed the gap width, the polymer density profile would not change, remaining at the density profile associated with a single pin at x_P^L. In effect, the barrier resides in the gap created by the pin, so the fact that the barrier width is finite has no impact.

The second situation follows when the barrier width *does* exceed the width of the gap created by the pin. Now, both ends of the barrier are in contact with polymers. Repeating the earlier integral-equation analysis, we find the resulting density profile (choosing units as before so that $w = \pi$) to be given

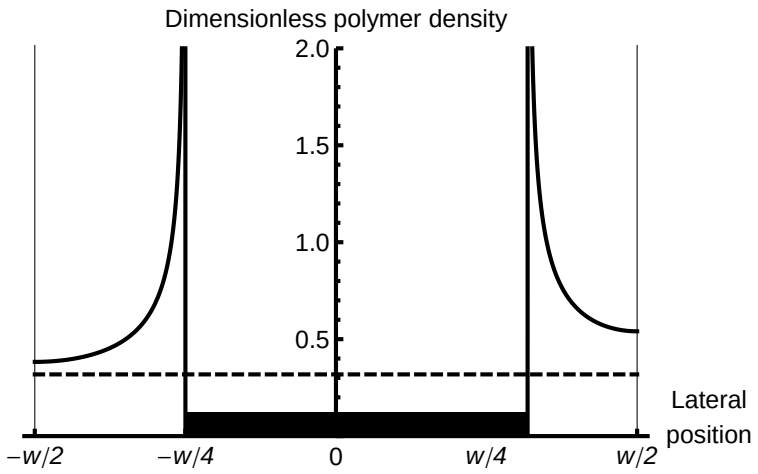

Figure 4.6: Equilibrium directed-polymer density along the line containing a barrier. The physical polymer density is the plotted quantity scaled by $N\pi/w$. The spatial extent of the barrier is indicated by the thick line. Note that for the chosen value of the polymer partitioning, the polymer density diverges on both sides of the barrier. The dashed line represents the density of the polymer system in the absence of the barrier. From Rocklin et al. [2].

by

$$\bar{\rho}(x) = \begin{cases} \dfrac{(A_0 + A_1 \sin x)\,\mathrm{sgn}(\sin x - \sin x_p^R)}{\sqrt{(\sin x - \sin x_p^L)(\sin x - \sin x_p^R)}}, & \text{for } -\pi/2 < x < x_p^L \\ & \text{or } x_p^R < x < \pi/2; \\ 0, & \text{for } x_p^L < x < x_p^R. \end{cases} \tag{4.23}$$

The two constants are now set by the numbers of polymers passing on either side of the barrier. The area of the "gap" is now precisely the area excluded by the barrier, and the polymer density diverges on either side of it, as shown in Fig. 4.6.

Although, in general, the effect of the barrier on the free energy is more complicated than the effect of a single pin, there is one case that may be addressed analytically. Consider an extended barrier of width small width b such that $w/N \ll b \ll w$, whose midpoint would be an equilibrium pin if b were set to 0. In this case, the equilibrium polymer density on either side of the barrier resembles the polymer density around a single pin that has been displaced a distance $b/2$ from an equilibrium position $x = w/2$. The free

energy cost of such a small barrier is then given by

$$\Delta\mathcal{F} = \frac{\pi^2}{8}\,T\left(\frac{N}{w}\right)^2 b^2. \tag{4.24}$$

4.6 Effects of multiple pins and/or barriers on noncrossing polymers

We now have all the tools we need to address multiple pins and even multiple finitely-wide barriers, as long as we continue to restrict these obstacles to lying on a common line $\tau = \tau_p$. Consider, then, M pins at the ordered locations $-(w/2) < x_1 < x_2 < \cdots < x_M < (w/2)$, such that N_ℓ polymers are constrained to pass between pin ℓ (located at x_ℓ) and the nearest pin (or wall) to its left (i.e., at smaller x). N_1 and N_{M+1} respectively denote the number of polymers passing to the left of the leftmost pin and the right of the rightmost pin. (We remind the reader that any barrier of finite width may be treated as an adjacent pair of pins with no polymers passing between them.) For such situations, the cost in free energy is determined, as usual, by maximizing the logarithm of the appropriate partition function $\mathcal{Z}$, given by (choosing here units so that $w = \pi$)

$$\ln\mathcal{Z} \sim \int_{\mathcal{C}} dx \int_{\mathcal{C}} dx'\,\rho(x)\,\rho(x')\ln\Big[\big(\sin x - \sin x'\big)^2\Big], \tag{4.25}$$

over the density profile $\rho(\cdot)$, subject to the constraints imposed by the pins and/or barriers. The symbol $\mathcal{C}$ now indicates the following collection of constraints for all ℓ:

$$\int_{\mathcal{C}_\ell} dx\,\rho(x) \;=\; N_\ell/N, \tag{4.26}$$

$$\rho(x) \;\geq\; 0, \quad \text{for} \quad -\pi/2 < x < \pi/2, \tag{4.27}$$

where $\mathcal{C}_\ell$ indicates that the integration range runs to the $\ell^{\,\text{th}}$ obstacle from the obstacle or wall that precedes it (or, in the rightmost case, from the rightmost obstacle to the right wall). The barrier constraints are implemented via a collection of Lagrange multiplier terms, which augment $\ln\mathcal{Z}$ and are given

by

$$\sum_{\ell=1}^{M+1} \lambda_\ell \left\{ \int_{\mathcal{C}_\ell} dx\, \rho(x) - \frac{N_\ell}{N} \right\}. \tag{4.28}$$

This is simply a more general form of the source term $s(x)$ discussed in Chapter 3, with λ_ℓ the value of the term for x on the ℓ^{th} interval. As with the cases already treated earlier in this chapter, functional differentiation—of the free energy functional augmented by the Lagrange multiplier terms—yields an integral equation that is solvable for a non-negative, and therefore physically acceptable, $\rho(\cdot)$, provided we (i) allow for the possibility of gaps in the polymer density profile, and (ii) determine their necessity and location by implementing the constraints on the numbers of polymers passing between the various obstacles. In general, some pins will lie within the interior of gaps; other pins will have a gap form on one side.

For cases involving more than one or two pins, the process of determining the gap structure that permits all constraints to be satisfied becomes quite tedious, but it should always yield a unique result for the density profile that minimizes the free energy. Moreover, denoting by $\{p_j\}$ the sets of points at which the polymer density diverges and by $\{g_k\}$ the set where it increases gradually from zero density, we may continue as before and thus obtain the mean polymer density in regions outside the gaps as

$$\bar{\rho}(x) = \frac{1}{w} \sqrt{\frac{\prod_k [\sin(\pi x/w) - \sin(\pi g_k/w)]}{\prod_j [\sin(\pi x/w) - \sin(\pi p_j/w)]}}. \tag{4.29}$$

4.7 Longitudinal impact of topological constraints

4.7.1 Classical hydrostatic approach

In describing the effects of a single pin, we have focused specifically on the equilibrium structure of the polymer system along the line $\tau = \tau_p$ which passes through the pin. To extend our understanding of the effect of topological constraints away from this line and into the longitudinal direction, it is useful to develop a treatment that is analogous to hydrodynamics, which we call a classical hydrostatic approach. This enables us to describe the large

fluctuations that are present around topological obstructions.

Consider an area of the $x-\tau$ plane of width w' much greater than the interpolymer spacing and length L' sufficient for ground-state dominance to be valid. Let this area be bounded by $x(\tau) \in [v\tau - w'/2, v\tau + w'/2]$ (i.e., the polymers are confined to a parallelogram such that their average slope is v). We can again map this onto a quantum problem with a time-independent Hamiltonian, provided we first make the tilt mapping $x(\tau) \to x(\tau) + v\tau$. To lowest order in v, the effect of this tilt is to increase the free energy per polymer per unit length by $Av^2/2$. Thus, the free energy density within the region is given by

$$\frac{\mathcal{F}}{w'L'} = A\rho\frac{v^2}{2} + \frac{\pi^2}{6}\frac{1}{\beta^2 A}\rho^3. \tag{4.30}$$

We may interpret this quantity as the *local* free energy density, expressed in terms of the *local* polymer density $\rho(x,\tau)$ and the *local* polymer slope $v(x,\tau)$ fields, provided we also require polymer line-length conservation, via the continuity equation

$$\partial_\tau \rho(x,\tau) + \partial_x \left(\rho(x,\tau)v(x,\tau)\right) = 0. \tag{4.31}$$

Now, around a topological constraint the polymer density and slope fields are dominated by configurations that minimize the free energy subject to the constraints. This minimization leads to the following nonlinear partial differential equation, obeyed by $\rho(x,\tau)$ and $v(x,\tau)$, which supplements the continuity equation:

$$\partial_\tau v + v\partial_x v = \frac{\pi^2}{\beta^2 A^2}\rho\partial_x\rho. \tag{4.32}$$

These equations may be combined into a single Hopf equation for the single complex field $w(x,\tau)$:

$$\partial_\tau w - iw\partial_x w = 0, \tag{4.33}$$

$$w(x,\tau) \equiv \frac{\pi}{\beta A}\rho(x,\tau) + iv(x,\tau) \tag{4.34}$$

Solutions of the Hopf equation take the form

$$w(x,\tau) = F\left(x + i(\tau - \tau_p)w(x,\tau)\right), \tag{4.35}$$

where $F(\cdot)$ is an analytic function determined by the boundary conditions.

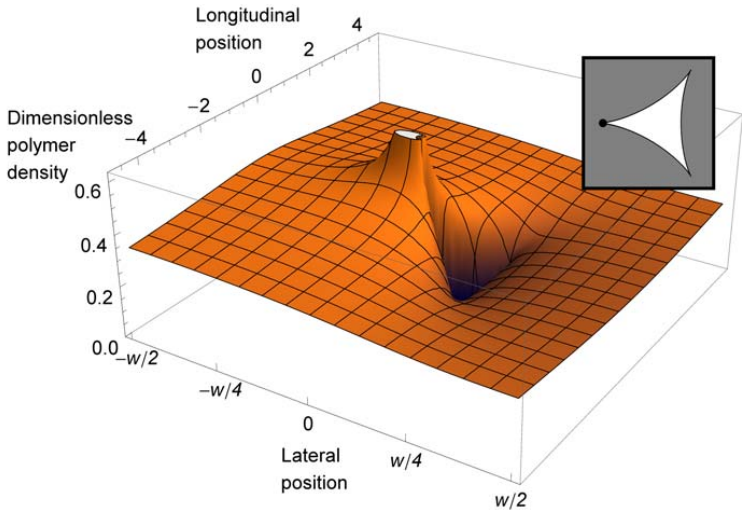

Figure 4.7: Variation of the equilibrium directed-polymer density over the (x,τ) plane in the vicinity of a pin constraint. The physical polymer density is the plotted quantity scaled by $N\pi/w$. Note that the gap (i.e., the region in which the present approximation scheme gives zero for the polymer density) is roughly triangular in shape, as shown by the unshaded area of the inset. The divergence in the polymer density occurs only at precisely the location of the pin, depicted by a black dot in the inset. From Rocklin et al. [2].

We have already obtained the dominant density profile $\rho(x,\tau_p)$. This profile serves as a boundary condition on the Hopf equation for the $\tau > \tau_p$ region of the plane (or for the $\tau < \tau_p$ region). By symmetry, it is clear that $\rho(x,\tau_p+\tau') = \rho(x,\tau_p-\tau')$ and $v(x,\tau_p+\tau') = -v(x,\tau_p-\tau')$. In particular, we have that $v(x,\tau_p) = 0$, serving as our second boundary condition at $\tau = \tau_p$. Provided that the pin is far from the boundaries of the system, the boundary

conditions there are simply that the polymer density field is uniform and the slope field vanishes. Thus, the analytic function $F(\cdot)$ is fully determined, and $w(x,\tau)$ may be obtained throughout the plane, at least numerically. The polymer density resulting from a pin at $x = -0.06w$ with the partitioning $N_L = .74N$ is shown in Fig. 4.7. We note that the divergence in the polymer density at the pin immediately subsides but the gap persists over a finite range in the longitudinal direction. At large longitudinal distances, however, the polymer density profile returns to the uniform distribution of the pin-less system.

As the free energy expression Eq. (4.30) is obtained by ignoring contributions associated with certain higher-gradient terms, the density profile thus obtained is expected to be quantitatively incorrect in the vicinity of any pins, because there the polymer density diverges and one expects the short-distance details of the inter-polymer interaction to control such divergences. Indeed, for a broad class of systems, nonlinearities can lead to shock-wave behavior even for initially fairly smooth density profiles [26], and even more readily for the divergent behavior around a pin.

4.7.2 Connection to quantum hydrodynamics

In the previous subsection we have used a hydrostatic description of the polymer system to describe the polymer density away from the line $\tau = \tau_p$. One may also address polymer density for $\tau \neq \tau_p$ in the quantum particle system language. This corresponds to determining the imaginary-time evolution of the quantum system away from the time $\tau = \tau_p$ in a manner consistent with the initial density profile $\bar{\rho}(x)$ at $\tau = \tau_p$. As this profile differs substantially from the equilibrium density profile for the pin-less case (i.e., a uniform density profile) the equivalent quantum system can be regarded as having undergone a large quantum fluctuation.

Systems of nonlinear equations analogous to hydrodynamical equations have been used to describe the evolution of one-dimensional systems of interacting particles around large fluctuations [27]. In terms of the particle

density and velocity fields, $\rho(x,t)$ and $v(x,t)$, these equations read

$$\partial_t \rho + \partial_x (\rho v) = 0, \tag{4.36a}$$

$$\partial_t v + v\partial_x v = m^{-1}\partial_x \partial_\rho (\rho \mathcal{E}(\rho)), \tag{4.36b}$$

where $\mathcal{E}(\rho)$ is the ground-state energy per particle, expressed as a function of the density ρ. In the quantum case, these equations come from minimizing the instantonic action whose dominant terms are the local internal energy density $(\rho\mathcal{E}(\rho))$ and the kinetic energy $(v^2\rho/2)$ associated with the large average local velocity. For the polymers, the competing physical quantities are the internal energy density and the local energy cost of large average polymer slopes.

For a system of free fermions $\mathcal{E}(\rho) = (\hbar^2\pi^2/6m)\rho^2$. In this case, the quantum hydrodynamical equations are identical to the classical hydrostatic ones for noncrossing polymers, Eqs. (4.31), (4.32), provided we make the familiar parameter identifications of Eq. (2.5). Indeed, we were led to the direct, classical hydrostatic approach after doing the mapping to the quantum particle system and following the quantum hydrodynamical approach to such systems developed by Abanov and co-workers; see, e.g., Refs [27, 26].

The analogy to quantum hydrodynamics also illustrates how the response to a topological obstruction depends on the *length* of the polymer system. A qualitative analysis of large quantum fluctuations indicates that the probability $P(R)$ of a large fluctuation over a length scale R has the form $P(R) \sim \exp(-\alpha R^2)$; see Ref. [27]. This corresponds to our finding in this work that when the pin displacement is small (compared to the overall system size) and all polymers lie on one side of the pin the free-energy cost is quadratic in the displacement. However, when the finite temperature of such a quantum system is taken into account, the probability of a fluctuation becomes $P(R) \sim \exp(-\gamma R)$. The analog of a finite temperature in the quantum system is a finite *length* in the polymer system. For a system in which the pin coordinate τ_p is located near enough to another system feature, such as another pin or an end of the system, the ground-state dominance approximation fails, and one instead finds that the free-energy cost of the pin would increase linearly with the displacement of the pin from its equilibrium position. Thus, a longitudinally short system, or one having longitudinally distributed pins, can display a super-Hookean response when a pin is displaced a small amount

from its equilibrium position.

We remark that although the polymer system we have been exploring is formally equivalent to its quantum analog, the polymer system is more readily controllable. Large quantum fluctuations are, due to their rarity, difficult to observe. In contrast, the probability of occurrence of the equivalent large thermal fluctuations of the polymer system can be measured indirectly, via the entropic force on a pin, which has the useful effect of forcing the system to assume what would otherwise be rare configurations.

CHAPTER 5

CROSSING POLYMERS

In previous chapters, we enforced the noncrossing condition $x_i(\tau) \neq x_j(\tau)$ for all $i \neq j$ by including an infinite repulsive contact potential. We now wish to relax the noncrossing condition and allow for a nonzero density of polymer crossings. Let us then consider a system with a finite contact repulsion between polymers, so that two polymer lines may cross, albeit with an energetic penalty:

$$U\left[\{x_n(\cdot)\}\right] = \frac{A}{2}\sum_{n=1}^{N}\int_0^L d\tau \left(\partial_\tau x_n(\tau)\right)^2 + 2c\sum_{1\leq n<n'\leq N}\int_0^L d\tau\, \delta\big(x_n(\tau) - x_{n'}(\tau)\big), \tag{5.1}$$

where $\delta(\cdot)$ is the one-dimensional Dirac delta function and $2c$, which has units of energy, is a positive parameter that describes the effective contact repulsion between polymers.

5.1 Origin of contact repulsion

Some of the physical systems we consider, such as step edges on a crystalline surface, are truly two dimensional. Polymers, in contrast, exist in three dimensions and can, in principle, cross over each other. Let us then parametrize our polymer configurations by paths through three dimensional space $\mathbf{r}(\tau) \equiv (x(\tau), y(\tau))$. As before, $x(\tau) \in (-w/2, w/2)$ but now polymers are permitted to move in a narrow band such that $y(\tau) \in (-\epsilon/2, \epsilon/2)$, with $\epsilon \ll w$. Suppose further that polymers have an effective diameter d such that the ensemble permits only configurations that for all n, n' and at all τ obey

$$\left|\mathbf{r}_n(\tau) - \mathbf{r}_{n'}(\tau)\right|^2 \geq d^2. \tag{5.2}$$

We wish to integrate out the polymer degrees of freedom associated with the small third dimension and thereby restore our effectively two-dimensional picture of polymer configurations. In particular, let us integrate out two polymer coordinates y_n and $y_{n'}$ at some particular value of τ. If $|x_n - x_{n'}| \geq d$ each of the two polymer coordinates may occupy any point on $(-\epsilon 2, \epsilon/2)$

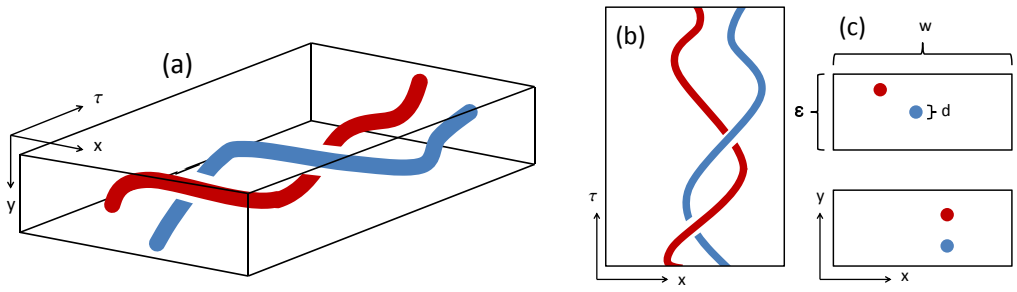

Figure 5.1: **(a)** A configuration of two directed lines of finite thickness d less than the thickness ϵ of the system in the y-direction. The polymers interact via an excluded-volume effect. **(b)** The projection of the configuration shown in (a) onto the $x - \tau$ plane. Because the width of the system in the x-direction is much greater than its thickness in the y-direction, we may neglect the additional tension energy associated with deflections in the y-direction. **(c)** Cross-sections of the configuration in the plane transverse to the preferred direction of the polymers. Because of the excluded volume effect, there are fewer ways to vary the y-coordinates of the polymer segments in the configuration in the bottom panel than in the configuration in the top panel. This leads to a finite effective entropic repulsion between polymer configurations in the $x - \tau$ plane. Prepared for Rocklin et al. [28].

(ignoring edge effects at $y = \pm\epsilon/2$). In contrast, if $x_n = x_{n'}$, then any value of y_n restricts $y_{n'}$ to a thickness $\epsilon - d$ in the y-direction (see Fig. 5.1). Thus, upon integrating out the third dimension we ought to reduce the weight of a polymer configuration $\{x_n(\cdot)\}$ by a factor of

$$\frac{\epsilon(\epsilon - d)}{\epsilon^2} \tag{5.3}$$

whenever one polymer crosses over another. We may take the number of polymer crossings to be proportional to

$$\sum_{n<n'} \int_0^L d\tau\, \delta\big(x_n(\tau) - x_{n'}(\tau)\big), \tag{5.4}$$

provided that we assume some cutoff length scale such that $\dot{x}(\tau)$ remains finite at a crossing. Then, we obtain an effective contact repulsion from this entropic effect, yielding the energy functional in Eq. (5.1) with parameter

$$2c = -T \ln(1 - d/\epsilon), \tag{5.5}$$

with T the temperature in units of energy. Note that in the limit that polymer width d approaches the thickness ϵ of the system in the third dimension, the condition that no polymer crossings occur is recovered.

In addition to the geometrical effects discussed here, we note that the configurations of polymers discussed here are also subject to topological effects associated with how they wind around one another. In Chapter 8, the effects of polymer topology will be considered.

5.2 Quantum picture

The analog of the polymer system with a contact repulsion as in Eq. (5.1) is a one-dimensional gas of bosons interacting via a contact potential. Such a system is governed by the Lieb-Liniger Hamiltonian:

$$\hat{H} = -\frac{\hbar^2}{2m} \sum_n \frac{\partial^2}{\partial x_n^2} + 2c \sum_{n<n'} \delta\left(x_n - x_{n'}\right). \tag{5.6}$$

This is an integrable system, with each eigenstate of the Hamiltonian characterized by a set of N quasimomenta $\{k_i\}$ [18].

Because the bosons are free particles when they do not coincide, an eigenstate of the Hamiltonian has the Bethe Ansatz form (for periodic boundary conditions) when $x_1 < x_2 < \ldots < x_n$:

$$\psi(\{x_n\}) = \sum_P e^{i\theta_P} \exp\left(i \sum_n k_n^P x_n\right), \tag{5.7}$$

where the $\{k_n\}$ are sets of quasimomenta associated with each eigenstate of the Hamiltonian. The P index the $N!$ permutations on the quasimomenta, and $e^{i\theta_P}$ is a phase factor associated with permutation P.

As Lieb and Liniger show by integrating the Schrödinger equation from $x_n = x_{n+1} - \delta$ to $x_n = x_{n+1} + \delta$ with $\delta \to 0$, the phase factor θ_n associated

with exchanging k_n and k_{n+1} is

$$e^{i\theta_n} = \frac{i\,(k_{n+1} - k_n) - c}{i\,(k_{n+1} - k_n) + c}. \tag{5.8}$$

This gives us N equations in N unknowns, which have solutions for certain sets of $\{k_n\}$, corresponding to the eigenstates of the Hamiltonian. Notice that for $c = 0$ the quasimomenta are merely the momenta of a system of free bosons. For $c \to \infty$ the hardcore bosons function as free fermions and the phase factors ensure that the wave function vanishes when any two particle coordinates coincide. For a finite repulsion strength c, the quasimomenta associated with the ground state of the system may be obtained via an integral equation (or a set of equations, for a finite number of particles). They lie in some band $k_n \in (-K, K)$, where K is less than the Fermi momentum of the corresponding system of free fermions. However, there is still an abrupt drop in the density of quasimomenta at K, just as there is at a true Fermi surface, so that the the logarithmic divergence in the x-ray form factor found for a system of strictly noncrossing (i.e., $c = \infty$) polymers by de Gennes at wave vector $k = 2\pi N/w$ [18] will instead occur at some lesser value that is dependent on the interaction strength.

5.3 Effect of crossings on polymer statistics

Having thus formulated the partition function of our polymer system we may determine the thermodynamic properties of the long polymer system (long so that the ground-state approximation is appropriate) in much the same way that Lieb and Liniger calculated various quantum observables of the Bose gas [18]. It is important to recall that when extracting polymer observables that depend on the polymer *slopes*, one must take into account the short-distance component of the partition function,

$$\mathcal{Z}_\ell = \left(\frac{2\pi\ell}{A\beta}\right)^{NL/2\ell}, \tag{5.9}$$

as well as the behavior encoded in the ground state of the Lieb-Liniger model.

As discussed in Chapter 2, the free energy per unit are of the long polymer system may be obtained from the ground-state energy of the quantum system, resulting in

$$\frac{\mathcal{F}}{wL} = \frac{1}{wL}\left(-\frac{1}{\beta}\right)\ln \mathcal{Z} = \frac{1}{2\beta}\frac{N}{w\ell}\ln\left(\frac{A\beta}{2\pi\ell}\right) + \frac{1}{2}\left(\frac{N}{w}\right)^3 \frac{1}{\beta^2 A} e(\gamma) \quad (5.10)$$

where $e(\cdot)$ is the dimensionless energy function that Lieb and Liniger derive via the Bethe Ansatz technique. In terms of polymer parameters, the dimensionless interaction parameter, γ is

$$\gamma = 2c\left(\frac{w}{N}\right)\beta^2 A \quad (5.11a)$$

$$= -\left(\frac{w}{N}\right) A\beta \ln\left(1 - d/\epsilon\right). \quad (5.11b)$$

$$\gamma \approx \left(\frac{w}{N}\right) A\beta \left(\frac{d}{\epsilon}\right) \quad (5.11c)$$

In the limit $\gamma \to \infty$, one has $e(\gamma) \to \pi^2/3$, recovering the result of strictly noncrossing polymers. Note however that this is *not* the high-density limit. Although the free energy per unit area increases with increasing polymer density, increasing polymer density *decreases* γ, indicating that the free energy of the high-density system depends more on the polymer deflections than on the polymer crossings. Given the entropic origin of our contact repulsion from Eq. (5.5), we also have that γ is *inversely* proportional to temperature. At low temperatures, the polymers are restricted to configurations with few crossings, whereas for high temperatures they cross more freely, although still less often than would truly noninteracting polymers.

One may in a similar way obtain the areal density of polymer crossings,

$$\frac{1}{wL}\Big\langle \sum_{n<n'} \int d\tau \delta\left(x_n - x_{n'}\right) \Big\rangle = -\frac{1}{2\beta}\frac{1}{wL}\frac{\partial}{\partial c}\ln \mathcal{Z} = \frac{1}{2}\left(\frac{N}{w}\right)^2 e'(\gamma). \quad (5.12)$$

As shown in Fig. 5.2, this quantity diverges as the interaction strength c is reduced to zero. This is true only when does not take the short-distance polymer cutoff length ℓ into account, so that polymers can wander back

and forth across one another an arbitrary number of times within a short distance. Taking the finite slope set by ℓ into account implies a residual density of polymer crossings in the noninteracting limit

$$\sim \left(\frac{N}{w}\right)^2 \frac{1}{\sqrt{A\beta\ell}}. \tag{5.13}$$

We saw in Chapter 2 that the noncrossing condition reduced the average slope of polymers below what it would be for noninteracting polymers by eliminating from the ensemble certain configurations that tended to have steep polymer slopes. Now, with a finite contact repulsion, those same configurations have more polymer crossings and therefore suffer a greater energetic penalty, again reducing the average polymer slope:

$$\langle \dot{x}^2(\tau)\rangle = -\frac{2}{\beta}\frac{1}{NL}\partial_A \ln \mathcal{Z} = \frac{1}{A\beta\ell} - \frac{1}{\beta^2 A^2}\left(\frac{N}{w}\right)^2 \left(e(\gamma) - \gamma e'(\gamma)\right). \tag{5.14}$$

One may also obtain the energy density, which includes both the deflection energy and the crossing energy:

$$\frac{1}{wL}\big\langle U\left[\{x_n\tau\}\right]\big\rangle = \tag{5.15}$$
$$\frac{1}{wL}\left(-\partial_\beta \ln \mathcal{Z}\right) = \frac{1}{2\beta}\frac{N}{w\ell} + \frac{1}{2}\left(\frac{N}{w}\right)^3 \frac{1}{\beta^2 A}\Big(2\gamma e'(\gamma) - e(\gamma)\Big).$$

Note that the second term, coming from the increase in interaction energy, includes a portion that comes from the temperature-dependence of the effective interaction strength as in Eq. (5.11a).

One may also obtain the pressure on the walls containing the polymers at $x = \pm w/2$ and $y = \pm\epsilon/2$. In the x-direction, the pressure P_x is given by

$$P_x = \frac{1}{\epsilon L}\frac{1}{\beta}\partial_w \ln Z = \left(\frac{N}{w}\right)^3 \frac{1}{\beta^2 A\epsilon} e(\gamma). \tag{5.16}$$

In the y-direction, on the other hand, the effect of interactions is to generate a P_y given by

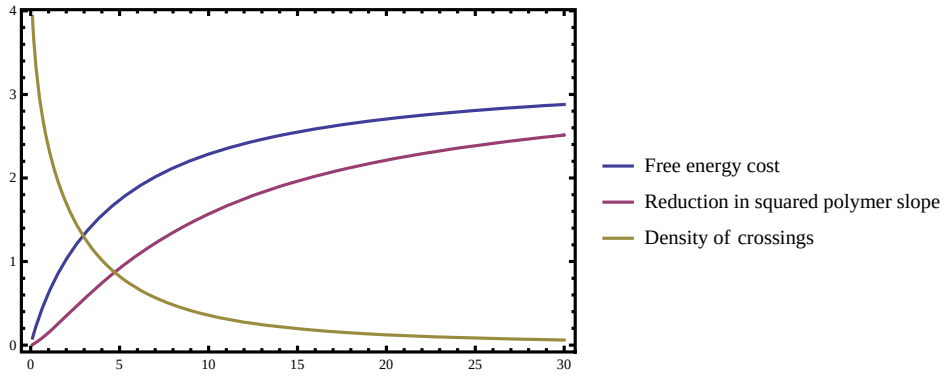

Figure 5.2: Basic (scaled) characteristic quantities of the polymer system are plotted as a function of the dimensionless parameter γ that describes the strength of polymer-polymer interactions. Both the free-energy density (blue line) and the reduction in the squared polymer slope $\langle \dot{x}^2(\tau) \rangle$ (red line) monotonically approach their noncrossing values for strictly noncrossing polymers as γ is increased. The yellow line, depicting the areal density of polymer crossings, diverges for small γ and approaches its own noncrossing value (i.e., zero) for large γ. Prepared for Rocklin et al. [28].

$$P_y = \frac{1}{wL}\frac{1}{\beta}\partial_\epsilon \ln Z = \frac{1}{\beta}N\frac{L}{\ell} + \frac{1}{2\beta}\left(\frac{N}{w}\right)^2 e'(\gamma)\frac{d}{\epsilon(\epsilon - d)}. \tag{5.17}$$

The second term on the right-hand side is simply the expected number of polymer crossings from Eq. (5.12) multiplied by the entropic cost of ensuring that the polymers pass around rather than through each other at each crossing separately. In addition to this term, there is the pressure that would persist even in the limit $d \to 0$ from the confinement of each polymer segment separately to a thickness ϵ. This term is simply that associated with confining each of NL/ℓ polymer segments separately to a thickness ϵ.

The free-energy cost density associated with the interaction is shown in Fig. 5.2. For a sufficiently long system, any interpolymer interaction, no matter how weak or short-range, suffices to generate a free energy that strongly modifies the behavior of the system as compared to a system of free polymers. As we have already seen for strictly noncrossing polymers, polymers with generic interactions have profoundly different physics in reduced dimensions than do free polymers.

5.3.1 Thick polymers

Previously, we considered polymers of nonzero diameter that were narrow enough to cross over one another, (i.e., $d < \epsilon$). Alternatively, one could return to the case of polymers whose effective thickness is too great to allow crossings, $d \approx \epsilon$, while still taking into account the finite thickness of the polymers. In this case, the noncrossing condition becomes the more stringent

$$-w/2 < x_1 - (d/2) < \cdots < x_j - d(j - (1/2)) < \cdots < w/2 - Nd \quad (5.18)$$

That is, not only do the polymer paths not cross, they never come within one polymer diameter of one another, or within one half-diameter of a wall.

This problem is readily solved by mapping the problem onto one of strictly noncrossing but zero-diameter polymers via $x'_j = x_j - d(j - 1/2)$. Then, the finite-diameter polymer system is equivalent to a zero diameter one with a system width narrower by Nd. This leads to the free-energy density

$$\frac{\mathcal{F}}{wL} = \frac{\pi^2}{6} \frac{N^3}{w\,(w - Nd)^2} \frac{1}{\beta^2 A}. \quad (5.19)$$

CHAPTER 6

POLYMERS WITH LONG-RANGE INTERACTIONS

In Chapter 3 we constructed a formalism that applied to polymer systems whose quantum ground states were of a modified product form which included both one-body and two-body terms. This class of systems does not include the crossing polymers of Chapter 5, and we have as yet applied the analysis only to systems of noncrossing polymers without any other interactions. We now wish to extend this class as much as possible. To this end, let us consider the Schrödinger equation for the ground state of a translationally invariant quantum system

$$H\psi(\{x_n\}) = \left[-\sum_{n=1}^{N}\frac{\hbar^2}{2m}\frac{\partial^2}{\partial {x_n}^2} \quad + \sum_{1\le n<n'\le N} V(x_n - x_{n'})\right]\psi(\{x_n\}) = E\psi(\{x_n\}), \quad (6.1)$$

where in this chapter we shall take $V(\cdot)$, the general interpolymer interaction, to be parity invariant, $V(x) = V(-x)$, and to forbid polymer crossings, i.e., $V(0) = \infty$. Following Sutherland [22], we may ask which such interactions produce a groundstate wave function of the product form, which, as we saw in Chapter 3, corresponds to a one-dimensional classical system with a long-range two-body interaction.

By Bose symmetry, if such a wave function $\Psi(\{x_n\})$ is known within the sector $x_1 < x_2 < \cdots < x_N$ it is known everywhere. Within such a sector, since $\Psi(\{x_n\}) > 0$ (a condition we found in Chapter 2 to hold generally providing that the interaction energy does not diverge within a sector) one may divide by it to obtain

$$\frac{1}{2\Psi(\{x_n\})}\sum_{n=1}^{N}\frac{\partial^2}{\partial {x_n}^2}\Psi(\{x_n\}) = \frac{m}{\hbar^2}\left[\sum_{1\le n<n'\le N} V(x_n - x_{n'}) - E\right]. \quad (6.2)$$

Now, let us *assume* that the groundstate wave function has the product form

$$\Psi(\{x_n\}) = \prod_{n<n'}\psi(x_n - x_{n'}). \quad (6.3)$$

In general, inserting such a form into the left-hand side of Eq. (6.2) will result in N terms which each separately depend on *three* particle coordinates, whereas each term on the right-hand side of the same depends only on two. Thus, one must have (regardless of the particular form of the interaction $V(\cdot)$) that for some function $B(\cdot)$ the terms involving, say, $x_n, x_{n'}, x_{n''}$ in the left-hand side are expressible as

$$B(x_n - x_{n'}) + B(x_{n'} - x_{n''}) + B(x_{n''} - x_n). \tag{6.4}$$

One can show [22] that this requirement leads to a differential equation for $\psi(\cdot)$ whose most general solution is the wave function

$$\psi(x_n - x_{n'}) = \vartheta_1^\lambda \left(\pi(x_n - x_{n'})/w|q\right), \tag{6.5}$$

where $\vartheta_1^\lambda(x|q)$ is the λ^{th} power of the Jacobi theta function with parameter q, and w is the width of the system (which we take to obey periodic boundary conditions). This then is the generic form that permits analysis of noncrossing polymer lines subject to a long-ranged interaction. Thus, this form (squared) is the most general form of the interaction $g(\cdot,\cdot)$ term in the charged fluid model described in Chapter 3, at least for translationally-invariant systems. For polymer systems whose quantum analogs do not have groundstate wave functions of the product form one must include effective three-body or more interactions in the charged fluid model.

6.1 Long-range interactions

Having identified the general form of product-form wave functions, we now specialize to $q \to 0$, for which the interaction becomes (first ignoring boundary conditions)

$$V_0(x_n - x_{n'}) = \frac{1}{2A\beta^2} \frac{\lambda(\lambda-1)}{(x_n - x_{n'})^2}. \tag{6.6}$$

Here, the parameter $\lambda > 0$ gives the strength of the interaction, either attrac-

tive or repulsive. For the attractive case (i.e., $\lambda < 1$) we nevertheless retain the noncrossing condition by assuming some additional short-range repulsion. Electrical dipole moments present on the lines lead to an interaction of this form, as has been noted in the context of crystalline step edges [29]. In addition to this, for the crystalline step edges the elasticity of the crystal also gives rise to an effective repulsive interaction between step edges of this form [30].

For periodic boundary conditions with period w, one must include additional potential terms with images of x_n at $x_n \pm w$, $x_n \pm 2w$, etc. Using the mathematical identity (see, e.g., [31])

$$\sum_{n=-\infty}^{n=\infty} \frac{1}{(n+a)^2} = \frac{\pi^2}{\sin^2(\pi a)}, \tag{6.7}$$

this leads to a potential

$$V_0(x_n - x_{n'}) = \frac{1}{2A\beta^2} \left(\frac{\pi}{w}\right)^2 \frac{\lambda(\lambda-1)}{\sin^2(x_n - x_{n'})}. \tag{6.8}$$

The corresponding quantum system is described by the Calogero-Sutherland model [32, 33]. This model is exactly-solvable. In particular, the (unnormalized) ground-state wave function is then

$$\Psi(\{x_n\}) = \prod_{n<n'} \left|\sin\left[\pi(x_n - x_{n'})/w\right]\right|^{\lambda}. \tag{6.9}$$

In the presence of hard walls at $x = 0$ and $x = w$, the interaction must be modified via images to include additional image charges at $-x_n \pm w$, $-x_n \pm 2w, \ldots$, yielding

$$V(x_i - x_j) = \frac{1}{2A\beta^2} \left(\frac{\pi}{w}\right)^2 \times \left(\frac{\lambda(\lambda-1)}{\sin\left[\pi(x_i - x_j)/w\right]^2} + \frac{\lambda(\lambda-1)}{\sin\left[\pi(x_i + x_j)/w\right]^2} \right). \tag{6.10}$$

For a system with hard-wall boundary conditions, the groundstate wave

function is [34]

$$\psi_{gs}(\{x_n\}) = \left(\prod_{n=1}^{N} \left| \cos \frac{\pi x_n}{w} \right|^{\lambda} \right) \left(\prod_{1 \le n < n' \le N} \left| \sin \frac{\pi x_n}{w} - \sin \frac{\pi x_{n'}}{w} \right|^{\lambda} \right). \quad (6.11)$$

Remarkably, for this choice of interpolymer interaction, the quantum wave function is precisely the λ^{th} power of the free fermion one given in Eq. (2.24), which applies to noncrossing polymers without a long-range interaction. This means that the free-energy cost per unit area of the interaction is

$$\frac{\mathcal{F}}{wL} = \frac{\pi^2}{6} \left(\frac{N}{w} \right)^3 \frac{1}{\beta^2 A} \lambda^2. \quad (6.12)$$

There is an additional free-energy cost associated with the normalization of the wave function, but one may show that it is $O(N \ln N)$, and so does not dominate for large numbers of polymers. This model includes both repulsive ($\lambda > 1$) and attractive ($0 < \lambda < 1$) polymer interactions. In the case of attractive interactions, we must assume some additional short-range repulsion that still prevents the polymers from crossing over one another. Repulsive (attractive) polymers are less (more) likely to be found near one another than polymers with only a short-range repulsion, and have a higher (lower) free energy.

Having determined the free-energy density (or, alternatively, the partition function) in terms of the interaction parameter λ, all of the polymer observables found in the previous chapter for crossing polymers may likewise be readily obtained for the polymers with long-range interactions. The energy density, which now includes deflection energy and the long-range interaction $V(\cdot)$ is

$$\frac{1}{wL} \big\langle U\left[\{x_n \tau\}\right] \big\rangle = \frac{1}{wL} \left(-\partial_\beta \ln \mathcal{Z} \right) = \frac{1}{2\beta} \frac{N}{w\ell} - \frac{\pi^2}{6} \left(\frac{N}{w} \right)^3 \frac{1}{\beta^2 A} \lambda^2. \quad (6.13)$$

Note that regardless of the value of λ the interaction reduces the energy (but not the free energy) of the polymer system. Repulsive interactions reduce the deflection energy more than they increase the interaction energy. Indeed, the

reduction in deflection energy is $O(N^3)$, while the interaction energy, positive or negative, is only $O(N^2)$. That reduction in deflection energy comes from the reduction in average squared polymer slope

$$\langle \dot{x}^2(\tau) \rangle = -\frac{2}{\beta} \frac{1}{NL} \partial_A \mathcal{Z} = \frac{1}{A\beta\ell} - \frac{\pi^2}{3} \frac{1}{\beta^2 A^2} \left(\frac{N}{w} \right)^2 \lambda^2. \tag{6.14}$$

As interpolymer interactions become very attractive ($\lambda \to 0$), the effect of the noncrossing condition becomes negligible. In the other limit, of strong repulsive interactions, the polymers become increasingly more resistant to deflection.

6.2 Polymer correlations

As discussed in Chapter 2, the density of polymers at a point (x, τ) corresponds to the density of particles in the analogous quantum system at a corresponding point in space-time. Thus, one may describe the lateral density-density correlations of the polymers in terms of the equal-time density-density correlations of the quantum system. Making the groundstate approximation, this yields

$$\langle \rho(x)\rho(0) \rangle = \int dx_3 \, dx_4 \, \ldots dx_N \, |\Psi(0, x, x_3, x_4, \ldots, x_N)|^2 \,, \tag{6.15}$$

where we now consider a translationally-invariant system so that the correlation depends only on the relative coordinate x. For certain values of λ, this correlation may be obtained exactly, and the results are shown Fig. 6.1. The techniques used to obtain such observables are discussed in Appendix B.

As one can see in Fig. 6.1, in all cases, the probability of two particles coinciding vanishes. The noncrossing condition, along with thermal fluctuations, overwhelms even attractive interactions. For attractive interactions, no oscillatory behavior appears. For long-range repulsion or for no long-range interactions, oscillations in the density correlation appear at $x = \pm w/N, \pm 2w/N \ldots$. In the former case, at these points polymers are actually more likely to be found than one would have for noninteracting (i.e.,

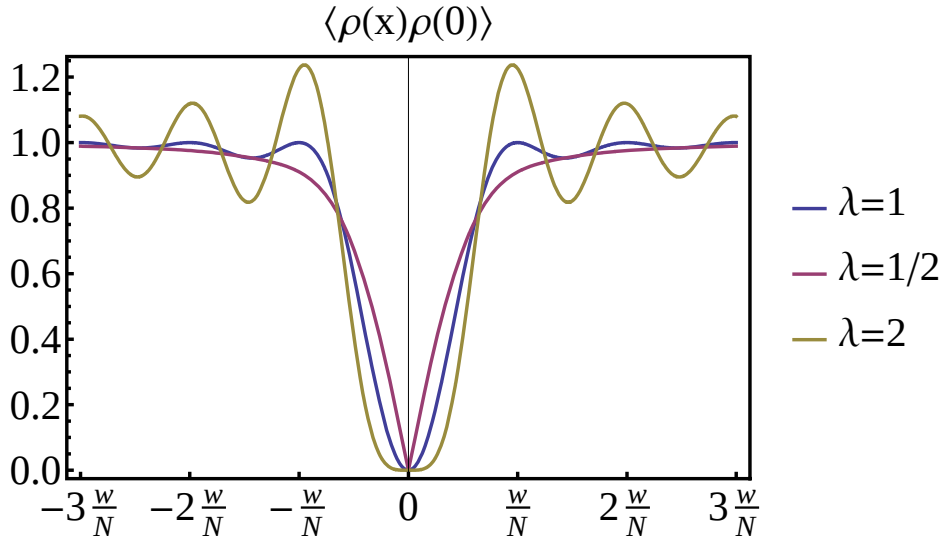

Figure 6.1: The density correlations $\langle \rho(x)\rho(0)\rangle$ (in units of the squared average density $(N/w)^2$) are plotted as a function of the lateral separation (in units of the average polymer spacing w/N) for various values of the interaction parameter λ. For $\lambda = 1/2$ (attractive long-range interactions) there is no oscillatory behavior. For $\lambda = 1$ and $\lambda = 2$, corresponding to no long-range interaction and to long-range repulsion respectively, there are oscillations in the correlations, in the latter case leading to negative correlations for $x = \pm w/n, \pm 2w/n, \ldots$ In all cases, the correlations decay as $\sim x^{-2}$.

freely crossing) polymers.

6.3 Large fluctuations of polymers with long-ranged interactions

Because the particular form of interactions considered yields a ground-state wave function so similar to that of noncrossing polymers, as found in Eq. (6.11), the analysis of large fluctuations or strong constraints may be readily generalized to the class of systems now under consideration. Recall the one-dimensional model introduced in Chapter 3, which describes the configuration of polymer coordinates $\{x_n\}$ on some line $\tau = \tau_p$. In this model, the effective interaction is given by

$$\beta U(\{x_n\}) = -\ln |\langle \Psi(\{x_n\})|^2 \,. \tag{6.16}$$

This means that for the class of interactions we consider, the effective interaction of the one-dimensional model scales as λ but otherwise has the same functional form. This applies equally when one considers the effect of a constraint on the polymer system. The free-energy cost of such a constraint scales as λ, and the polymer distribution on the dominant polymer distribution $\bar{\rho}(x)$ on the line $\tau = \tau_p$ is *independent of the interaction* λ. The more general effective interaction in Eq. (6.5) yields a distinct density profile $\bar{\rho}(x)$ that can nevertheless be addressed via the charged fluid model discussed in Chapter 3.

As one moves off the line $\tau = \tau_p$ the behavior of the polymer system is no longer governed solely by the ground-state properties of the quantum system, but the behavior of the Calogero-Sutherland system around a large fluctuation may be treated in a similar manner to a system of free fermions [35, 36]. Thus, the qualitative features of the polymer structure around a pin, including the two-dimensional extent of the gap, should persist.

CHAPTER 7

POLYMERS WITH GENERIC INTERACTIONS TREATED VIA BOSONIZATION

7.1 Introduction to bosonization

Bosonization is a powerful technique in the study of one-dimensional quantum many-body systems in which the microscopic degrees of freedom are eliminated and the low-energy behavior of the system is characterized by its dominant long-length scale density fluctuations. Because of the mapping between polymer lines and quantum particles, bosonization can also be used to analyze the behavior of systems of interacting directed polymers in two dimensions.

The bosonization technique applies generally to quantum Hamiltonians of the form

$$H = \int dx \, \frac{\hbar^2}{2m} \left(\partial_x \Psi^\dagger(x)\right) \left(\partial_x \Psi(x)\right) + \int \int dx \, dx' \, \Psi^\dagger(x) \Psi(x) V(x - x') \Psi^\dagger(x') \Psi(x'), \tag{7.1}$$

where $\Psi^\dagger(x)$ represents either a bosonic or fermionic particle creation operator. For a full description of bosonization, see, e.g., the book by Giamarchi [12], whose notation we adopt. The original bosonic creation operator may be expressed as

$$\Psi_B^\dagger(x) = \left[\frac{N}{w} - \frac{1}{\pi}\frac{\partial \phi}{\partial x}\right]^{1/2} \sum_{p=-\infty}^{\infty} e^{2ip(N\pi x/w - \phi(x))} e^{-i\theta(x)}, \tag{7.2}$$

in terms of the emergent fields $\phi(x)$ and $\theta(x)$, which respectively correspond to changes in the polymer density and slope (or, in the quantum case, to the amplitude and phase of the one-particle creation operator). The emergent fields obey the bosonic canonical relationship

$$[\partial_x \phi(x), \partial_{x'} \theta(x')] = i\pi \delta'(x - x'), \tag{7.3}$$

where $\delta'(\cdot)$ is the first derivative of the Dirac delta function. The polymer density is

$$\rho(x,\tau) = [N/w - \partial_x \phi(x)/\pi] \sum_{p=-\infty}^{\infty} e^{2ip(N\pi x/w - \phi(x,\tau))}, \tag{7.4}$$

where the $p \neq 0$ terms correspond to the short-distance polymer structure.

The benefit of this procedure is that for a wide variety of interactions in Eq. (7.1), the Hamiltonian governing the low-energy excitations may be expressed in terms of the emergent bosonic fields as

$$H = \frac{1}{2\pi} \int dx \, \frac{uK}{\hbar} \left(\partial_x \theta(x)\right)^2 + \frac{u}{K\hbar} \left(\partial_x \phi(x)\right)^2, \tag{7.5}$$

where the two Tomonaga-Luttinger parameters, u and K, depend on the microscopic model. The first, u, plays the role of a renormalized "Fermi velocity," which would relate the time and space dimensions of the quantum system. In the polymer system, it is unitless and relates the lateral and longitudinal coordinates. The second parameter, K, can be treated via a rescaling of the fields ($\phi(x) \to \phi(x)/\sqrt{K}$, $\theta(x) \to \sqrt{K}\theta(x)$) which maps the system back onto the $K = 1$ case, which corresponds to the noncrossing polymers considered in Chapters 2 and 3. In this way, systems with a wide range of interactions, including those considered in Chapters 5 and 6, can be mapped onto noncrossing but otherwise noninteracting polymers, the very system considered in the early chapters. The cost to this rescaling of the fields is that it destroys the relatively straightforward relationship between $\theta(\cdot)$ and $\phi(\cdot)$ (which describe the emergent polymer fluid) and the microscopic degrees of freedom (the original polymer lines) given in Eq. (7.2).

Although the bosonized Hamiltonian lacks the interpolymer length-scale w/N explicitly, the definitions of the fields in Eq. (7.2) retain the short-distance behavior. From this Hamiltonian, the bosonized action follows as well:

$$S = \frac{\hbar}{2\pi K} \int dx \, d\tau \, \left[\frac{1}{u} \left(\partial_\tau \phi\right)^2 + u \left(\partial_x \phi\right)^2\right], \tag{7.6}$$

associated with which there is a polymer partition function

$$\mathcal{Z} = \int \mathcal{D}\phi(x,\tau) \exp\left(-\frac{1}{2\pi K}\int dx\, d\tau\, \left[\frac{1}{u}\left(\partial_\tau \phi\right)^2 + u\left(\partial_x \phi\right)^2\right]\right). \quad (7.7)$$

This partition function characterizes the polymer system in terms of the configurations of the field $\phi(x,\tau)$, which is related to polymer density via Eq. (7.4). The normalization condition that the system contain N polymers then leads to *periodic* boundary conditions on $\phi(x,\tau)$:

$$\phi(w/2,\tau) - \phi(-w/2,\tau) = 0. \quad (7.8)$$

Alternatively, we could obtain an action solely in terms of the field $\theta(x,\tau)$, related to the polymer slope field. Because of the lack of polymer free ends in the interior of the system, either polymer density or polymer slope fully defines a given configuration of the system.

7.2 Polymer observables via bosonization

The characterization of the polymer system in terms of the harmonic fluid of the bosonization approach allows one to obtain the polymer correlations in the 2D plane. In particular, the density correlations of a large, clean polymer system are

$$\langle \rho(x+x_0,\tau+\tau_0)\rho(x_0,\tau_0)\rangle = \left(\frac{N}{w}\right)^2 \left[1 + \frac{K}{2\pi^2}\frac{(u\tau)^2 - x^2}{\left(x^2+(u\tau)^2\right)^2} + \sum_{m=1}^{\infty} A_m \frac{\cos(2\pi m N x/w)}{\left(x^2+(u\tau)^2\right)^{2m^2K}}\right]. \quad (7.9)$$

Note that although the partition function appears isotropic, the polymer correlations are sharply anisotropic, owing to the preferred direction of the polymer lines. In particular, the first nonconstant term in Eq. (7.9) indicates positive (negative) density correlations over longitudinal (lateral) displacements. This correctly indicates that if polymers occupy a point (x_0,τ_0) they are also likely to occupy a nearby point $(x_0,\tau_0+\delta\tau)$ in the preferred direction, but that there are likely to be fewer polymers at the laterally displaced nearby point $(x_0+\delta x,\tau_0)$ because no polymer line can be at that point and

at (x_0, τ_0). The other terms, with nonuniversal coefficients A_m, describe oscillatory changes in the density correlations over lengths of the average interpolymer spacing, w/N; they are analogous to Friedel oscillations. When $K < 1$, as it is for polymers with long-range repulsion, this oscillatory behavior is the dominant correlation over long length-scales. For $K > 1$, as is the case for polymers with a finite contact repulsion or for noncrossing polymers with a long-range attraction, the non-oscillatory component dominates instead.

These long-range correlations are characteristic of the clean polymer system. One can also consider the object of including columnar or point-like impurities into the polymer system. This leads to a rich variety of phases in superconducting vortex arrays in two or three dimensions [3, 4, 5, 6]. A single column at, say, $x = 0$ corresponds to a point impurity in the Luttinger liquid at $x = 0$.

This is the situation considered by Kane and Fisher in the transport of interacting electrons in one dimension across an impurity [37, 38]. They found that when the Luttinger parameter K was greater than one, transmission did not occur at zero temperature, but that for $K < 1$ electrons freely cross he impurity. In the polymer context, this result indicates that for long polymers which cross over *one another*, columnar impurities could be freely crossed, but that for noncrossing polymers the column would be impenetrable. This result shows that the response of the polymers to the column is entirely determined by interpolymer interactions rather than by single-polymer effects. This circle of ideas has been applied to vortex lines subject to a pinning column and point disorder [17], where it was found that even when the pinning was irrelevant, in the renormalization-group sense, large numbers of lines could become pinned, with Friedel-type oscillations in the polymer density around the column.

One may also bosonize a line fluid containing a *dynamical* linelike impurity. For example, one may have a polymer system with a single impurity polymer. If the impurity polymer is much stiffer than the polymers making up the polymer fluid, this corresponds to a heavy impurity in a Luttinger liquid, as considered by Castro Neto and Fisher [39]. Applying their analysis to a polymer system, one finds that the long polymers (corresponding to a low-temperature quantum system), the effective parameter A_i describing the stiffness of the impurity line against transverse fluctuations is increased by a

quantity

$$\frac{1}{t\beta^2}\left(\frac{N}{w}\right)^2, \tag{7.10}$$

where t describes the small transmissibility of polymers across the impurity line. As before, we see that the effect of the polymer fluid on an impurity (in this case a long impurity line rather than a pin or small barrier) is of order N^2, reflecting the significance of interactions over single-polymer effects.

7.3 Large fluctuations of the bosonized fluid

We now return to the type of issues discussed in Chapters 3 and 4 and ask: What is the effect of the pin on the bosonized polymer fluid? More generally, we address the task of determining the probability of a given polymer density profile $\bar{\rho}(x, \tau_p)$. Let us impose some configuration $\bar{\phi}(x)$ of the field $\phi(x, \tau)$ on the line $\tau = \tau_p$ and in addition require that $\phi(x, \tau)$ vanish (corresponding to uniform polymer density) far from this line.

Bosonization is most easily addressed in the infinite 2D plane, and so rather than considering a system of width w we extend the lateral coordinate x to any real number, with the requirement that $\phi(x + w) = \phi(x)$ to enforce normalization of the number of polymers on $|x| < w/2$.

As in the wave-function formalism, we search for the dominant polymer configuration that minimizes the free energy subject to the constraint. Now, rather than searching for the wave function $\psi(\{x_n\})$ that is the ground state of a Hamiltonian, we require a configuration of the field to minimize the bosonized action in Eq. (7.6), i.e., to obey

$$\left(\frac{1}{u^2}\partial_\tau^2 + \partial_x^2\right)\phi(x, \tau) = 0 \tag{7.11}$$

for $\tau \neq \tau_p$. The configuration that satisfies this condition and the boundary condition is

$$\phi(x,\tau) = \frac{u\,(\tau-\tau_p)}{\pi}\int dr \frac{\bar{\phi}(r)}{(x-r)^2 + u^2\,(\tau-\tau_p)^2}. \tag{7.12}$$

One may obtain from Eq. (7.7) the free energy associated with this configuration. After performing certain straightforward contour integrals , one obtains the effective free energy associated with a boundary field $\bar{\phi}(\cdot)$:

$$\mathcal{F}_p = \frac{1}{\pi^2\beta K}\int_{-\infty}^{\infty}\int_{-\infty}^{\infty} dr\,dr'\,\frac{\bar{\phi}(r)\bar{\phi}(r')}{(r-r')^2}. \tag{7.13}$$

This result applies generally to an infinite system. Now we wish to consider our system of finite width w by considering a configuration $\bar{\phi}(r)$ that is periodic in w, allowing us to relate these infinite integrals to integrals over the finite system of width w. Using the mathematical identity of Eq. (6.7) one finds a potential

$$\mathcal{F}_p = \frac{1}{w^2\beta K}\int_{-w/2}^{w/2}\int_{-w/2}^{w/2} dr\,dr'\,\frac{\bar{\phi}(r)\bar{\phi}(r')}{\sin^2\left[\pi\,(r-r')\,/w\right]}. \tag{7.14}$$

In the continuum limit, in which one considers only length-scales greater than the interpolymer length, one may use $N/w - \partial_x\phi(x)/\pi \sim \rho(x)$ and integration by parts to obtain the free energy cost of the large fluctuation in terms of the polymer density on the line $\tau = \tau_p$:

$$\mathcal{F} = \frac{1}{\beta K}\int_{-w/2}^{w/2}\int_{-w/2}^{w/2} dr\,dr'\rho(r)\rho(r')\ln\sin\left[\pi\,(r-r')\,/w\right]. \tag{7.15}$$

Strikingly, this is the exact expression for the equivalent quantity for the noncrossing polymers, scaled by $1/K$, that was derived from the free-Fermion wave function in Chapter 4 for systems of noncrossing polymers. This indicates that a wide variety of polymer systems (and other systems of linelike objects), including those with polymer crossings and with long-range interactions, respond to strong constraints in the same way. In particular, the density profile around a pin will lead to the same density profile $\bar{\rho}(x)$ already obtained.

7.4 Bosonization as linearized hydrodynamics

In this section, we return to the hydrostatic approach used in Chapter 4 to describe the evolution of the polymer density profile in the longitudinal direction. As we will see, bosonization corresponds to the linearized version of this theory. Recall that, as in Eq. (4.30), the free energy density of a region of the polymer system may be expressed in terms of local coarse-grained polymer density and slope fields in a region of width w' and length L' as

$$\frac{\mathcal{F}}{w'L'} = A\rho\frac{v^2}{2} + \rho\mathcal{E}(\rho). \tag{7.16}$$

One may expand this around the equilibrium density as $\rho(x,\tau) = \rho_0 + \delta\rho(x,\tau)$. The lowest-order nonconstant contributions to the free energy have the form (following some renormalization of the constant coefficients)

$$\beta\mathcal{F} = \frac{1}{2\pi}\int\int dx\, d\tau\, \frac{1}{uK}\rho_0^2 v(x,\tau)^2 + \frac{u}{K}\left(\delta\rho(x,\tau)\right)^2. \tag{7.17}$$

The continuity condition becomes

$$\partial_\tau\delta\rho(x,\tau) + \rho_0\partial_x v(x,\tau) = 0, \tag{7.18}$$

which may be satisfied automatically, provided that we associate the density and slope with a field $\phi(x,\tau)$ via

$$\begin{pmatrix} \delta\rho(x,\tau) \\ \rho_0\, v(x,\tau) \end{pmatrix} = \begin{pmatrix} \partial_x\phi(x,\tau) \\ -\partial_\tau\phi(x,\tau) \end{pmatrix}. \tag{7.19}$$

Having made this association, we recover the form of the bosonized free energy from Eq. (7.7). Thus, we see that the bosonization is valid only when the polymer density fluctuations $\delta\rho(x,\tau)$ are small. Indeed, the quantum techniques used to bosonize the Hamiltonian rely on a *linear* dispersion, which is only valid in the limit of low-energy excitations of a generic system. Thus, strong constraints such as the pin do not strictly permit bosonization.

Bosonization predicts, e.g., the correct profile on the line $\tau = \tau_p$. But it incorrectly predicts that polymer density grows linearly as one moves longitudinally away from the pin. In fact, we know from the exact techniques of Chapters 3 and 4 based on the wave function that nonlinear terms lead to a gap of finite area around the pin. We expect then that the gap structure is qualitatively as found for noncrossing polymers, with the Luttinger liquid parameter u describing dilation or contraction of the gap and other features in the polymer density.

Finally, we note that there are regimes of constraints that are still strong but that leave the polymer system close enough to equilibrium to justify the use of bosonization. For example, bosonization may describe the polymer evolution around the constraint requiring $\rho(x, \tau_p) = \rho_0 + (\delta\rho_0)\mathrm{sgn}(x)$, with $(\delta\rho_0) \ll \rho_0$. In such a situation, the linearized hydrodynamic equations and/or bosonization suffice to describe the polymer structure around the constraint.

CHAPTER 8

POLYMERS IN $2+1$ DIMENSIONS

8.1 Introduction to bulk polymers

In previous chapters, we considered systems of noncrossing directed lines in $1+1$ dimensions. In Chapter 5 we included a small third dimension so that polymers could cross over one another. We now wish to consider a fully $2+1$-dimensional system of nonintersecting polymers. The configuration of a single polymer line is now given by $\mathbf{r}_n(\tau) \equiv (x_n(\tau), y_n(\tau))$, where the x and y directions are treated on an equal basis.

The energy of a given polymer configuration from Eq. (1.3) generalizes readily to the $(2+1)$-dimensional case:

$$U\left[\{\mathbf{r}_n(\cdot)\}\right] = \frac{A}{2}\sum_{n=1}^{N}\int_0^L d\tau \left(\partial_\tau \mathbf{r}_n(\tau)\right)^2 + \frac{1}{L}\sum_{n=1}^{N}\int_0^L d\tau\, \Phi\big(\,|\mathbf{r}_n(\tau)|\,\big) + \frac{1}{L}\sum_{1\le n<n'\le N}\int_0^L d\tau\, V\big(\,|\mathbf{r}_n(\tau)-\mathbf{r}_{n'}(\tau)|\,\big). \quad (8.1)$$

The one-body potential $\Phi\big(\,|\mathbf{r}_n(\tau)|\,\big)$ will be chosen to confine the polymers in a finite area:

$$\mathbf{r}_n(\tau)^2 \le R^2. \quad (8.2)$$

This leads to an average density of polymers

$$\rho_0 = \frac{N}{\pi R^2}, \quad (8.3)$$

where unlike in previous chapters ρ_0 is an *areal* density.

The two-body interaction will serve to make the polymers nonintersecting, the equivalent in $2+1$ dimensions of the noncrossing condition in $1+1$ dimensions:

$$\left(\mathbf{r}_n(\tau)-\mathbf{r}_{n'}(\tau)\right)^2 \ge d^2. \quad (8.4)$$

Here, we will take the effective thickness d of the polymer line to be negligibly

small compared to the average interpolymer spacing.

8.2 Polymer topology

Unlike noncrossing polymers in $1+1$ dimensions, nonintersecting polymers in $2+1$ dimensions have topological properties that describe their entanglement about one another. Consider now a single polymer whose configuration $\mathbf{r}(\tau)$ for simplicity we assume to obey periodic boundary conditions in the longitudinal coordinate:

$$\mathbf{r}(0) = \mathbf{r}(L). \tag{8.5}$$

Now, following Edwards [40] we may define the *winding number* W of a configuration as

$$W\left[\mathbf{r}(\tau)\right] = \frac{1}{2\pi}\int_0^L d\tau\, \frac{d}{d\tau}\theta(\mathbf{r}(\tau)), \tag{8.6}$$

where $\theta(\mathbf{r}(\tau))$ is the angle of $\mathbf{r}(\tau)$ relative to the positive x axis:

$$\theta(\mathbf{r}) = \tan^{-1}\left(\frac{y}{x}\right). \tag{8.7}$$

The winding number is an integer which counts the net number of times the polymer configuration circles around the line $\mathbf{r} = 0$. It is topological in the sense that continuous deformations of the polymer configuration (respecting the condition that the polymer cannot cross $\mathbf{r} = 0$) cannot change it. It may be seen that this term is equivalent to the Aharanov-Bohm one governing a charge following a path $\mathbf{r}(\tau)$ around a fixed flux through the origin:

$$\mathbf{A}(\mathbf{r}) \sim \frac{\hat{\tau}\times\mathbf{r}}{|\mathbf{r}|^2}, \tag{8.8}$$

$$\frac{d}{d\tau}\theta(\mathbf{r}) = \mathbf{A}(\mathbf{r})\cdot\dot{\mathbf{r}}(\tau). \tag{8.9}$$

This suggests that when we attempt the quantum picture of polymers in $2+1$ we may be able to account for their interactions via the insertion of Aharanov-Bohm flux tubes into the polymer lines.

If we wish to require that this winding number have some particular value W^*, then it is necessary to insert a delta function into the measure over polymer configurations:

$$\mathcal{D}\mathbf{r}(\cdot) \to \mathcal{D}\mathbf{r}(\cdot)\delta\left(W\left[\mathbf{r}(\tau)\right] - W^*\right). \tag{8.10}$$

More generally, one may define the winding number between two polymer configurations $\mathbf{r}_n(\tau)$ and $\mathbf{r}_{n'}(\tau)$:

$$W_{n,n'} \equiv W\left[\mathbf{r}_n(\tau) - \mathbf{r}_{n'}(\tau)\right] = \frac{1}{2\pi}\int_0^L d\tau\, \frac{d}{d\tau}\theta(\mathbf{r}_n(\tau) - \mathbf{r}_{n'}(\tau)). \tag{8.11}$$

We treat our polymers as being restricted to some particular set of winding numbers $\{W_{n,n'}\}$. This could be enforced by holding fixed the polymer endpoints at $\tau = 0$ and $\tau = L$. Even if the ends are not strictly fixed, it has been shown that for systems of dense directed lines without free ends the time required for lines to untangle themselves grows very quickly with the length of the system [41], so that the lines will behave as though they were topologically restricted over any reasonable experimental lifetime.

Even in the absence of a finite polymer thickness, restricting the polymer system to a particular topological sector will lead to nonintersecting polymers repelling one another. We saw for noncrossing polymers in 1D that it was unlikely to find one polymer very close to another because a thermal fluctuation could drive the polymers across one another, and the noncrossing condition forbids that. In contrast, polymers that were far apart could fluctuate more freely, and so these were more likely configurations.

Now, nonintersecting polymers restricted to a given topological sector suffer a similar penalty when brought close to one another. That is, a thermal fluctuation could alter the winding number $W_{n,n'}$ between two nearby polymers, which is forbidden by the topological restriction. Thus, thermal fluctuations will drive the polymers apart.

The finite line thickness d has a similar effect. When polymers are close

to one another thermal fluctuations may bring them within a distance d of one another— a configuration forbidden by the interaction in Eq. (8.4). Thus, thermal fluctuations drive polymers of finite thickness apart in $2+1$ dimensions, even without any topological restriction. Thus we see that *either* the restriction to a particular topological sector of $\{\mathbf{r}_n(\cdot)\}$ *or* the finite thickness of the lines will, in the presence of thermal fluctuations, drive the lines apart from each other. In contrast, infinitely thin nonintersecting lines not under any topological restriction are effectively noninteracting in $2+1$ dimensions, since unlike in $1+1$ dimensions the fraction of configurations $\{\mathbf{r}_n(\cdot)\}$ of polymers which include an intersection is negligible.

8.3 Quantum picture

As in previous chapters, we shall attempt to describe the the statistics of the polymer system via the ground state of a quantum Hamiltonian:

$$H = \frac{1}{2m}\sum_n \mathbf{p}_n^2 + \sum_n \Phi\big(\,|\mathbf{r}_n(\tau)|\,\big) + \sum_{n<n'} V\big(\,|\mathbf{r}_n(\tau) - \mathbf{r}_{n'}(\tau)|\,\big). \qquad (8.12)$$

As discussed in Chapter 2, the natural ground state of this Hamiltonian, as in the 1D case, is bosonic, real, and nonnegative. Also as in the $1D$ case, we wish to incorporate the interpolymer repulsion by ensuring that the wave function vanish when any two particle coordinates coincide:

$$\psi(\mathbf{r}_1, \ldots, \mathbf{r}, \ldots, \mathbf{r}, \ldots \mathbf{r}_n) = 0. \qquad (8.13)$$

In the 1D case, this was accomplished by de Gennes by a trivial mapping directly onto fermions [1]. Girardeau showed that in 1D a bosonic wave function could be mapped onto a fermionic wave function simply by including a fermion-like phase factor -1 whenever any two particle coordinates were exchanged. We could attempt the same thing for our 2D case, but while this would indeed require that the wave function vanish when particle coordinates coincide, it would mean that the transformed wave function was no longer an eigenstate of the Hamiltonian of Eq. (8.12). Indeed, such a trans-

formation requires us to be able to associate a phase factor of ± 1 with any ordering of the one-dimensional coordinates $\{x_n\}$, one that changes abruptly as any x_n is brought across another $x_{n'}$. The two-dimensional particle coordinates $\{\mathbf{r}_n\}$ cannot be said to have any order, and so any phase factor ought to vary gradually, since any $\mathbf{r}_n$ can be brought *around* another $\mathbf{r}_{n'}$. Fortunately a transformation exists that achieves Fermi statistics through gradually-changing phase factors exists [42], the well-known singular gauge transformation of Chern-Simons theory. For any bosonic eigenstate of the Hamiltonian in Eq. (8.12), one may define a fermionic one

$$\Psi_f \equiv \exp\left[i\phi \sum_{n<n'} \theta\left(\mathbf{r}_n - \mathbf{r}_{n'}\right)\right] \Psi_b, \tag{8.14}$$

where the angle function $\theta(\mathbf{r})$ has the same definition as that used to describe the winding of one polymer around another in Eq. (8.7) and ϕ is a real parameter.

Now, let us examine the statistics of our new wave function. Suppose one exchanges the particles at $\mathbf{r}_{n'}$ and $\mathbf{r}_n$ by taking them along paths such that $\mathbf{r}_{n'}$ is rotated by π radians about $\mathbf{r}_n$ but that the two particles follow the same path relative to the remaining $N-2$ particles. This exchange will take $\theta_{n,n'} \to \theta_{n,n'} + \pi$, but will leave the sum of the other phase factor unchanged, as well as the original bosonic wave function. Thus, particle exchange yields

$$\Psi_f \to \exp(i\pi\phi)\Psi_f. \tag{8.15}$$

Thus, Fermi statistics (and therefore the nonintersection of the polymer lines) are ensured provided that we choose ϕ to be an odd integer. For simplicity, we will focus on $\phi = 1$.

Unlike in the 1D case, the transmutation of the wave function now leads to a nontrivial change in the energy eigenproblem

$$H'\Psi_f = E\Psi_f. \tag{8.16}$$

The energy values E are unchanged by the transmutation, but the Hamil-

tonian is now

$$H' \equiv \frac{1}{2m}\sum_{n=1}^{N} |\mathbf{p}_n - q\mathbf{A}_n(\mathbf{r}_n)|^2, \tag{8.17a}$$

$$\mathbf{A}_n(\mathbf{r}) \equiv \frac{\phi h}{2\pi q}\sum_{n'(\neq n)} \nabla'_n \theta_{n,n'} = \frac{\phi h}{2\pi q}\sum_{n'(\neq n)} \frac{\hat{\boldsymbol{\tau}} \times (\mathbf{r} - \mathbf{r}_{n'})}{|\mathbf{r} - \mathbf{r}_{n'}|^2}. \tag{8.17b}$$

If, in Eq. (8.17a), $\mathbf{A}_n(\mathbf{r}_n)$ were to depend only on $\mathbf{r}_n$, and not on any $\{\mathbf{r}_{n'(\neq n)}\}$, the Hamiltonian $\mathcal{H}'$ would describe independent particles in a magnetic field $\mathbf{B} = \nabla \times \mathbf{A}$. However, as shown in Eq. (8.17b), $\mathbf{A}_n$ does depend on $\{\mathbf{r}_{n'(\neq n)}\}$, which implies (nonlocal) interactions between all particles. Eq. (8.17b) states that $\{\mathbf{A}_n\}$ describes particles that have ϕ quanta of fictitious magnetic flux attached (i.e., localized at the position of every particle, each quantum carrying h/q flux, where q is a fictitious charge and units are such that the speed of light is unity). Thus, $\mathcal{H}'$ describes composite fermions—composed of particles obeying Fermi statistics and flux tubes [43, 44]. This transmutation of statistics is the Hamiltonian form of Chern-Simons theory.

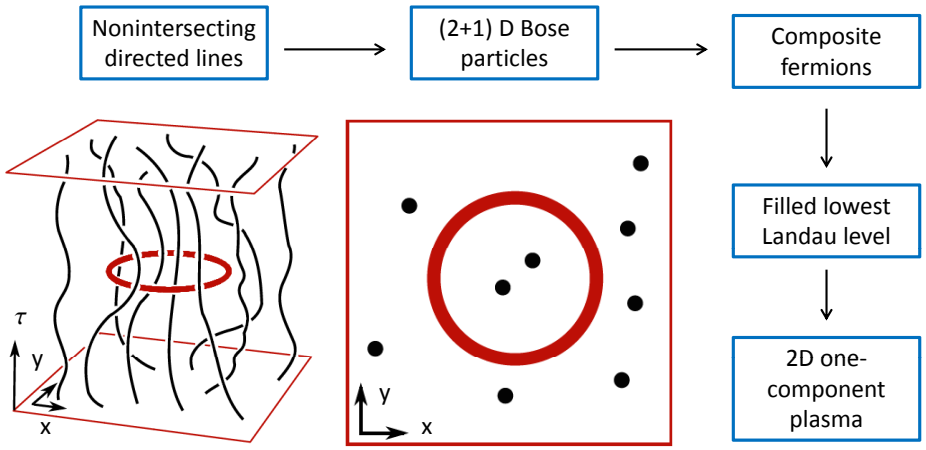

Figure 8.1: (Sequence of transformations of a liquid of directed polymers with a spatially extended constraint, shown as a ring (thick line), threaded by a fixed number of polymers used to obtain the free energy and polymer density of the constrained system. The directed polymer liquid is transformed to a two-dimensional one-component plasma, whose the Coulomb repulsion results from integrating out the long noncrossing chains.

This composite fermion theory has been used in many contexts, including

discussion of the fractional quantum Hall effect [44, 43], anyon superconductivity [43] and reptation dynamics in polymer melts [45]. The topological nature of Chern-Simons field theory has been used to study the winding [46], writhe [47] and knot invariants [48] of entangled polymers. The Lagrangian form of Chern-Simons theory involves coupling the Bose particles to a gauge field and integrating out the gauge field to find an effective fermion theory [42, 49] and naturally leads to the powerful second-quantized Landau-Ginzburg-Chern-Simons (LGCS) theory in terms of a Lagrangian density $\mathcal{L}$ [50, 49, 51].

Although the composite fermion formulation effectively incorporates the hard-core restriction, it remains intractable, and thus we are led to take advantage of a natural approximation (see, e.g., Refs. [43, 44]), which we now describe. Instead of having an odd number of flux tubes attached to each particle, we smear the magnetic field associated with one flux tube per particle uniformly over the area of the system, and gauge-transform away the remaining flux tubes. In this so-called Average Field Approximation (AFA), the fermions are *non-interacting* and subject to a *homogeneous* magnetic field $\nabla \times \mathbf{A} = B\hat{\boldsymbol{\tau}}$, corresponding to one quantum of magnetic flux per particle. [In the symmetric gauge, $\mathbf{A} = \frac{B}{2}(y, -x, 0)$.] In the language of directed lines, the magnetic field is equal to the number of lines per unit area ρ_0 times a quantum of flux (i.e., $B = \rho_0 h/q$). In this magnetic field, the many-body ground-state has the energy $E = NB\hbar q/2m$ and the Slater determinant takes the Vandermonde form [52],

$$\Psi_f^a(\mathbf{R}) \propto e^{-\sum_{n=1}^{N} |w_n|^2/4\ell^2} \prod_{1 \le n < n' \le N} (w_n - w_{n'}), \tag{8.18}$$

where $w_n = x_n + iy_n$. Strikingly, this wave function in fact closely resembles the one obtained for noncrossing polymers in $1D$. If one sets the $\{y_n\}$ identically to zero, one would obtain a wave function for 1D fermions (confined to a harmonic potential rather than bound by hard walls). Within our approximations, the quantum ground state energy and wave function describe the long noncrossing directed line liquid. In particular, for its free energy per unit volume, we obtain the result

$$\frac{\mathcal{F}}{\pi R^2 L} = \frac{\pi \rho_0^2}{A\beta^2}. \tag{8.19}$$

the many-body effect of the crowding of the polymers, an effect absent for free directed lines.

8.4 Large fluctuations and constraints

Proceeding in analogy with the 1+1 dimensional case, we can use the ground-state wave function to effectively integrate out the bulk of the polymer system and describe the effective energy of a given polymer configuration $\{\mathbf{r}_n\}$ in a transverse plane $\tau = \tau_p$:

$$\beta U(\{\mathbf{r}_n\}) \approx -\ln|\Psi_f^a|^2 = -2\sum_{n<n'} \ln|\mathbf{r}_n - \mathbf{r}_{n'}| + \pi\rho_0 \sum_{n=1}^{N} |\mathbf{r}_n|^2. \tag{8.20}$$

Interpreted as a potential energy, U describes a two-dimensional one-component plasma (2DOCP) [53, 54]. In the general case of the plasma, particles of (e.g., negative) charge $-e$ live in a uniform background that maintains overall charge neutrality, and they interact via two-dimensional Coulomb repulsion: $e^2 \ln(|\mathbf{r}_n - \mathbf{r}_{n'}|)$. This βU corresponds to a specific value, viz. 2, of the plasma coupling constant βe^2. As in the $1+1$-dimensional case, integrating out the bulk polymers gives rise to an effectively long-ranged repulsion between the polymer segments, even though the original polymer interaction is local. This term would, by itself, lead to polymers being driven apart by thermal fluctuations until the polymer density dropped to zero. The second term in the effective energy in Eq. (8.20) serves to counteract this tendency and confine the N polymer segments to the area $\mathbf{r}^2 \leq R^2$.

This completes our reduction of the three-dimensional classical system of a liquid of noncrossing directed lines to the classical Two-Dimensional One-Component Plasma (2DOCP), which enables us to compute physical properties such as the free-energy cost and the equilibrium density profiles associated with the imposition of spatially extended constraints. The long-range planar interactions within the 2DOCP arise from the short-range interactions

between the fluctuating directed lines, integrated over their length.

We now introduce the ring constraint into the system, as depicted in Fig. 8.2. The ring is the boundary of the region

$$\mathbf{r}^2 < a^2 \tag{8.21}$$

in the plane $\tau = \tau_p$ through which some fixed number of polymers pass. The special case for which no polymers pass through the ring represents the effect of inserting a solid object, a disk of radius a, into the polymer fluid. We refer to a general such constraint (not necessarily circular) as encompassing some simply-connected region $\mathcal{D}$. This is the analog of the pin discussed in Chapter 4, which fixed some number N_L of polymer lines passing through part of the system. As with the pin, the ring will in general either compress or rarefy the polymers passing through $\mathcal{D}$, with the opposite effect on the remaining polymers.

To calculate the free energy and the equilibrium density of directed lines in the presence of a ring constraint, we analyze the 2DOCP first at the level of classical electrostatics, and then allow for fluctuations. To minimize the electrostatic energy, any excess mobile charge is forced up against the boundary of $\mathcal{D}$. Moreover, on the other side of the boundary, a region fully depleted of mobile charge (i.e., a gap) opens up, out to a radius within which the net charge is zero. This electrostatic argument fails for the 1D case used to consider a pin because the particles are confined to the one-dimensional line $y = 0$ which does not have a true interior. For a simply-connected region of arbitrary boundary $\mathcal{D}$ in two dimensions, the charge distribution may be found by conformally mapping the problem onto one with a circular boundary.

Similarly, at the level of electrostatic energy minimization one can readily determine the energy of the charge distribution and, hence, the free energy cost of the ring constraint $\Delta\mathcal{F}(Q, Q_0)$, in terms of the mobile charge $-Q$ (that is, the number of polymers passing through the ring) and the background charge in $\mathcal{D}$, Q_0 ($\equiv \pi a^2 \rho_0$), both in units of e [57]; see Fig. 8.2. For the special case $Q = 0$ (i.e., $\mathcal{D}$ empty, corresponding to an inclusion) the free energy cost has a simple form:

$$\Delta\mathcal{F} = Q_0^2/4 = \pi^2 a^4 \rho_0^2/4. \tag{8.22}$$

This simple electrostatic result is significant for the noncrossing-directed-line liquid, as it differs qualitatively from the case of a noninteracting directed line liquid, for which a particle inclusion incurs a free-energy cost *linear* in $a^2\rho_0$. Instead, as for the case of polymers in $1+1$ dimensions, the response of polymers in $2+1$ dimensions to a strong constraint grows as N^2, indicating that polymer interactions rather than single-polymer effects dominate the response of the system to impurities. Not only does the ring displace some number of polymers proportionate to ρ_0, but the cost of displacing each of these polymers is itself proportionate to ρ_0 due to interpolymer interactions.

To improve upon the electrostatic approximation, we take into account the effect of thermal fluctuations on the polymer density profile. We rely on the exact solution of the 2DOCP with the appropriate plasma coupling constant, i.e., 2 [55, 56, 57, 54, 59, 60]. In the limit of a large ring, $a \gg 1/\sqrt{\rho_0}$, the exact density profile outside the region of constraint depends only on a, ρ and Q through the combination $(Q - Q_0)/\sqrt{2Q_0}$ [55]. The layer of excess mobile charge on one side forms an electrical double layer of thickness of order $1/\sqrt{\rho_0}$; see Fig. 8.2c and Ref. [55]. The region partially depleted of mobile charge does develop a soft gap, in which the charge is small but nonzero. The mobile charge density profile progresses smoothly, according to a qualitatively error-function-like curve, through the boundary region, rapidly approaching the value that exactly compensates the background charge density ρ_0; see Fig. 8.2c and Ref. [55]. The mobile charge density profile for the depleted side of the constraint applies to both cases, $Q > Q_0$ and $Q < Q_0$, and similarly for the excess-charge side. For Q small relative to Q_0, the remaining mobile charge in $\mathcal{D}$ forms a droplet whose shape is essentially the density profile of a system of electrons that fill the lowest Landau level: a flat central profile and a decay into the soft gap; see, e.g., Ref. [61]. Thus, we have established that when some fixed portion of the lines of a directed line liquid is constrained to thread $\mathcal{D}$, the equilibrium density profile in the slice containing $\mathcal{D}$ is that of the correspondingly constrained 2DOCP.

The behavior of the gap formed around the ring differs substantially from the gap around the pin discussed in Chapter 4. The size of that gap was less

than the pin displacement as the polymers sagged upward to take advantage of the extra space on the depleted side of the pin. In $2+1$ dimensions, the gap is exactly the size necessary so that the polymer density averaged over a region including the ring and the gap remains ρ_0. And the polymer density around a pin remained substantially modified over the entire width of the system. In contrast, the gap fills in over a distance on the order of the interpolymer spacing $1/\sqrt{\rho_0}$.

Recapping our strategy, we progressed from a three-dimensional liquid of thermally fluctuating lines, to a two-dimensional quantum many-boson fluid, to a two-dimensional quantum many-fermion fluid coupled to a Chern-Simons gauge field, which we treat in the Average Field Approximation to obtain the filled lowest Landau level picture. The phenomenology of a lowest Landau level filled with non-interacting fermions is well studied, and suggests various analogous phenomena for the corresponding hard-core boson fluid. However, as the AFA is an approximation, these analogous phenomena may be artifacts of the approximation, and we now use physical intuition to identify any such artifacts. For example, the quantum Hall effect suggested by the AFA is one such artifact: the boson fluid does not have broken time-reversal symmetry, and therefore shows no Hall effect [62, 63] (By Hall effect we mean the occurrence of a transverse particle current in response to a longitudinal potential gradient). A second artifact is suggested by the incompressibility of the filled lowest Landau level, which would incorrectly imply the incompressibility of the boson fluid. However, by reinstating the inter-particle interactions $\mathbf{A}(\mathbf{r}) - \mathbf{A}_a(\mathbf{r})$, for example via the Random Phase Approximation, the compressibility of the boson fluid is restored, as shown in Refs. [62, 63]. In the context of the directed line liquid, the thermodynamic (areal) compressibility κ is defined in terms of the free energy density f via $\kappa^{-1} \equiv \rho_0^2 \, \partial^2 f / \partial \rho_0^2$, and thus, using Eq. (8.19), we obtain $\kappa = A\beta^2/2\pi\rho_0^2$. A particularly noteworthy consequence of the residual interactions $\mathbf{A}(\mathbf{r}) - \mathbf{A}_a(\mathbf{r})$ is their ability to renormalize the effective plasma coupling constant e^2/T in the plasma analogy away from the exactly solvable case, viz. 2. Nevertheless, we expect the general picture presented here of the energetics and structure of the directed line liquid in the presence of spatially extended constraints to hold.

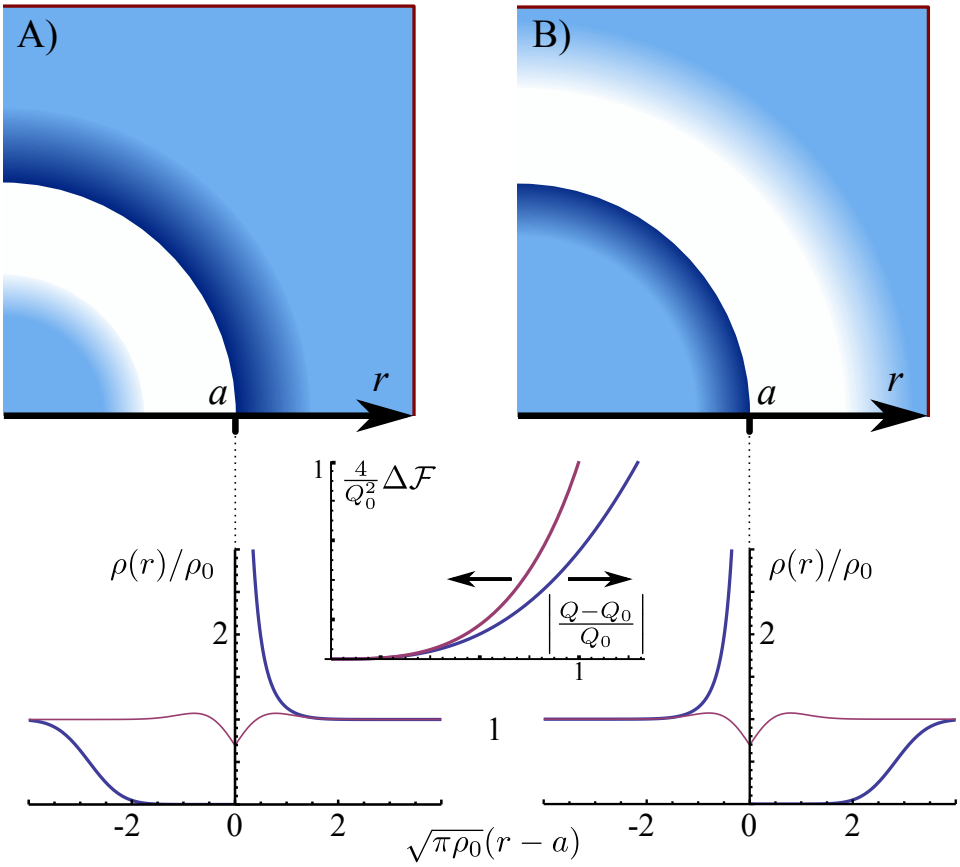

Figure 8.2: (Two-Dimensional One-Component Plasma (2DOCP) with a spatially extended constraint. The electrostatic approximation predicts a gap in the mobile charge density and an accumulated surface charge for cases (A), for which excess mobile charge stays outside of the ring, and (B), for which excess mobile charge is confined inside the ring. This approximation also predicts mobile-charge-density discontinuities, which in the exact solution are smeared out due to thermal fluctuations of mobile charges around the energy minimum. The exact solution leads to the density profiles $\rho(r)/\rho_0$ shown for $(Q-Q_0)/\sqrt{2Q_0} = \pm 4$ (thick) and 0 (thin), where $-Q$ and Q_0 ($\equiv \pi a^2 \rho_0$) are the mobile and the background charges inside the ring, respectively [55, 56]. The inset shows the rescaled energy cost $(4/Q_0^2)\Delta\mathcal{F}$ [top: case (A), bottom: case (B)] [57]. The curves are valid for macroscopic values of the charge deficiency, i.e., for not-too-small values of the argument, when $\Delta\mathcal{F}$ is dominated by electrostatic energy. In the text, we establish that these profiles corresponds to the planar distribution of noncrossing directed lines due to a planar spatially extended constraint. Based on a figure prepared for Souslov et al. [58].

CHAPTER 9

CONCLUDING REMARKS

Our central aim with this work has been to develop a statistical-mechanical treatment of macroscopic systems of directed classical polymers and other linelike objects that are subject to various interactions. This framework has been developed chiefly by mapping the various polymer systems onto corresponding quantum systems undergoing imaginary-time evolution. This mapping allows us to exploit a variety of powerful techniques from quantum many-body physics to shed light on the associated polymer system. This framework has allowed us not only to describe the equilibrium structure and thermodynamic properties of polymer systems, but also how these systems respond to strong constraints or undergo large fluctuations.

Strong constraints such as the topological pin have the effect of altering the equilibrium value of the spatial profile of the local polymer density and reducing the entropy (and therefore increasing the free energy) of directed polymer systems. Generically, this increase in the free energy gives rise to forces that act on the constraints (and between them, if there are several of them).

The determination of the alteration of statistical weight resulting from the presence of constraints for the polymer system is then ascertained via consideration of a particular quantum amplitude: the matrix element of the imaginary-time evolution operator between the many-particle ground state and the set of states consistent with the constraint. This technique readily yields results for situations in which the constraints are located collinearly on a line that runs perpendicular to the direction preferred by the polymers. By supplementing this technique with a hydrodynamical approach we are able to establish the form of the polymer density not only along the aforementioned line on which the constraints lie but also at points away from this line.

The archetypal constraint that we consider is a topological point-like pin, which fixes the number of polymers that flow to one side of it, generically compressing part of the polymer system. Strikingly, in the limit of large numbers of polymers, in which fluctuations are small and the polymer density may be approximated as a continuous fluid, we find that the effect of such a pin is to cause a divergent pile-up of the polymer density on the compressed side of the pin and a zero-density region (or gap) on the low-density side, the latter giving way to a continuously rising density beyond the gap. In addition, via a quantum-hydrodynamical approach we find that the gap opened by the pin has a nonzero extent in the polymer preferred direction, only

gradually narrowing and closing. Fluctuations around the dominant density profile replace the zero-density region by a region of very small polymer density. We also find for pins that are only mildly displaced from a zero-force (i.e., equilibrium) position that the force acting on them is sub-Hookean, growing less than linearly with the displacement via a factor logarithmic in the displacement, and the gap created by them similarly grows sub-linearly with the displacement. One can regard these nonlinear responses as resulting from the effectively long-range interactions between polymer segments that emerge via short-range interactions between long polymer strands in regions that reach far from the segments in question.

We have also determined how the form of polymer interactions modifies the statistical properties of the polymer system. Polymers of nonzero thickness that cross over one another are related to bosons with a contact interaction and treated via the Bethe Ansatz technique. We have described how the effective interaction is related to polymer parameters, and how various statistical properties of the polymer system may be derived from the quantum model. Polymers with long-range interactions may instead be described via the quantum Calogero-Sutherland model. In this case, one finds that the ground-state wave function is closely related to that for noncrossing polymers, showing that the response of a wide class of polymer systems to strong constraints mirrors that of noncrossing polymers without any additional interactions.

Bosonization has been developed as a universal technique that applies to two-dimensional classical statistical systems as well as one-dimensional quantal many-body ones. We have used it to describe the density correlations of the polymer system and its response to impurities. We have also used bosonization to show that the response of a generic polymer system to a strong constraint in some ways perfectly mirrors that of a system of noncrossing polymers. Care must be taken, however, in applying bosonization to polymer systems subject to strong constraints.

Finally, we have discussed the response of polymers in $2+1$ dimensions to obstructions. We have described how in the quantum picture interactions may be treated via Chern-Simons theory, just as Fermi statistics enforces noncrossing in $1+1$ dimensions. We have found that there is an effective two-dimensional statistical model, the Two-Dimensional One-Component Plasma (2DOCP), which mirrors the form of the one-dimensional model used to de-

scribe polymers in $1+1$ dimensions. Although the effective interaction has the same form (logarithmic), in either $2+1$ or $1+1$ dimensions, its effect is very different due to the differing dimensionality. Gaps still form in depleted regions but excess polymers build up near the surface of nanoparticle inclusions, rather than modifications to the density profile extending far across the system.

In conclusion, we have explored the rich behavior of a variety of directed polymer systems both subject to and not subject to strong constraints.

APPENDIX A

N FERMION GROUND-STATE WAVE FUNCTION

Consider a system of N noninteracting fermions moving freely one dimension on the line segment $0 < x < \pi$ and subject to homogeneous (i.e., homogeneous Dirichlet) boundary conditions at $x = 0$ and $x = \pi$. The normalized wave functions associated with the single-particle energy eigenstates of such a system are given by

$$\phi_j(x) = \sqrt{2/\pi}\sin(jx), \quad j = 1, 2, \ldots. \tag{A.1}$$

In terms of these, the normalized N-particle ground-state wave function of the N-fermion system may be expressed in terms of a Slater determinant, as follows:

$$\psi(x_1, \ldots, x_N) = \frac{1}{\sqrt{N!}} \det_{N\times N} \big[\phi_j(x_k)\big], \tag{A.2}$$

where $[\phi_j(x_k)]$ is the $N \times N$ matrix having (jk) element $\phi_j(x_k)$. Omitting N factors of $\sqrt{2/\pi}$, the matrix $[\phi_j(x_k)]$ takes the form

$$\begin{pmatrix} \sin x_1 & \sin x_2 & \cdots & \sin x_N \\ \sin 2x_1 & \sin 2x_2 & \cdots & \sin 2x_N \\ \vdots & \vdots & \ddots & \vdots \\ \sin Nx_1 & \sin Nx_2 & \cdots & \sin Nx_N \end{pmatrix}. \tag{A.3}$$

To simplify the evaluation of the determinant of this matrix, we add linear combinations of the rows of the matrix to other rows, a procedure that leaves its value unchanged. Specifically, we make the replacements

$$\phi_j(x_k) \to \phi_j(x_k) + \phi_{j-2}(x_k) - 2\cos x_N \ \phi_{j-1}(x_k),$$

where we make the definition $\phi_j(x_k) = 0$ for $j < 1$. The resulting matrix is then given by

$$\left(\begin{array}{c|c} \sin x_1 \;\; \sin x_2 \;\; \cdots \;\; \sin x_{N-2} \;\; \sin x_{N-1} & \sin x_N \\ \hline & 0 \\ 2(\cos x_k - \cos x_N) \sin\left((j-1)x_k\right) & \vdots \\ & 0 \end{array}\right). \tag{A.4}$$

Note, specifically, the vanishing of the elements in the lower $N-1$ rows in the N^{th} column. In evaluating the determinant of this matrix, we may extract $N-1$ factors of the form $2(\cos x_k - \cos x_N)$ from the rows in the lower left block of the matrix. Thus, we obtain the recursive result, linking Slater determinants for N-particle and $(N-1)$-particle systems:

$$\begin{aligned} \det_{N\times N}\big[\phi_j(x_k)\big] &= (-1)^{N-1} \sin x_N \\ &\times \prod_{k=1}^{N-1} (2\cos x_k - 2\cos x_N) \times \det_{\substack{(N-1)\\ \times(N-1)}}\big[\phi_j(x_k)\big]. \end{aligned} \tag{A.5}$$

Next, we apply this relation recursively, and this arrive at the following, desired form for the N-particle ground-state wave function:

$$\begin{aligned} \psi(x_1, x_2, \ldots, x_N) = \frac{2^{N^2/2}}{\pi^{N/2}\sqrt{N!}} \Big(\prod\nolimits_{j=1}^{N} \sin x_j\Big) \\ \times \prod_{1\le j<k\le N} \big(\cos x_j - \cos x_k\big). \end{aligned} \tag{A.6}$$

Note that for a system of hard-core bosons the corresponding ground-state wave function is simply the absolute value of this fermionic wave function.

APPENDIX B

GAUSSIAN RANDOM MATRICES AND CHARGED FLUIDS

Following Mehta [64], when an $N \times N$ Hermitian matrix is drawn from a random ensemble of Hermitian matrices whose real parameters are Gaussian random variables, the joint probability density of its eigenvalues $\{x_n\}$ is

$$P_{N\lambda} = \exp\left(-\lambda \sum_n x_n^2\right) \prod_{n<n'} |x_n - x_{n'}|^{2\lambda} . \tag{B.1}$$

Here, $\lambda = 1/2, 1, 2$ correspond to orthogonal, unitary, and symplectic ensembles of matrices respectively. That is, the ensembles are invariant under orthogonal, unitary and symplectic transformations, respectively.

The integral over such a probability density of eigenvalues may be interpreted as the partition function of a one-dimensional system of interacting particles. This falls within the charged fluid model described in Chapter 3, with a harmonic confining potential $f(\cdot)$ and a logarithmic interaction $g(\cdot, \cdot)$ whose repulsive strength is proportionate to λ. Taking into account the harmonic potential centered at $x = 0$ rather than hard walls at $x = \pm w/2$, this also corresponds to three instances of systems of noncrossing polymers with attractive interactions, no long-range interactions, and repulsive interactions for $\lambda = 1/2, 1, 2$ respectively. Thus we see that the lateral statistics of polymer segments correspond to the statistics of Gaussian random matrices.

For a system with hard walls and no additional strong constraints, the equilibrium density of polymers is nearly uniform , with short-ranged Friedel oscillations near the walls. In contrast, the equilibrium distribution for the harmonic confining potential is nontrivial. Proceeding in a manner similar to the one employed in Chapters 3, 4, one may arrive at an integral equation for the equilibrium polymer density, whose solution is given by Wigner's semicircle law [65]

$$\bar{\rho}(x) = \frac{1}{\pi}\sqrt{2N - x^2}\,\theta(2N - x^2). \tag{B.2}$$

That is, the polymers when confined by a harmonic potential rather than hard walls assume an equilibrium density profile shaped like a semicircle.

One may also derive the n-point density function for the polymer system by performing integrations over the distribution in Eq. (B.1). The two-point density correlations, found by Mehta [64], give the lateral density-density correlations of the polymer system and are plotted in Fig. 6.1. In an infinite system, the choice of boundary conditions (harmonic or hard-wall) does not affect the local density correlations.

APPENDIX C

ELLIPTIC INTEGRAL REPRESENTATIONS OF THE PIN CONSTRAINT AND FREE ENERGY

Given the form of the polymer density found in Chapter 4 the pin constraint Eq. (4.5) may be constructed in terms of the elliptic integral of the third kind as

$$\frac{N_R}{N} = \frac{2(s_g - s_p)}{\pi\sqrt{(1-s_p)(1+s_g)}}\,\Pi\left(\frac{1+s_p}{1+s_g}, \frac{(1+s_p)(1-s_g)}{(1-s_p)(1+s_g)}\right), \quad \text{(C.1a)}$$

$$\Pi(n,m) \equiv \int_0^1 \frac{ds}{1-ns^2}\frac{1}{\sqrt{(1-ms^2)(1-s^2)}}. \quad \text{(C.1b)}$$

We may describe how s_g varies with s_p for a given partitioning by requiring that the partitioning given by N_R is constant with respect to variations of s_p, so that

$$\frac{dN_R}{ds_p} = \frac{\partial N_R}{\partial s_p} + \frac{\partial N_R}{\partial s_g}\frac{\partial s_g}{\partial s_p} = 0. \quad \text{(C.2)}$$

By using Eq. (C.1a), we thus find the result

$$\frac{\partial s_g}{\partial s_p} = \frac{1+s_g}{1+s_p}\left(1 - \frac{E\left(\frac{(1+s_p)(1-s_g)}{(1-s_p)(1+s_g)}\right)}{K\left(\frac{(1+s_p)(1-s_g)}{(1-s_p)(1+s_g)}\right)}\right), \quad \text{(C.3)}$$

where K and E are elliptic integrals of the first and second kind, respectively:

$$K(k) \equiv \int_0^1 \frac{ds}{\sqrt{(1-k^2s^2)(1-s^2)}}, \quad \text{(C.4a)}$$

$$E(k) \equiv \int_0^1 ds\,\frac{\sqrt{1-k^2s^2}}{\sqrt{1-s^2}}. \quad \text{(C.4b)}$$

For a pin infinitesimally displaced from its equilibrium position, so that $s_p - s_g \approx \gamma \cos x_p$ with $\gamma \ll 1$, the right-hand side version of the pin constraint (4.5), may similarly be asymptotically expanded in γ to obtain the condition

$$\pi \frac{N_R}{N} \approx \int_{s_g}^{1} \frac{ds}{\sqrt{1-s^2}} \left[1 + \frac{\gamma \cos x_p}{2} \frac{1}{s - s_p} \right]$$
$$\approx \frac{\pi}{2} - x_g + \frac{\gamma}{2} \ln \left[\frac{2 \cos^2 x_p}{|\gamma|} \right]. \tag{C.5}$$

This equation yields the asymptotic relation between gap size and displacement given in Eq. (4.15).

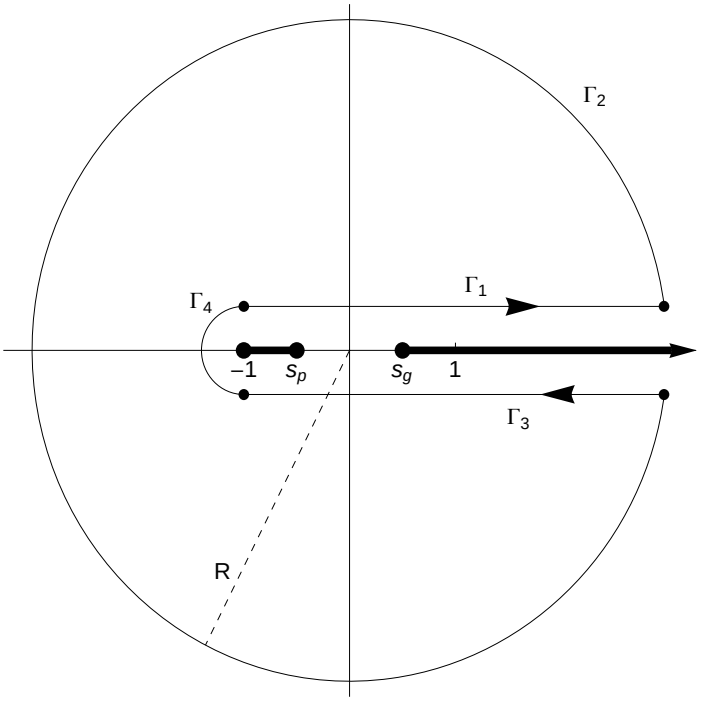

Figure C.1: The contour Γ used in Eq. (C.10). Branch cuts run from $s = -1$ to $s = \min(s_p, s_g)$ and from $s = \max(s_p, s_g)$ to $s = +\infty$. The arc Γ_4 has a radius ϵ which will be taken to zero, and the arc Γ_2 has a radius R which will be taken to infinity. From Rocklin et al. [2].

We turn our attention now to the free energy cost of the pin, Eq. (4.16), which can be written in terms of the scaled effective potentials ϕ_L and ϕ_R experienced by polymers on the left and right side of the pin, respectively, as

$$\frac{\Delta\mathcal{F}}{N^2T} = \frac{N_L}{N}\phi_L + \frac{N_R}{N}\phi_R, \tag{C.6a}$$

$$\phi_L \equiv \int_{-1}^{1} ds\, \ln\left[2(1+s)\right] Q(s), \tag{C.6b}$$

$$\phi_R \equiv \int_{-1}^{1} ds\, \ln\left[2(1-s)\right] Q(s), \tag{C.6c}$$

with the transformed coordinate s and polymer density $Q(s)$ defined in the main text; see Eq. (4.9). As we shall see, it is useful to represent ϕ_R as an elliptic integral, and to do this it is necessary to obtain a form without the logarithm. To this end, we extend s into the complex plane, and make use of the residue theory result

$$\oint_\Gamma ds \ln(1-s) Q(s) = 0, \tag{C.7}$$

where the keyhole contour Γ comprises the segments $\Gamma_1, \ldots, \Gamma_4$ as shown in Fig. C.1. Now, the integrand has the form

$$\ln(1-s)\, Q(s) = \frac{1}{\pi}\Big(\ln|1-s| + i\arg(1-s)\Big) \times\sqrt{\left|\frac{s-s_g}{(1-s^2)(s-s_p)}\right|}\, e^{i\phi(s)}, \tag{C.8a}$$

$$\phi(s) \equiv \big(\arg(s-s_g) - \arg(1-s) - \arg(1+s) - \arg(s-s_p)\big)/2, \tag{C.8b}$$

which is analytic in the complex plane except on the branch cuts. Note that although the physical polymer density is zero in the gap, we are allowing $Q(s)$ to be nonzero but imaginary in the gap, and complex in the complex s plane. We choose the branch cuts to run from $s = -1$ to $s = \min(s_p, s_g)$ and from $s = \max(s_p, s_g)$ to $s = +\infty$, as shown in Fig. C.1.

While the integral along the inner contour Γ_4 vanishes as its radius ϵ goes to zero, the integral along the outer contour Γ_2 (i.e., along $|s| = R$), does not vanish. In the limit $R \gg 1$ this contour integral becomes

$$\int_{\Gamma_2} ds \ln(1-s)\, Q(s) \approx$$
$$\int_0^{2\pi} \left(iRe^{i\theta}d\theta\right) \Big[\ln R + i\,(\theta-\pi)\Big] \frac{i}{\pi R e^{i\theta}} = -2\ln R. \quad \text{(C.9)}$$

Thus, the contour integral of Eq. (C.10) yields

$$2\ln R \approx \int_{-1}^{1} ds \ln|1-s|\, Q(s+i\epsilon) + \int_1^R ds \Big[\ln|1-s| - \pi i\Big] Q(s+i\epsilon)$$
$$+ \int_R^1 ds \Big[\ln|1-s| + \pi i\Big] Q(s-i\epsilon) + \int_1^{-1} ds \ln|1-s|\, Q(s-i\epsilon). \quad \text{(C.10)}$$

Elementary cancellations among parts of these integrals occur, so that upon taking the limit $R \to \infty$, Eq. (C.10 (which is exact in this limit) yields

$$\phi_R = \int_1^\infty ds \left[\frac{1}{s} - \sqrt{\frac{s-s_g}{(s^2-1)(s-s_p)}}\right], \quad \text{(C.11a)}$$

$$\phi_L = \int_1^\infty ds \left[\frac{1}{s} - \sqrt{\frac{s+s_g}{(s^2-1)(s+s_p)}}\right]. \quad \text{(C.11b)}$$

Using these representations of ϕ_L and ϕ_R, the free energy may be expressed in terms of elliptic integrals, although the complete expression is rather complicated. Strikingly, however, a simple result follows for the force on the pin, $-d\mathcal{F}/dx_p$. In particular, by differentiating Eq. (C.6a) we find

$$\frac{1}{N^2 T}\frac{d\mathcal{F}}{ds_p} = \frac{N_L}{N}\frac{d\phi_L}{ds_p} + \frac{N_R}{N}\frac{d\phi_R}{ds_p}, \quad \text{(C.12)}$$

where

$$\frac{d\phi_{L/R}}{ds_p} = \frac{\partial\phi_{L/R}}{\partial s_p} + \frac{\partial s_g}{\partial s_p}\frac{\partial\phi_{L/R}}{\partial s_g}. \quad \text{(C.13)}$$

Thus, by consideration of the elliptic integral representation, it can be shown that

$$\frac{1}{N^2 T}\frac{d\mathcal{F}}{ds_p} = \frac{s_p - s_g}{1 - s_p^2}, \tag{C.14}$$

and from this result follows the force on the pin given in Eq. (4.20).

REFERENCES

[1] P.-G. de Gennes, "Soluble model for fibrous structures with steric constraints," *J. Chem. Phys.*, vol. 48, p. 2257, 1968.

[2] D. Z. Rocklin, S. Tan and P. M. Goldbart, "Directed-polymer systems explored via their quantum analogs: Topological constraints and their consequences," *Phys. Rev. B*, vol. 86, p. 165421, 2012.

[3] D. R. Nelson and V. M. Vinokur, "Boson localization and correlated pinning of superconducting vortex arrays," *Phys. Rev. B*, vol. 48, p. 13060, 1993.

[4] T. P. Devereaux, R. T. Scalettar and G. T. Zimanyi, "Effect of competition between point and columnar disorder on the behavior of flux lines in (1+1) dimensions," *Phys. Rev. B*, vol. 50, p. 13625, 1994.

[5] M. P. A. Fisher, "Vortex-glass superconductivity: A possible new phase in bulk high-Tc oxides," *Phys. Rev. Lett.*, vol. 62, p. 1415, 1989.

[6] T. Giamarchi and P. L. Doussal, "Elastic theory of flux lattices in the presence of weak disorder," *Phys. Rev. B*, vol. 52, p. 1242, 1995.

[7] N. C. Bartelt, T. L. Einstein and E. D. Williams, "The influence of step-step interactions on step wandering," *Surf. Sci*, vol. 240, p. L591, 1990.

[8] M. Kulkarni and A. Lamacraft, "From GPE to KPZ: finite temperature dynamical structure factor of the 1D Bose gas," *arXiv:1201.6363v1 [cond-mat.quant-gas]*, 2012.

[9] M. E. Fisher, "Walks, Walls, Wetting, and Melting," *J. Stat. Phys.*, vol. 34, p. 667, 1984.

[10] R. D. Kamien, P. Le Doussal and D. R. Nelson, "Theory of directed polymers," *Phys. Rev. A*, vol. 45, p. 8727, 1992.

[11] F. Wiegel, "An exactly solvable two-dimensional biomembrane model," *J. Stat. Phys.*, vol. 13, p. 515, 1975.

[12] T. Giamarchi, *Quantum Physics in One Dimension*. Oxford: Oxford University Press, 2004.

[13] M. Kardar, G. Parisi and Y.-C. Zhang, "Dynamic scaling of growing interfaces," *Phys. Rev. Lett.*, vol. 56, p. 889, 1986.

[14] M. Kardar, "Roughening by impurities at finite temperatures," *Phys. Rev. Lett.*, vol. 55, p. 2923, 1985.

[15] M. Kardar and Y.-C. Zhang, "Scaling of directed polymers in random media," *Phys. Rev. Lett.*, vol. 58, p. 2087, 1987.

[16] R. Feynman, *Statistical Mechanics: A Set of Lectures, Frontiers in Physics*. San Francisco: Benjamin Cummings, 1972.

[17] A. Polkovnikov, Y. Kafri and D. R. Nelson, "Vortex pinning by a columnar defect in planar superconductors with point disorder," *Phys. Rev. B*, vol. 71, pp. 014 511–1, 2005.

[18] E. Lieb and W. Liniger, "Exact Analysis of an Interacting Bose Gas. I. The General Solution and the Ground State," *Phys. Rev.*, vol. 130, p. 1605, 1963.

[19] M. Girardeau, "Relationship between Systems of Impenetrable Bosons and Fermions in One Dimension," *J. Math. Phys.*, vol. 1, p. 516, 1960.

[20] H. Kleinert, *Path Integrals in Quantum Mechanics, Statistics, and Polymer Physics, and Financial Markets*. Singapore: World Scientific Publishing, 2004.

[21] R. Feynman and A. Hibbs, *Quantum Mechanics and Path Integrals*. New York: McGraw-Hill, 1965.

[22] W. Sutherland, *Beautiful Models: 70 Years of Exactly Solved Quantum Many-Body Problems*. Singapore: World Scientific, 2004.

[23] M. Doi and S. Edwards, *The Theory of Polymer Dynbamics*. Oxford: Oxford University Press, 1986.

[24] R. Pathria, *Statistical Mechanics*. Burlington, MA: Elsevier, 1972.

[25] R. Estrada and R. P. Kanwal, "Integral Equations with Logarithmic Kernels," *IMA J. Appl. Math.*, vol. 43, p. 133, 1989.

[26] E. Bettelheim, A. G. Abanov and P. Wiegmann, "Nonlinear Quantum Shock Waves in Fractional Quantum Hall Edge States," *Phys. Rev. Lett.*, vol. 97, p. 246401, 2006.

[27] A. G. Abanov, "Hydrodynamics of correlated systems," in *Applications of Random Matrices in Physics*, E. Brézin *et al*, Ed. Amsterdam, The Netherlands: Springer, 2006, ch. 5, p. 139.

[28] D. Z. Rocklin, S. Tan and P. M. Goldbart, "Directed-polymer systems explored via their quantum analogs: general polymer interactions and their consequences," to be published.

[29] C. Jayaprakash, C. Rottman and W. F. Saam, "Simple model for crystal shapes: Step-step interactions and facet edges," *Phys. Rev. B*, vol. 30, p. 6549, 1984.

[30] V. I. Marchenko and A. Ya. Parshin, "Elastic properties of crystal surfaces," *Sov. Phys. JETP*, vol. 52, p. 129, 1980.

[31] J. Hofbauer, "A simple proof of $1+1/2^2+1/3^2+\ldots=\pi^2/6$ and related identies," *Am. Math. Monthly*, vol. 109, p. 196, 2002.

[32] F. Calogero, "Solution of the One-Dimensional N-Body Problems with Quadratic and/or Inversely Quadratic Pair Potentials," *J. Math. Phys.*, vol. 12, p. 419, 1971.

[33] B. Sutherland, "Exact Results for a Quantum Many-Body Problem in One Dimension," *Phys. Rev. A*, vol. 4, p. 2019, 1971.

[34] H. Frahm and S. I. Matveenko, "Correlation functions in the Calogero-Sutherland model with open boundaries," *Eur. Phys. J. B.*, vol. 5, p. 671, 1998.

[35] A. G. Abanov and P. Wiegmann, "Quantum Hydrodynamics, the Quantum Benjamin-Ono Equation, and the Calogero Model," *Phys. Rev. Lett.*, vol. 95, p. 076402, 2005.

[36] A. G. Abanov, E. Bettelheim and P. Wiegmann, "Integrable hydrodynamics of Calogero-Sutherland model: bidirectional Benjamin-Ono equation," *J. of Phys. A*, vol. 42, p. 135201, 2009.

[37] C. L. Kane and M. P. A. Fisher, "Transmission through barriers and resonant tunneling in an interacting one-dimensional electron gas," *Phys. Rev. B*, vol. 46, p. 15233, 1992.

[38] C. L. Kane and M. P. A. Fisher, "Transport in a one-channel Luttinger liquid," *Phys. Rev. Lett.*, vol. 68, p. 1220, 1992.

[39] A. H. Castro Neto and M .P. A. Fisher, "Dynamics of a heavy particle in a Luttinger liquid," *Phys. Rev. B*, vol. 46, p. 15233, 1992.

[40] S. Edwards, "Statistical mechanics with topological constraints: I," *Proc. Phys. Soc.*, vol. 91, p. 513, 1967.

[41] S. P. Obukhov and M. Rubinstein, "Topological Glass Transition in Entangled Flux State," *Phys. Rev. Lett.*, vol. 65, p. 1279, 1990.

[42] D. P. Arovas, J. R. Schrieffer, F. Wilczek and A. Zee, "Statistical mechanics of anyons," *Nucl. Phys. B*, vol. 251, p. 117, 1985.

[43] F. Wilczek, *Fractional Statistics and Anyon Superconductivity.* Singapore: World Scientific, 1990.

[44] J. Jain, *Composite Fermions.* Cambridge: Cambridge University Press, 2007.

[45] A. L. Kholodenko and T. A. Vilgis, "The tube diameter in polymer melts, its existence and its relation to the quantum Hall effect," *J. Phys. I France*, vol. 4, p. 843, 1994.

[46] B. Drossel and M. Kardar, "Winding angle distributions for random walks and flux lines," *Phys. Rev. E*, vol. 53, p. 5861, 1996.

[47] D. Moroz and R. D. Kamien, "Self-avoiding walks with writhe," *Nucl. Phys. B*, vol. 506, p. 695, 1997.

[48] F. Ferrari and I. Lazzizzera, "Polymer topology and Chern-Simons field theory," *Nucl. Phys. B*, vol. 559, p. 673, 1999.

[49] S. C. Zhang, T. H. Hansson and S. Kivelson, "Effective-field-theory model for the fractional quantum Hall effect," *Phys. Rev. Lett.*, vol. 62, p. 82, 1989.

[50] N. Read, "Order Parameter and Ginzburg-Landau Theory for the Fractional Quantum Hall Effect," *Phys. Rev. Lett.*, vol. 62, p. 86, 1989.

[51] A. Lopez and E. Fradkin, "Fractional quantum Hall effect and Chern-Simons gauge theories," *Phys. Rev. B*, vol. 44, p. 5246, 1991.

[52] R. B. Laughlin, "Quantized motion of three two-dimensional electrons in a strong magnetic field," *Phys. Rev. B*, vol. 27, p. 3383, 1983.

[53] R. B. Laughlin, "Anomalous quantum Hall effect: an incompressible quantum fluid with fractionally charged excitations," *Phys. Rev. Lett.*, vol. 50, p. 1395, 1983.

[54] B. Jancovici, "Exact results for the two-dimensional one-component plasma," *Phys. Rev. Lett.*, vol. 46, p. 286, 1981.

[55] B. Jancovici, "Charge distribution and kinetic pressure in a plasma: a soluble model," *J. Phys. Lett.*, vol. 42, p. 223, 1981.

[56] B. Jancovici, "Classical Coulomb systems near a plane wall. I," *J. Stat. Phys.*, vol. 28, p. 43, 1982.

[57] B. Jancovic, J. L. Lebowitz and G. Manificati, "Charge distribution and kinetic pressure in a plasma: a soluble model," *J. Stat. Phys.*, vol. 72, p. 773, 1993.

[58] A. Souslov, D. Z. Rocklin and P. M. Goldbart, "Organization of strongly interacting directed polymer liquids in the presence of strong constraints," *arXiv:1304.5267 [cond-mat.soft]*, 2013.

[59] B. Jancovici, "Classical Coulomb systems near a plane wall. II," *J. Stat. Phys.*, vol. 29, p. 263, 1982.

[60] B. Jancovici, "Surface properties of a classical two-dimensional one-component plasma: exact results," *J. Stat. Phys.*, vol. 34, p. 803, 1984.

[61] X. Wen, *Quantum Field Theory of Many-Body Systems*. Oxford: Oxford University Press, 2004.

[62] A. L. Fetter, C. B. Hanna and R. B. Laughlin, "Random-phase approximation in the fractional-statistics gas," *Phys. Rev. B*, vol. 39, p. 9679, 1989.

[63] Q. Dai, J. L. Levy, A. L. Fetter, C. B. Hanna and R. B. Laughlin, "Quantum mechanics of the fractional-statistics gas: Random-phase approximation," *Phys. Rev. B*, vol. 46, p. 5642, 1992.

[64] M. L. Mehta, *Random Matrices*. San Diego: Academic Press, 1991.

[65] E. P. Wigner, "Characteristic Vectors of Bordered Matrices With Infinite Dimensions," *Ann. Mathematics*, vol. 62, p. 548, 1955.